DYNAMICS AND CONTROL OF THE

CONTINUOUS CRYSTALLIZER WITH FINES TRAP

by

Shang-jen Lei

A dissertation submitted to the
Graduate Faculty in Chemical Engineering
in partial fulfillment of the requirements
for the degree of Doctor of Philosophy,
The City University of New York.

1970

This manuscript has been read and accepted for the Graduate Faculty in Engineering in satisfaction of the disertation requirement for the degree of Doctor of Philosophy.

18th May 1970
date

Stanley Katz
Chairman of Examining Committee

18 May 1970
date

Executive Officer

Prof. Jacques Benveniste

Prof. Robert Graff

Prof. Stanley Katz - Chairman

Prof. George Kranc

Prof. Reuel Shinnar

Supervisory Committee

The City University of New York

Acknowledgment

It has been a considerable time, since I first decided to pursue my studies toward a doctor's degree. During this long period of education, I have become indebted to many persons for their kind advice and assistance. To these people, I now can only express my sincere thanks and appreciation, since there is no way to repay them for their encouragement and concern. Several persons, however, deserve special mention here. Without them it would have been impossible for me to complete this work.

Professor A Thesdore Trimble,jr., who was the acting dean of the Engineering School of Tunghai University, and Professor Harvey List, whom I first met at Tunghai when I graduated, gave their recommendation, so that I had the opportunity to study in this country. Professor Alois X. Schmidt, Chairman of the Chemical Engineering Department, gave me the chance to continue my study in City College. There is no adquate way for me to express my heartful thanks for these opportunities which they have made possible, but to wish them continued success in their endeavors.

Professor Stanley Katz and Professor Reuel Shinnar, my advisers, made possible the successful completion of this work. Their direction of my study, their patience with my short-comings, their keen insight into the heart of the problem and their familiarity with the tools required for this study, made it possible for me to accomplish my goal. My daily contact with these scholars has not only benefited my general engineering development, but also provide me with a new insight into life.

I also thank my pardents who not only supported me through the early phases of my education but also provided me with moral inspiration and encouragement, through some of the darken moments. Thanks are also due to my wife, Rei-hsian, for typing this thesis. She enjoyed my successes as if they were her own.

I am also appreciative of partial financial support from the National Science Foundation for this work.

Table of Contents

Abstract

A mathematical model is presented for studying the stability and control of a continuous crystallizer with fines trap.

Working equations are developed for the open-loop operation of the crystallizer. A linearized stability analysis is carried out, and it is shown how proper operation of the fines trap can stabilize the crystallizer at large crystal product sizes that would otherwise lead to instability. An analytical stability criterion is developed for a crystallizer with point fines trap, that is, one with small fines destruction size and large recirculation rate. Dynamic studies for the full non-linear equations are carried out numerically, and stable limit cycles exhibited around unstable equilibrium points.

Various feedback control mechanisms for the regulation of continuous crystallizers are studies as well. It is discovered that modes of operation unstable in open loop can be stabilized by measuring the surface area of the fines population and manipulating the throughput rate. A corresponding manipulation of the fines recirculation rate rather than of the bulk throughput rate cannot readily stabilize an unstable operation, but seems to smooth stable operations quite efficiently. The stabilization criteria are developed from a linearized stability analysis of a crystallizer with point fines trap. The analytical results are tested numerically with the full working equations.

Nomenclature

a = $\left[6-(6+6\lambda+3\lambda^2+\lambda^3)e^{-\lambda}\right] / \left[2-(2+2\lambda+\lambda^2)e^{-\lambda}\right]$

A = a dimensionless constant in Volmer's kinetics of nucleation.

b = $6kB(c)G(c)^3\theta^4\left\{1+(\rho-c)B'(c)/B(c)\right\}$, sensitivity nucleation rate.

$B(c)$ = general nucleation rate function.

C, C_i = solute concentration, and inlet solute concentration.

C_s, C_m = solute saturated concentration, and a critical concentration level higher than C_s

$f(r,t)$ = number density of the crystal size distribution function.

g = $6kB(c)G(c)^3\theta^4(\rho-c)G'(c)/G(c)$, sensitivity growth rate.

$G(c)$ = general growth rate function.

$G(s)$ = transfer function of the plant, $1/G(o)$ is the static sensitivity of the feedback control system.

$h(x)$ = One form of the fines selection function, here $x=r/r_o$.

$H(x)$ = a component function of the characteristic equation (4.12), see eq. (4.13)

k = particle shape factor.

K_b = rate constant of nucleation function.

K_g = rate constant of growth rate function.

$K(x)$ = a component function of the haracteristic equation (4.12), see eq.(4.13).

$K(s)$, K = transfer function of the controller, and proportional control constant.

L = $(\rho - C_s)/(C_i - C_s)$

M = $(C_m - C_s)/(C_i - C_s)$

n, n_o = total number of crystals and fines particles per unit volume, also an subscript.

r = a characteristic linear dimension for particle.

r_o = a critical size for fines destruction.

r^* = $r_o/(G\theta)$, a dimensionless paramter of the system.

$\bar{r}$ = the weight average particle size.

S = $(C_i - C_s)/C_s$

s = dimensionless, Laplace transform variable

t = time dimension

u = δu is the control action of the feedback control

v = the active volume of the system

w, w_o = the volumetric throughput rate, and fines recirculated rate.

x, y = dummy variables, δx also used as response variable of control system.

Greek letters:

α = $6k_B(c)G(c)^3\theta^4$ a parameter of linearized system.

ϵ = liquid volume fraction in the crystallizer

θ, θ_o = the overall holdup time of the crystallizer, and the fines retention time

σ, σ_o = the bulk surface and fines surface per unit volume

$\sigma(x)$ = $(21x^3+87x^2+128x+64)/(x+4)^2$

ρ = the crystal density

$\nu_n(x)$ = a dimensionless function defined in eq (3.10)

φ = the total solute-crystal resource function

$\eta(r)$ = the fines selection function

λ = $r_o/(G\theta_o)$ a parameter of the fines trap

μ_n = n^{th} moment function of $f(r,t)$

Prefix:

δ : refers to the perturbation var ables of the system.

Subscripts:

i : refers to the variables or functions of the inlet condition.

o : pertains to the var ables or parameters of the fines trap.

e : refers to the steady-state (equilibrium) values.

Miscellany:

$\mathcal{L}$: refers to the Laplace transfer form of the system variables

Dimensionless parameters:

θ = $\theta \cdot (kB_iG_i^3)^{1/4}$

θ_o = $\theta_o(kB_iG_i^3)^{1/4}$

$\bar{r}$ = $\bar{r}/(G_i/kB_i)^{1/4}$

r_o = $r_o/(G_i/kB_i)^{1/4}$

B = B/B_i

G = G/G_i

t = t/θ

r = $r/(G\theta)$

$\delta f(r,t)$ = $\delta f(r,t)/(\epsilon B/G)$

$\delta\varphi$ = $\delta\varphi(t)/\left[6k\epsilon\frac{B}{G}(G\theta)^4(\rho-c)\right]$

Figures

CHAPTER 1
INTRODUCTION

Continuous removal of fines or small crystals from the crystal magma to increase the average particle size has become a standard practice in industrial crystallization [2,4,5,12,13]. The fraction of fines removal is often quite high and may reach up to 30% of the production rate on a mass basis.

A schematic diagram of a typical fines trap is given in fig. 1 [1,12,13]. Part of a mixed crystallizer is shielded by a baffle. The circulation of the magma through the baffled zone is slow so larger particles fall to the bottom. Only fines particles reach the top, from which a stream is drawn off to a heater in which the smaller crystals are dissolved, or to a mechanical fines removal device, and the clear solution is fed back to the crystallizer.

The design of the baffle and the crystallizer itself allows one to fix the maximum particle size r_o that will be elutriated into the fines trap region. This design will determine the size distribution and magma density at the inlet to the fines trap. The amount of fines dispersion circulated through the fines trap, w_o, is separately adjustable by the operator. The operator, in most cases, has very little direct control of r_o. In some designs a change in w_o also effects the maximum size which is elutriated into the fines zone, but this thesis deals with the first case.

Fines traps are important tools in the control of the crystallizer. Not only do they allow adjustment of particle size at more or less constant production rate, but proper adjustment of the fines trap also allows one to stabilize the operation of the crystallizer[1,2] and prevent continued cycling.

Continued cycling of this kind is a serious problem in the scale-up and operation of commercial continuous crystallizers [1,3,8], and quantitative treatment for both mixed and classified crystallizers has been presented by several investigators [1,6,8, 10,15,12,16,19]. In these cases the particle size fluctuates in a periodic way. A few cases of such cyclic operation are reported in the literature [1,3]. An industrial example of such cycling is given in figure 2.

This thesis presents a detailed quantitative treatment of stabilizing and regulating strategies for a crystallizer with fines trap. It presents first an open loop dynamic analysis, which shows quantitatively how proper setting of the fines trap can stabilize the crystallier operation even at large crystal product sizes. The explicit mathematical results are for a linearized stability analysis, and for a point fines trap, that is, one with small fines destruction size and large recirculation rate, an analytical stability criterion is presented. For the finite fines

trap, the characteristic equation is developed analytically, and stability curves plotted numerically. To test the results of the linear analysis, dynamic studies for the nonlinear operating equations are carried out numerically.

With the open loop analysis in hand, transfer functions are calculated, and some simple schemes for feedback control are presented. The most promising are those, directly applicable to crystallizers with fines trap, that measure the surface area of the fine crystals and manipulate either the fines recirculation rate or the bulk throughput rate. The latter has the capability of stabilizing modes of operation that are unstable in open loop. The former cannot readily perform this stabilization, but it seems to smooth quite efficiently modes of operation that are already stable. The mathematical analysis of the control system is all carried out for a crystallizer with point fines trap. The mathematical methods are those of linear analysis. The analytical results are tested numerically with the full working equations for the systems in question.

The reults presented in this thesis should provide a theoretical background for a better understanding of the operation and design of continuous crystallizers with fines trap.

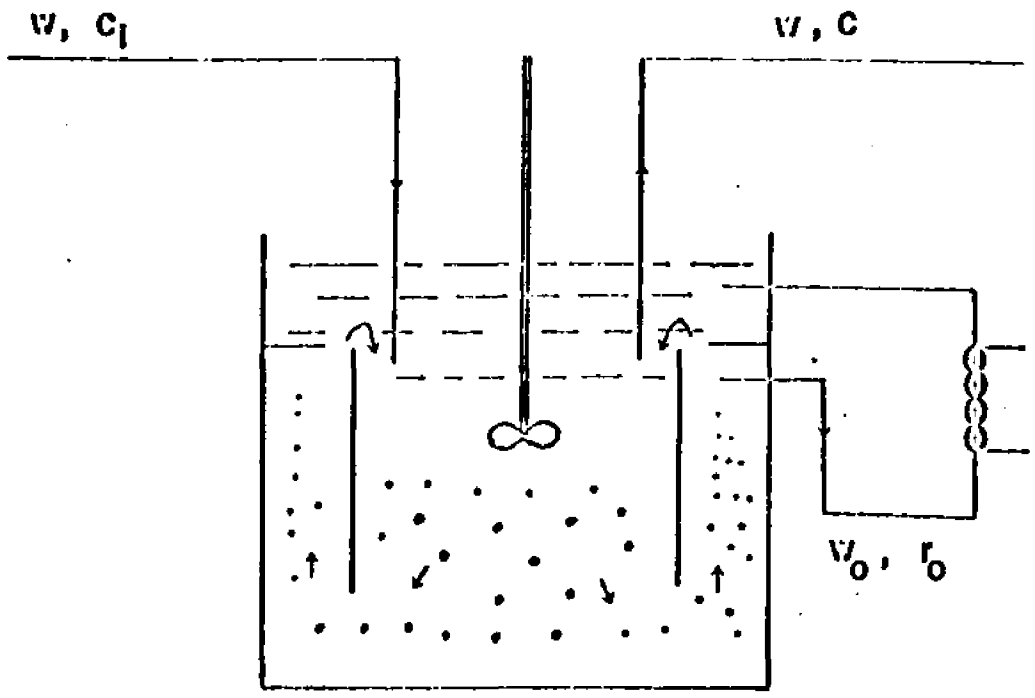

Figure 1 A Schematic Diagram of A Continuous Crystallizer With Fines Trap

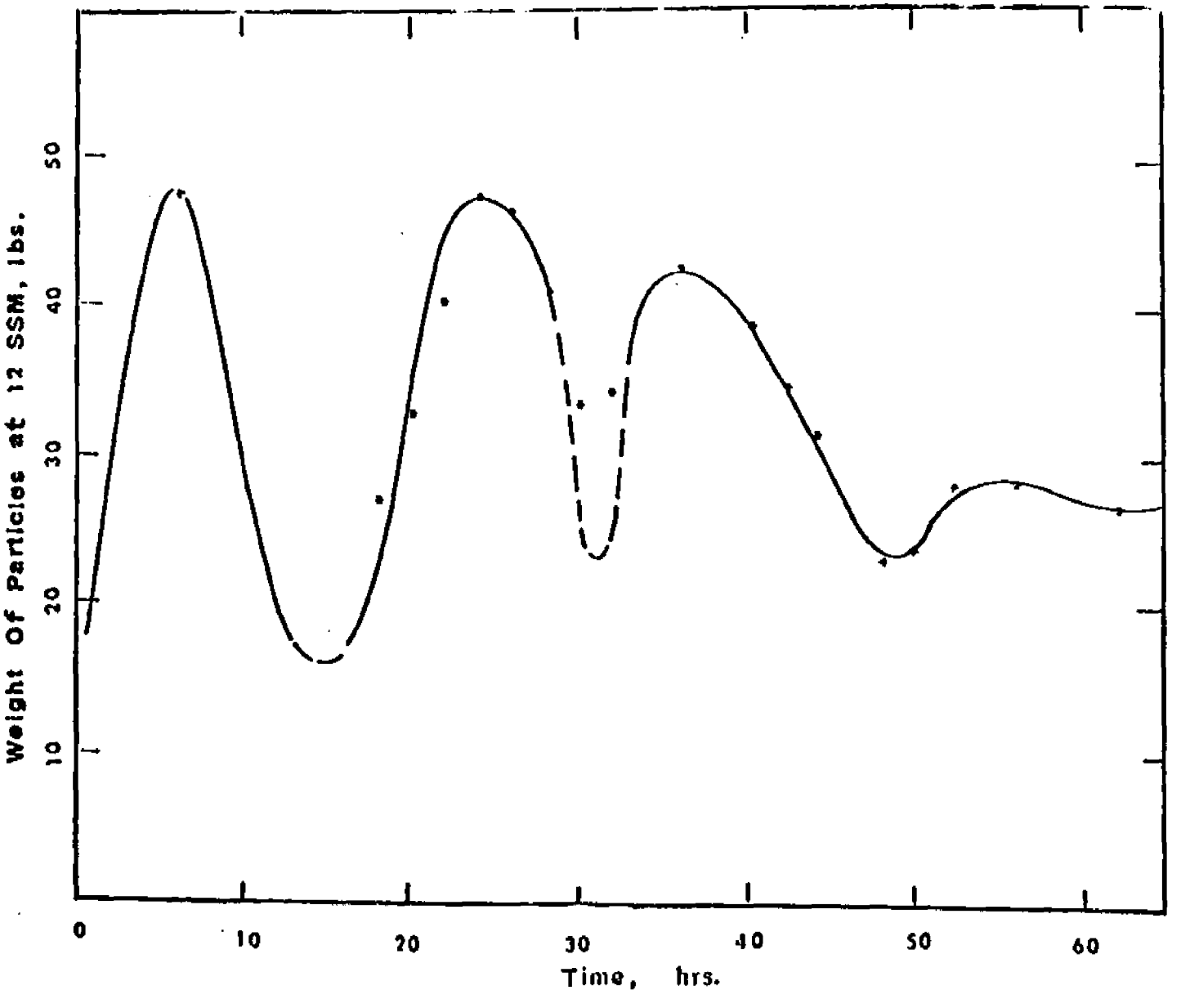

Figure 2 Cycling In A Continuous Crystallizer (Courtesy of Swenson Co.)

CHAPTER 2

Kinetic of Nucleation and Growth

In any analysis of crystallizer behavior the definition of the underlying kinetic regime is very important. We make here the following assumptions.

1. The crystallizer itself is ideally mixed and the product removed is a representative fraction of the dispersion inside the crystallizer.
2. The crystal growth rate is proportional to the supersaturation and is independent of particle size.

$$G(C) = k_g \cdot (C-C_s) \tag{2.1}$$

3. The nucleation rate B is a function of supersaturation alone. For most cases the form suggested by Mier, will be adopted:

$$B(C) = k_b \ (C-C_m)^n \tag{2.2}$$

where C_m is some critical concentration level higher than the saturation concentration C_s, and n is an exponent, $n \geq 1$.

If one limits oneself to a narrow range of growth rates then it is often possible to express this dependence as a simple power law [8]. We might note at this point that all our results

depend very strongly on Assumption 1, but that much of the mathematical analysis is independent of the particular rate expressions embodied in Assumption 2 and 3.

These three are of course strong simplifying assumptions. ref. [1,6,7,8] show that even simple mixed crystallizers give size distributions which strongly differ from those predicted by Assumption 1 and 2 (Assumption 3 has no effect on the steady state size distribution). On the other hand the problem is already very difficult in its simple form and it was shown in ref.[15] that if the growth rate is slightly nonlinear or size dependent this does not effect the basic results of the stability analysis.

The most critical assumption is the form of the dependence of nucleation rate on supersaturation or on growth rate. In a real crystallizer nucleation occurs mostly by secondary nucleation and often by attrition. While these depend on the moments of the size distribution the dependence is weak and for stability purposes there is some justification to express the nucleation rate as a function of supersaturation (or growth rate) only.

Basically we distinguish two cases of interest for crystallizers with fines traps, the first in which the nucleation sensitivity parameter (b/g) (which is equivalent to the exponent in the local approximation of ref.8) is low, and therefore the

size is insensitive to residence time. Control of particle size is only possible by a fines trap. The second case deals with crystallizers with high values of b/g under practical conditions. Equation (2.2) allows one to approximate both cases and the general results can be applied to any case for which the kinetics is known. To illustrate this, LnB is plotted versus LnG in figure 3 for equation (2.2) and as well for a Volmer relation.

Figure 3 Nucleation Kinetics

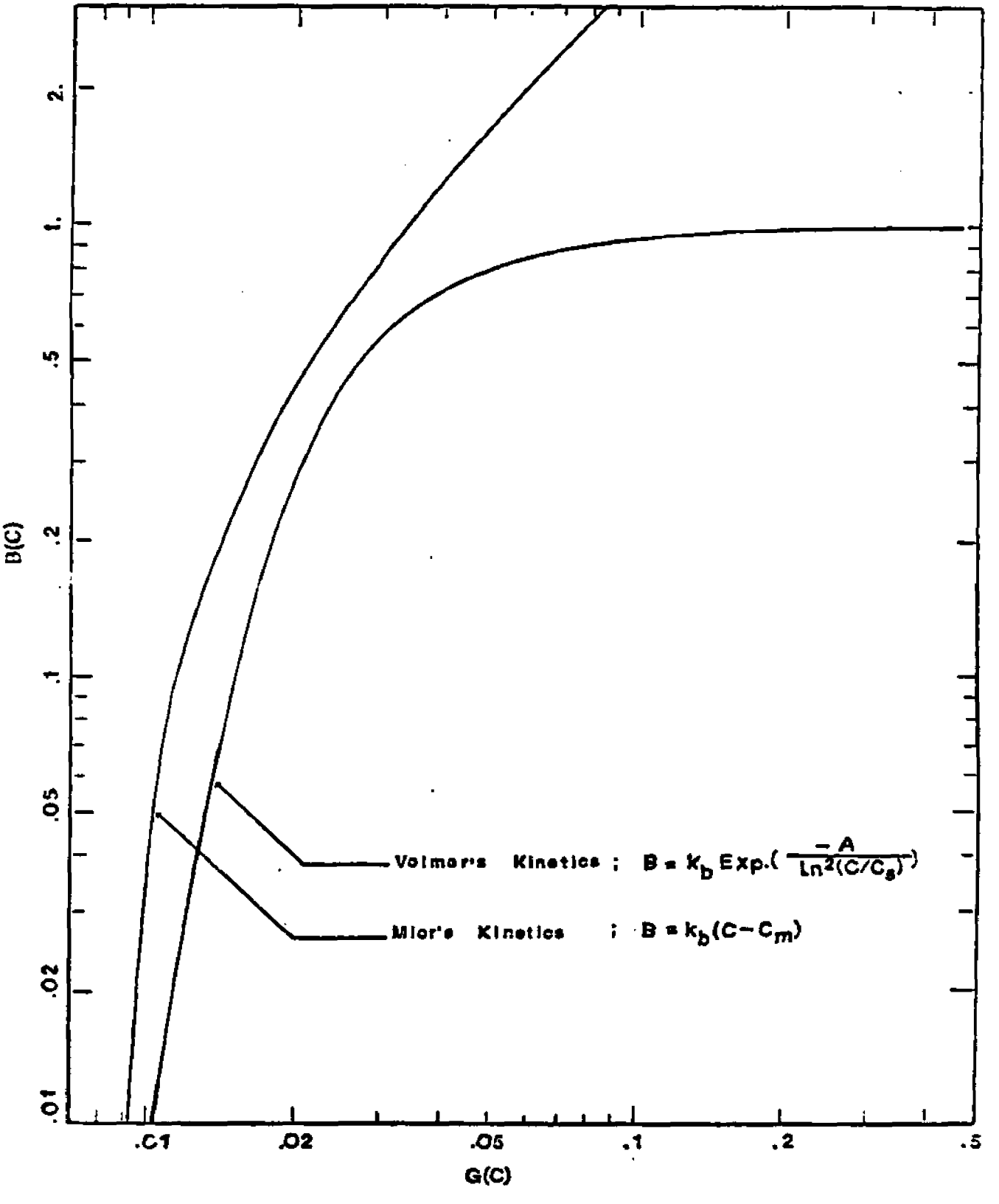

CHAPTER 3

Steady State Relationships

In this chapter, we set down the basic differential equations for a continuous crystallizer with fines trap and find their steady state solution. The results are illustrated by numerical examples based on the kinetics of equations (2.1) and (2.2).

The crystals in the system are assumed to be geometrically similar solids; "r" is used as a characteristic linear dimension for the solid. The growth kinetics of (2.1) are taken to apply to this linear dimension r, so that while a particle is in the system, $dr/dt = G$. A crystal of size r is taken to have volume kr^3, the parameter k serving as a particle shape factor. The dispersion in the crystallizer we characterize by a number density $f(r,t)$; that is, $f(r,t)\,dr$ is, at time t, the number of crystals per unit working volume of the crystallizer with sizes in the range r, r+dr. The fraction of the working volume occupied by solid is then $k\int_0^\infty r^3 \cdot f \cdot dr$, and the liquid fraction is accordingly

$$\epsilon(t) = 1 - k\int_0^\infty r^3 \cdot f(r,t)dr \qquad (3.1)$$

The nucleation kinetics of (2.2) we take to hold in this liquid volume only, so that, per unit working volume of the crystallizer, ϵB is the number of crystals formed per unit time; these nuclei are all taken to be of vanishingly small size. The kinetic

functions B and G are recognized as depending on the solute concentration C(t).

Now, from the schematic in fig. 1, we see that we may set down immediately an overall material balance on the system without taking explicit account of the fines trap operation:

$$\frac{d}{dt}\left\{\varepsilon \cdot C + (1-\varepsilon)\cdot \rho\right\} = \frac{1}{\theta} C_i - \frac{1}{\theta}\left\{\varepsilon \cdot C + (1-\varepsilon)\rho\right\} \qquad (3.2)$$

Here, $\theta = v/w$ is the mean residence time of material in the unit, C_i is the inlet solute concentration, and ρ is the true crystal density. The feed to the crystallizer is taken to be clear liquid.

Describing the operation of the fines trap calls for the introduction of another characteristic time $\theta_o = v/w_o$ to stand alongside the mean residence time θ. The quantity $1/\theta_o$ may be interpreted as a (probability) rate at which particles are circulated through the fines trap: that is, dt/θ_o represents the fraction of particles circulated through the fines trap in a (short) time dt. A balance on particles of size r may accordingly be written in the form:

$$\frac{\partial f}{\partial t} + G(c).\frac{\partial f}{\partial r} = \varepsilon \cdot B(c).\delta(r) - \frac{1}{\theta}.f - \frac{1}{\theta_o}.\eta(r).f \qquad (3.3)$$

The three terms on the right hand side of (3.3) represent respectively the formation of new crystals, the removal of crystal pro-

duct, and the destruction of crystals in the fines trap. The function $\eta(r)$ represents a selection curve for fines destruction. We take it in the form:

$$\eta(r) = h(r/r_o) = \begin{cases} 1 & ; \text{ for } r<r_o \\ o & ; \text{ for } r>r_o \end{cases} \tag{3.4}$$

where r_o is a critical size for fines destruction.

The $\delta(r)$ function in the nucleation term of (3.3) represents the understanding that all new crystals are formed at size r=0. mathematically speaking, this term has the force of a boundary condition (at r=0) for the partial differential equation (3.3). We recognize accordingly that (3.3) can, so to speak, be expanded out into the more explicit form;

$$\begin{cases} G(c)\cdot f(0,t) = \epsilon(t)\cdot B(c) & r = 0 \\ \dfrac{\partial f}{\partial t} + G(c)\dfrac{\partial f}{\partial r} = -\dfrac{1}{\theta}\cdot f(r,t) - \dfrac{1}{\Omega_o}\cdot\eta(r)\cdot f(r,t) & r > 0 \end{cases} \tag{3.3a}$$

The equations (3.1-3.3) form a self-contained system for the determination of the solute concentration C(t) and the particle number density f(r.t). Besides the underlying assumptions about the nature of the kinetic regime discussed in the preceding section, their validity depends on two further assumptions. First,

we note, we take the system to be isothermal; the temperature does not appear explicitly, and there is no need to set down energy balances. Also, we neglect volume changes on crystallization, so that the system in fact operates at fixed volume v, with a common flow rate w in and out of the crystallizer, and a common flow rate w_o in and out of the fines trap. (The fines are redissolved in the destruction unit, not mechanically removed from the system). The flow rates may of course change with time, and this change will be reflected in θ and θ_o .

We turn now to a consideration of the steady-state solutions of the basic equation (3.1-3.3). This offers no special difficulties, the ordinary differential equation (3.2) reducing to an algebraic equation, and the partial differential equation (3.3) reducing to an ordinary differential equation. The solution to this ordinary differential equation in f(r) is

$$f(r) = \epsilon \frac{B}{G} \cdot \exp. \left\{ - \frac{r}{\theta G} - \frac{1}{\theta_o G} \int_o^r \eta(s)ds \right\} \qquad r \geqslant 0 \quad (3.5)$$

Here, B and G are to be evaluated for the steady-state concentration C, but we do not show this functional dependence explicitly. Bringing (3.5) to (3.1) give an explicit formula for ϵ

$$\epsilon = \frac{1}{1 + k\frac{B}{G}\int_o^\infty r^3 \exp.\left\{-\frac{r}{\theta G} - \frac{1}{\theta_o G}\int_o^r \eta(s)ds\right\}dr} \qquad (3.6)$$

and bringing this expression for ϵ to the steady-state form of (3.2) gives

$$\frac{C_i - C}{\rho - C_i} = \frac{kB}{G}\int_o^\infty r^3 \exp.\left\{-\frac{r}{\theta G} - \frac{1}{\theta_o G}\int_o^r \eta(s)ds\right\}dr \qquad (3.7)$$

This is not an explicit formula for C, since B and G depend on C. One may see nevertheless that it is satisfied by only a single C since the left hand size is a decreasing function of C and the right hand side an increasing function (at least for any customary kinetics). Finally, from (3.5) we may evaluate the weight average crystal size

$$\bar{r} = \frac{\int_o^\infty r^4 \cdot f(r)dr}{\int_o^\infty r^3 \cdot f(r)dr}$$

in the crystallizer (and the product) as

$$\bar{r} = \frac{\int_o^\infty r^4 \exp.\left\{-\frac{r}{\theta G} - \frac{1}{\theta_o G}\int_o^r \eta(s)ds\right\}dr}{\int_o^\infty r^3 \exp\left\{-\frac{r}{\theta G} - \frac{1}{\theta_o G}\int_o^r \eta(s)ds\right\}dr} \qquad (3.8)$$

Equations (3.7) and (3.8) summarize important aspects of

the steady-state behavior of the crystallizer. Given a knowledge of the physical system (ρ,k), of the kinetics (B and G as functions of C), of the feed (C_i), and of the fines-trap operations (θ_o,η), these equations contain implicitly the dependence of G and B on C, and hence on each other. To make these dependencies as explicit as may be, we first rewrite (3.7) and (3.8), making suitable changes of variables in the integrals and taking account of the form of η in (3.4):

$$\begin{cases} \bar{r} = G\theta \cdot \dfrac{\nu_4}{\nu_3} \\ \dfrac{C_i - C}{\rho - C_i} = kBG^3\theta^4\nu_3 \end{cases} \tag{3.9}$$

with

$$\nu_n = \int_o^{\infty} X^n \exp\left\{-X - \frac{r_o}{\theta_o G}\int_o^{\theta GX/r_o} h(y)dy\right\}dx \tag{3.10}$$

These relationships can perhaps be seen more clearly in dimensionless form. We normalize the rate functions B and G on their values B_i and G_i for the feed concentration C_i; we normalize the particle sizes $\bar{r}$, r_o and the flow times θ, θ_o on suitable constructs of these same inlet kinetic values B_i, G_i. That is, we carry

$$\begin{cases} \theta \to \dfrac{\theta}{(kB_i G_i^3)^{1/4}}, \quad \theta_o \to \dfrac{\theta_o}{(kB_i G_i^3)^{1/4}} \\ \bar{r} \to \left(\dfrac{G_i}{kB_i}\right)^{1/4} \bar{r}, \quad r_o \to \left(\dfrac{G_i}{kB_i}\right)^{1/4} r_o \\ G \to G_i \mathcal{G}, \quad B \to B_i \mathcal{B} \end{cases} \tag{3.11}$$

These dimensionless variables will be used throughout the rest of this section. We recognize that, according to the linear growth kinetics of (2.1), the dimensionless G is simply

$$G = \frac{C - C_s}{C_i - C_s}$$

and so may serve as a dimensionless measure of the supersaturation. The concentration C may be expressed in terms of this G, and we may accordingly regard the nucleation rate B as also expressed in terms of G. Bringing all this to (3.9), we find

$$\begin{cases} \dfrac{1-G}{L-1} = BG^3\theta^4\nu_3 \\ \bar{r} = G\theta \dfrac{\nu_4}{\nu_3} \end{cases} \tag{3.12}$$

where $$L = \frac{\rho - C_s}{C_i - C_s}$$

The quantities ν_3 and ν_4 may still be taken from (3.10), since expressions of the form $\frac{r}{\theta G}$ remain unaltered by the scale changes (3.11)

This is about as far as the development can be carried in general. To develop from (3.12) some general quantitative feelings about the effect of the fines trap parameters θ_o, r_o on the crystallizer performance, we turn first to the important special case where the critical size r_o is, in a suitable sense, small. If r_o is very small as compared to the average particle size $\bar{r}$ the total mass contained in the distribution for all particles less than r_o is negligible. Furthermore, the time needed for a nucleus to grow to size r_o is very small as compared to θ. We can, therefore, with some justification assume that for very small values of $r_o/\bar{r}$, we may completely neglect the contribution of all particles less than r_o to the mass balance, and also assume that the destruction of nuclei in the fines trap is instantaneous. In mathematical terms, we implement these ideas by letting $r_o/G\theta \to 0$. Formally, the same result can be obtained by approximating η by $\eta(r) = r_o\delta(r)$ that is , approximating h, on consulting (3.4), by $h(y) = \delta(y)$ In any case, to this approximation

$$\nu_n = n!\ \exp.\ \left(-\frac{r_o}{\theta_o G}\right) \qquad (3.13)$$

and the equations (3.12) can be solved in turn for θ and $\bar{r}$ in terms of G to give

$$\begin{cases} \theta = \left\{ \dfrac{1}{6(L-1)} \cdot \dfrac{1-G}{BG^3} \cdot \exp.\left(\dfrac{r_o}{\theta_o G} \right) \right\}^{1/4} \\ \bar{r} = \left\{ \dfrac{256}{6(L-1)} \cdot \dfrac{G(1-G)}{B} \cdot \exp.\left(\dfrac{r_o}{\theta_o G} \right) \right\}^{1/4} \end{cases} \tag{3.14}$$

It will be convenient to have a form of words for this small r_o approximation, and we shall say that (3.14) describes the behavior of a point fines trap, while the general equations (3.12) and (3.10) describe the behavior of a finite fines trap. We see from (3.14) that the point fines trap approximation amounts simply to replacing the actual nucleation rate B by an effective nucleation rate B exp. $(-r_o/\theta_o G)$ which depend explicity on the growth rate G. Thus 1 - exp.$(-r_o/\theta_o G)$ represents the fraction of nuclei destroyed in the fines trap. This interpretation is quite consistent with the intuitive ideas about the smallness of r_o noted above. While r_o/G, the time a nucleus needs to grow to size r_o, is small with respect to the mean residence time θ, it is finite with respect to the much smaller mean recirculation time θ_o. Indeed, for small r_o, the ratio r_o/θ_o completely characterizes the operation of the fines trap.

The dimensionless equation (3.14) may be regarded as the parametric representation of $\bar{r}$-θ curves for a crystallizer with point fines trap. To this approximation, as noted above, the two fines trap parameters r_o, θ_o merge into a single parameter r_o/θ_o, and each choice of r_o/θ_o leads to an $\bar{r}$-θ curve. The dimensionless growth rate G serves as the parameter in the parametric representation of these curves, and to make all complete we need to express B in terms of G. This can readily be done, and for the nucleation kinetics of (1.2), we find for the dimensionless B.

$$B = \left(\frac{G-M}{1-M}\right)^n \quad ; \quad n > 1 \tag{3.15}$$

where

$$M = \frac{C_m - C_s}{C_i - C_s}$$

Fig. 4 shows a family of these curves with L=5, M=1/400, n=1. We see from these curves how, for a given θ, $\bar{r}$ increases with the fines trap operating parameters r_o/θ_o. Since $r=4G\theta$, this increase of $\bar{r}$ with r_o/θ_o reflects a corresponding increase in the supersaturation. We see further from these curves how a given product size $\bar{r}$ can be attained in many different ways, by playing off θ against r_o/θ_o. The stability curves superimposed on fig.4, and on figs. 5,6,7 following, will be developed in the next chapter of this thesis, and we defer a discussion of them until that time.

The dimensionless equation (3.14) for a point fines trap may also be examined from a somewhat different point of view. That is, we may regard

$$\lambda = \frac{r_o}{\theta_o G} \tag{3.16}$$

as a single parameter descirbing the fines trap operation, in place of r_o/θ_o. This serves as a design rather than as an operating parameter for the fines trap, since in operation its value depends on the supersaturation actually attained in the crystallizer. A choice of λ thus represents a design decision to destroy a fraction $1-e^{-\lambda}$ of the nuclei formed. Bringing (3.16) to (3.14) accordingly gives the parametric representation of a family of $\bar{r} - \theta$ curves

$$\begin{cases} \theta = \left\{ \dfrac{1}{6(L-1)} \cdot \dfrac{1-G}{BG^3} \cdot e^{\lambda} \right\}^{1/4} \\ \\ \bar{r} = \left\{ \dfrac{256}{6(L-1)} \cdot \dfrac{G(1-G)}{B} \cdot e^{\lambda} \right\}^{1/4} \end{cases} \tag{3.17}$$

that we may interpret as design curves for a crystallizer with point fines trap. A family of these curves is shown in fig. 5, with the nucleation kinetics of (3.15), and the same values of L, M, n, as in fig. 4. These curves show the same general behavior as those of fig. 4. (Equivalent results for power law kinetics are given in ref. 10).

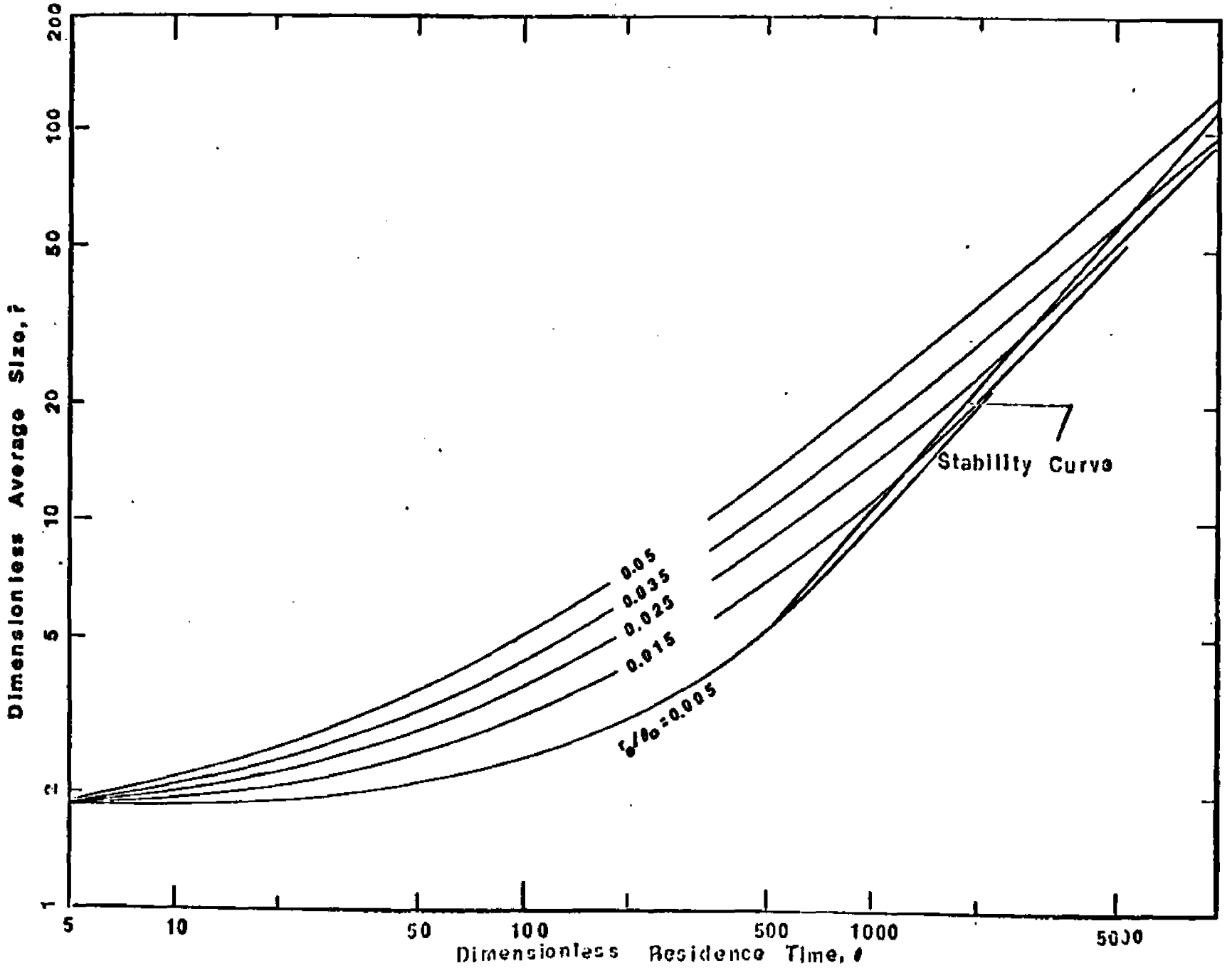

Figure 4 Illustrative Operating Curves For A Crystallizer With Point Fines Trap

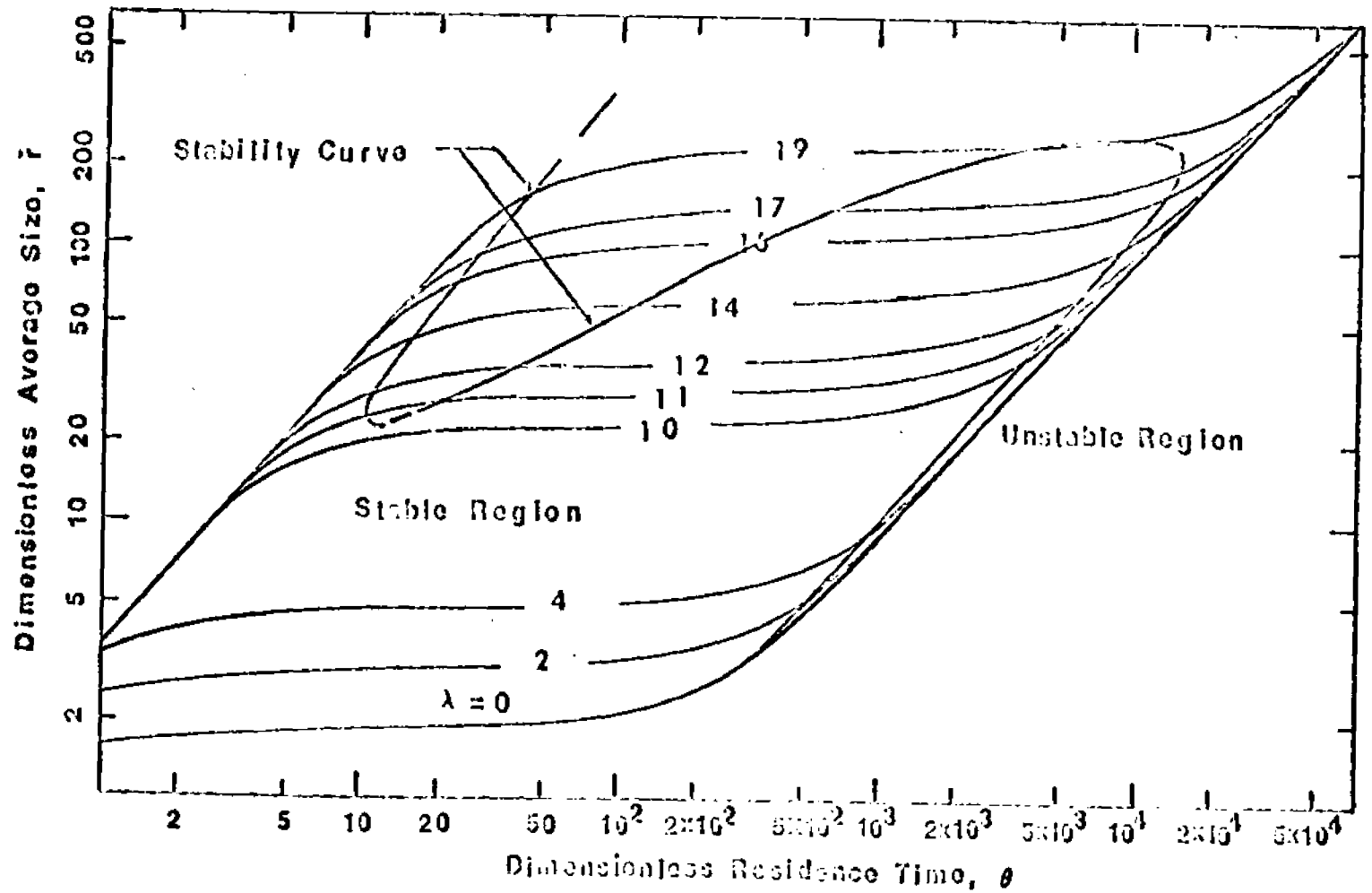

Figure 5 Illustrative Design Curves For A Crystallizer With Point Fines Trap

We turn next to a consideration of how the general character of the curves of figs. 4 and 5 is affected by relaxing the small r_o assumption that leads to a point fines trap. We shall not make this analysis in great detail, but simply illustrate the effects by showing some typical cases. To see this we bring (3.16) to (3.10), and write

$$\nu_n = \int_o^\infty x^n . \exp. \left\{ -x - \lambda \int_o^{x/r^*} h(y)dy \right\} dx \tag{3.18}$$

where we have set

$$\frac{r_o}{\theta G} = r^* \tag{3.19}$$

We note that $r^* \to o$ for the point fines trap. With r^* as a free parameter in place of r_o, the quantities ν_n no longer depend on θ, and we may solve the equations (3.10) for θ and F directly in terms of θ:

$$\begin{cases} \theta = \left\{ \frac{1}{L-1} \cdot \frac{1-\theta}{\theta G^3} \cdot \frac{1}{\nu_3} \right\}^{1/4} \\ \tilde{r} = \left\{ \frac{1}{L-1} \cdot \frac{\theta(1-\theta)}{\theta} \cdot \frac{\nu_4^4}{\nu_3^5} \right\}^{1/4} \end{cases} \tag{3.20}$$

The equations (3.20) and (3.18) thus give the finite fines trap behavior corresponding to the point fines trap equations (3.17).

Fig. 6 shows the results of some typical calculations. We see there how the behavior of the system varies with λ for a fixed r^*. The plots are made with the nucleation kinetics (3.15), and the same values of L, M, n, as in figs. 4 and 5.

We may note finally that the general monotone character of the curves of figs. 4 and 5 does not depend on the particular numerical values chosen there for illustration. As long as we stay with the nucleation kinetics (3.15) that correspond to (2.2), $\bar{r}$ will increase steadily with θ on each curve, and the general configuration will be as shown. This will also be the case if the nucleation rate is a simple power of the supersaturation, in our dimensionless variables, if $B=G^n$ with $n > 1$. But it need not be true for other common forms in which one descirbes the nucleation rate. With Volmer kinetics, for example, where we have for the nucleation rate in its customary physical units

$$B = K_b \exp. \left(\frac{-A}{L^2 (C/C_s)} \right) \tag{3.21}$$

we may for suitable choices of parameters find a downturn in the $\bar{r}$ - θ curve followed by a later upswing.

In terms of our dimensionless variables, the nucleation kinetics (3.21) may be written

Figure 6 Design Curves For A Crystallizer With Finite Fines Trap

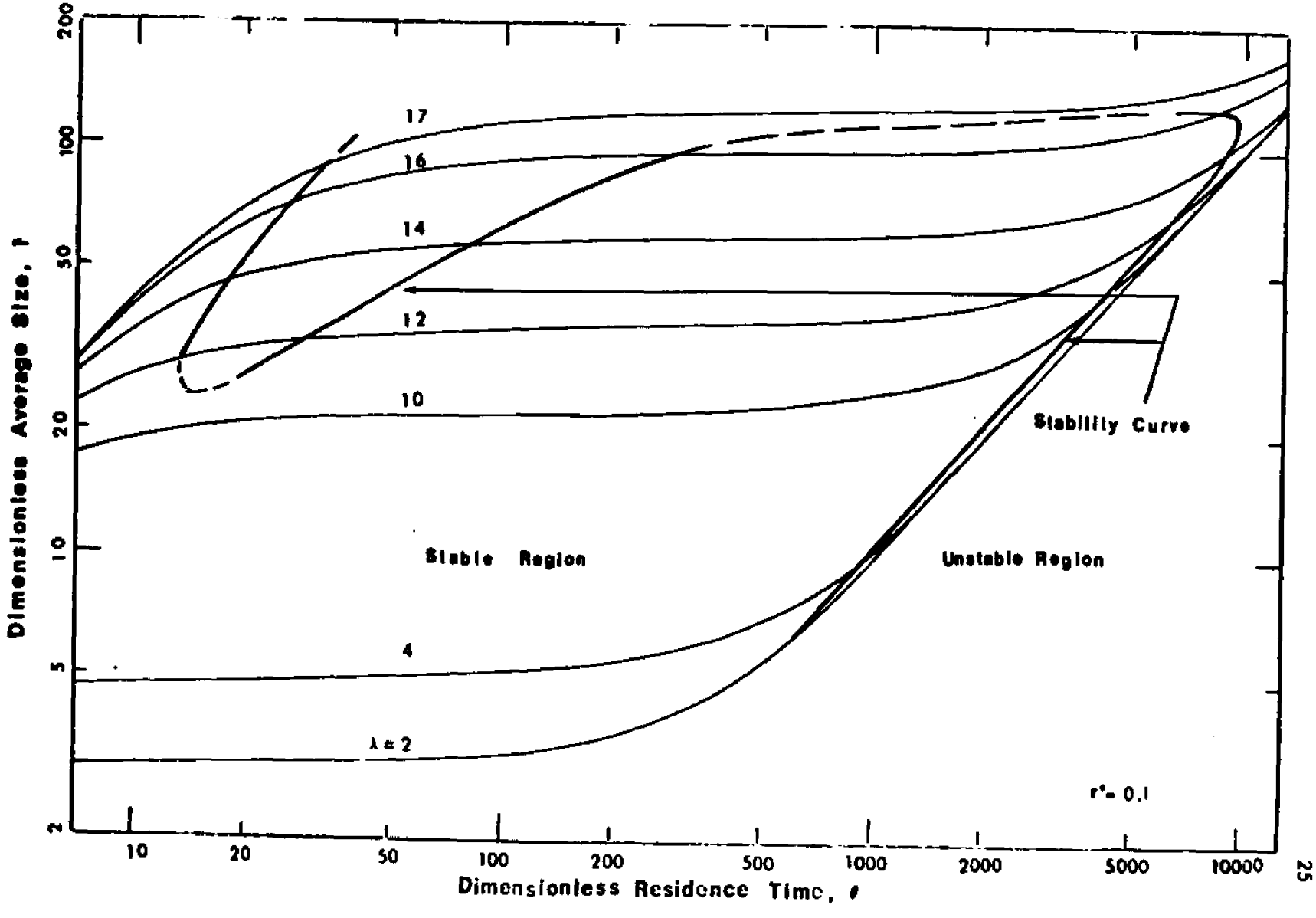

$$B = \exp.\left\{\frac{A}{Ln^2(1+S)} - \frac{A}{Ln^2(1+SG)}\right\} \tag{3.22}$$

where

$$S = \frac{C_i - C_s}{C_s}$$

Fig. 7 shows an $\bar{r}$ - θ plot for a point fines trap with the nucleation kinetics (3.22) for various λ for comparison with fig. 5. All the curves are for L=5, S=1, $A=5\times10^{-3}$. The existence of the local maxima and minima in these curves depends on the particular values of the parameters chosen, and the curves can be made monotone by taking, for example, a somewhat larger value of A.

This phenomenon of $\bar{r}$ falling as θ increases over a suitable range is not particularly a question of fines trap operation but rather of the form of the nucleation kinetics. It may be observed for a simple mixed crystallizer, and indeed, taking $r_o/\theta_o=0$ in (3.14) or $\lambda=0$ in (3.17), or, more generally, $h(y)=0$ in (3.10) and (3.12), leads to a common set of equations.

$$\begin{cases} \theta \left\{\frac{1}{6(L-1)} \cdot \frac{1-G}{G^3 B}\right\}^{1/4} \\ \bar{r} = \left\{\frac{256}{6(L-1)} \cdot \frac{G(1-G)}{B}\right\}^{1/4} \end{cases} \tag{3.23}$$

describing the behavior of a mixed crystallier without fines

Figure 7 Characteristic Curves For A Crystallizer With Point Fines Trap For Volmer's Kinetics

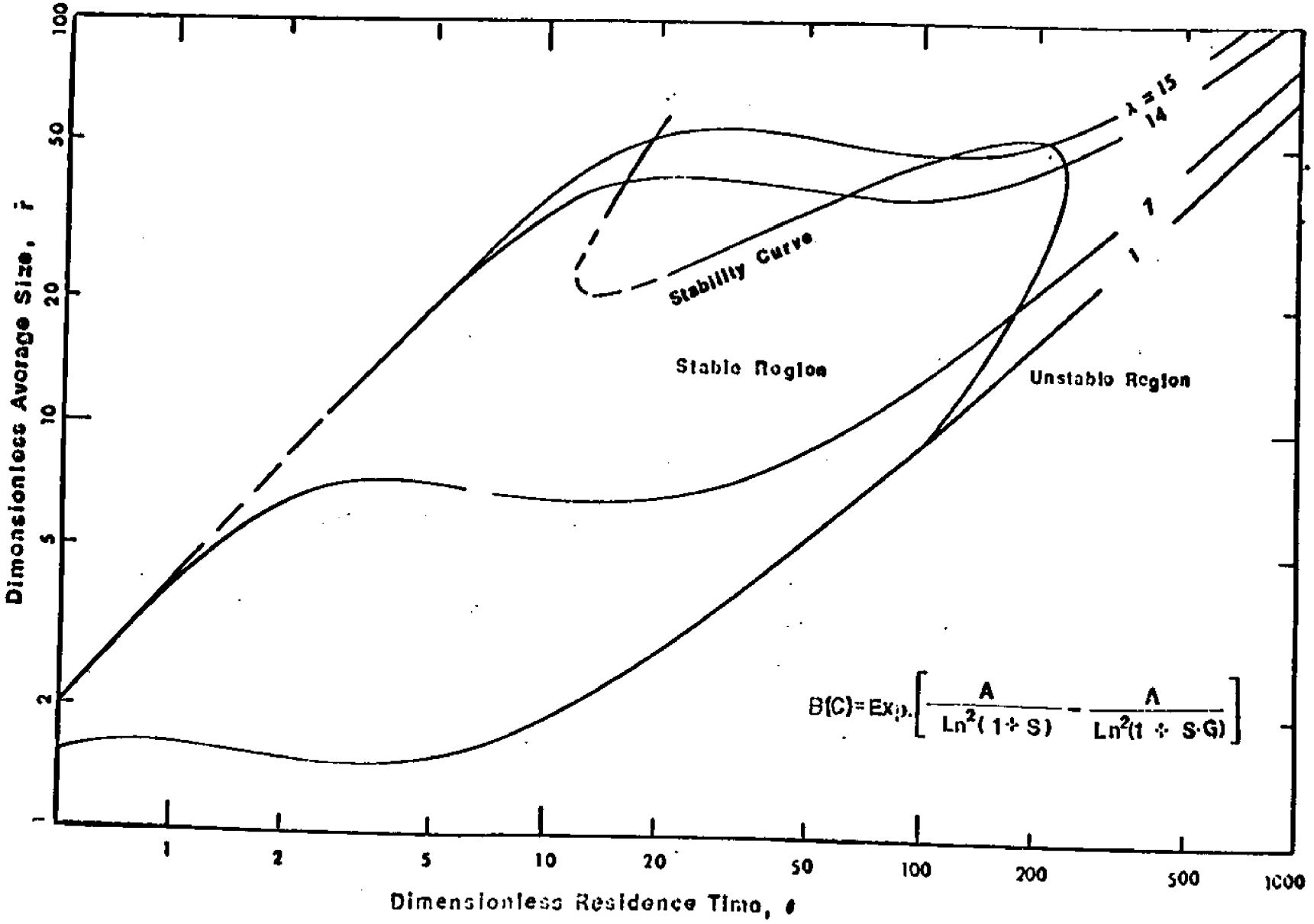

trap. Curves based on (3.23) show the same behavior. The existence of regions in which $\bar{r}$ decreases as θ increases has been predicted [8] for certain kinds of power law kinetics (with exponent<1), and has in fact been observed in practice [3] .

One can also use figures 4 - 7 to understand the effect of fines trap on crystallizers with power law kinetics. Eqn.(3.15) for $G \gg M$ reduces to $B = G^n$, and for this case b/g will be equal to n. (The sensitivity parameters b and g will be defined in Eqn.(4.10)) For our example n = 1, and one would therefore expect (ref. 8) that for $G \gg M$ particle size becomes independent of θ, which in our example is true for $\theta < 100$. For large θ, the supersaturation becomes small and approaches asymptotically the metastable limit. b/g increases without bound. For high values of θ, all the curves $\bar{r}(\theta)$, have a linear asymptote $\bar{r} = 4G\theta$. Similar considerations hold for the Volmer model for very high supersaturations. B becomes independent of G and therefore $\bar{r}$ decreases with increasing θ. At high values of θ the supersaturation drops and one again notes that equation (1.2) appraximates the basic behavior of the Volmer relation very well. Now in the region of high supersaturation, introducing a point fines trap changes the dependence of the effective nucleation rate B_{eff} on G as the probability of a nucleus surviving till r_o, depends on G. We note therefore that at constant fines trap setting (constant r_o/θ_o), $\bar{r}$ is now a function of

θ. It is hard to express this new dependence as a power law as in this case

$$(b/g)_{eff} = \frac{d\ \ln B_{eff}}{d\ \ln G} = (b/g)_{r_o = 0} + r_o/r\theta$$

CHAPTER 4

Linearized Stability Analysis

In this chapter, we develop stability criteria for the operation of a continuous crystallizer with fines trap. The results are expressed in terms of suitable dimensionless parameters characterizing the steady-state operation point under study, and applied to the steady-state operating and design curves developed in the preceding section. Mathematically speaking, the methods are entirely those of linear analysis.

Our starting point here is the basic set of differential equations (3.1-3.3), with the variables all in their customary physical units. It is convenient to rewrite them in terms of a total solute-crystal resource function:

$$\varphi(t) = \epsilon(t)\cdot C(t) + (1-\epsilon(t))\cdot\rho \tag{4.1}$$

so that, consulting (3.1),

$$C = \frac{\varphi - \rho\cdot k\cdot\int_0^\infty r^3\cdot f\cdot dr}{1 - k\int_0^\infty r^3 f\cdot dr} \tag{4.2}$$

and the equations (3.2,3.3) give in turn

$$\frac{d\varphi}{dt} = \frac{1}{\theta}\,(C_i-\varphi) \tag{4.3}$$

$$\begin{cases} G(c)\cdot f = (1-k\int_0^\infty r^3 f)\cdot B(c) & ; \quad r = 0 \\ \dfrac{\partial f}{\partial t} + G\,\dfrac{\partial f}{\partial r} = -\dfrac{1}{\theta}\cdot f - \dfrac{1}{\theta_o}\cdot\eta(r)\cdot f & ; \quad r > 0 \end{cases} \tag{4.4}$$

We now linearize the equations (4.2-4.4) about the steady-state solution of the preceding section. That is, we carry

$$\omega(t) \Longrightarrow \varphi + \delta\omega(t)$$

$$C(t) \Longrightarrow C + \delta C(t)$$

$$f(r,t) \Longrightarrow f(r) + \delta f(r,t)$$

where C and f(r) are given in equations (3.5-3.7) and the corresponding φ by (4.1). The functions $\delta\omega$, δC and δf are regarded as small perturbations, so that their squares and products may be neglected. The details are tedious, but straightforward, and we omit them here. The variable δC can be eliminated altogether by consulting the linearized form of (4.2), and we are left with

$$\frac{d(\delta\varphi)}{dt} + \frac{1}{\theta} \cdot \delta\varphi = 0 \tag{4.5}$$

from (4.3), and

$$\begin{cases} G\cdot\delta f + \left\{1 + (\rho - c)\left(\frac{B'}{B} - \frac{G'}{G}\right)\right\} B\cdot k\int_0^\infty r^3 \delta f \\ \qquad = \left(\frac{B'}{B} - \frac{G'}{G}\right) B\cdot\delta\varphi \quad ; \quad r = 0 \\ \\ \frac{\partial(\delta f)}{\partial t} + G\,\frac{\partial(\delta f)}{\partial r} + \left(\frac{1}{\theta} + \frac{\eta}{\theta_o}\right)\cdot \delta f \\ + \left(\frac{1}{\theta} + \frac{\eta}{\theta_o}\right)\cdot \mathrm{Exp.}\left(-\frac{r}{\theta\cdot G} - \frac{1}{\theta_o G}\int_0^r \eta\right)(\rho - C)\frac{G'}{G}\cdot\frac{B}{G}\, k\int_0^\infty r^3\delta f \\ \qquad = \left(\frac{1}{\theta} + \frac{\eta}{\theta_o}\right) e^{-\frac{r}{\theta G} - \frac{1}{\theta_o G}\int_0^r \eta} \frac{G'}{G}\,\frac{B}{G}\,\delta\varphi \quad ; \quad r > 0 \end{cases} \tag{4.6}$$

from (4.4). Here B and G are the values of the nucleation and growth rates at the steady-state under study, and B' and G' the values of their derivative (with respect to the concentration C) at this steady state.

It is convenient at this point to introduce dimensionless variables into (4.5, 4.6). We carry

$$\begin{cases} t \longrightarrow \theta t \\ r \longrightarrow \theta G r \\ \delta f \longrightarrow \epsilon \frac{B}{G} \delta f \\ \delta\varphi \longrightarrow 6k\epsilon \frac{B}{G} \cdot (G\theta)^4 \cdot (\rho - C) \cdot \delta\varphi \end{cases} \tag{4.7}$$

where the quantities C, ϵ, B, G are evaluated for the steady-state under study. We may note a difference between this scaling and that made in (3.11) for the analysis of steady-state behavior; here quantities are scaled in terms of the steady state being studied, there, in terms of feed parameters. At any rate, the dimensionless variables of (4.7), will be used throughout the remaineder of this chapter. And in terms of them, we have

$$\frac{d(\delta\varphi)}{dt} + \delta\varphi = 0 \tag{4.8}$$

from (4.5), and

$$\begin{cases} \delta f + (b-g)\int_0^\infty \frac{r^3}{6} \cdot \delta f = (b-g-\alpha)\delta\varphi \quad ; \quad r = 0 \\ \frac{\partial(\delta f)}{\partial t} + \frac{\partial(\delta f)}{\partial r} + (1+R\cdot\eta)\cdot\delta f + g(1+R\eta)e^{-r-R\int_0^r \eta} \int_0^\infty \frac{r^3}{6}\delta f \\ \qquad = g(1+R\cdot\eta)e^{-r-R\int_0^r \eta} \cdot \delta\varphi \quad ; \quad r > 0 \end{cases} \tag{4.9}$$

In the dimensionless form given by the equations (4.8,4.9), the linearized behavior of the crystallizer with fines trap depends on a number of dimensionless parameters. We have for the system overall the nucleation and growth rate sensitivity parameters

$$\begin{cases} b = 6kBG^3\theta^4 \left\{ 1 + (\rho - C)\frac{B'}{B} \right\} \\ g = 6kBG^3\theta^4(\rho - C)\frac{G'}{G} \end{cases} \tag{4.10}$$

as well as the auxiliary parameter

$$\alpha = 6kBG^3\rho^4$$

(which will not in fact appear in the stability conditions to be developed). For the fines trap itself, we have the recirculation ratio

$$R = \frac{\theta}{\theta_o} = \frac{W_o}{W} \tag{4.11}$$

and the knowledge of the critical fines destruction size contained in the selection curve $\eta(r)$. (This last will be brought out explicitly a little bit later).

Our stability analysis for the system is based on the equations (4.8,4.9). We carry it out here by a formal spectral (eight-value) analysis, which we feel is free of some of the ambiguities of the customary Laplace transform methods. Since these spectral methods may be of some interest in related problems, we lay them out for equations (4.8,4.9) in Appendix I, and simply quote the results here. The upshot of the argument is that the characteristic equation for (4.8,4.9) is given by

$$1 + (b-g)\,H(s) + g\cdot K(s) = 0 \tag{4.12}$$

with

$$H(s) = \int_0^{\infty} \frac{r}{6}^3 \cdot \exp.\left\{ -(s+1)r - R\int_0^r \eta(x)dx \right\} dr$$

$$K(s) = \int_0^{\infty} \frac{r}{6}^3 \exp.\left\{-(s+1)r - R\int_0^r \eta(x)dx\right\} \cdot \left[\frac{e^{sr}-1}{s}\right. \tag{4.13}$$

$$\left. + R\int_0^r \eta(y)e^{sy}dy\right].dr$$

The characteristic equation (4.12) determines formally the eigenvalues S associated with the system (4.8,4.9) and the stability condition for the system is accordingly that all the roots of (4.12) have negative real parts.

We now introduce explicitly the dependence of η on the critical fines destruction size r_o. Accordingly to (3.4), $\eta(r)=h(r/r_o)$ where r and r_o are in their ordinary physical units.

If r is taken in the dimensionless form given by (4.7), then r must be so taken also. That is, r_o must be replaced by $r_o/\theta G$. But this is simply the r* of (3.19), and in the dimensionless variables of (4.7), we accordingly set

$$\eta(r) = h(r/r^*)$$

where

$$h(x) = \begin{cases} 1 & ; \quad x < 1 \\ 0 & ; \quad x > 1 \end{cases} \tag{4.14}$$

We note from (4.11) and (3.19) that

$$Rr^* = \lambda \tag{4.15}$$

the parameter introduced in (3.16) to characterize the steady-state operation of the fines trap. The functions H and K of (4.13) may now be written

$$\begin{aligned} H(s) &= \int_o^\infty \frac{r^3}{6} \exp.\left\{-(s+1)r - \lambda \int_o^{r/r^*} h(x)dx\right\} dr \\ K(s) &= \int_o^\infty \frac{r^3}{6} \exp.\left\{-(s+1)r - \lambda \int_o^{r/r^*} h(x)dx\right\} \\ &\quad \cdot \left(\frac{e^{sr}-1}{s} + \lambda \int_o^{r/r^*} h(y)e^{syr^*} dy\right) dr \end{aligned} \tag{4.16}$$

While in (4.16), the fines trap is described in terms of the parameters λ and r*, we see from (4.15) that any two of the three parameters R, r*, λ could equally well be used.

The form of H and K in (4.16) is not especially transparent, and to develop some quantitative feeling about the stability

condition based on (4.12), we turn first, as in the steady-state studies of the preceding section, to the important special case of the point fines trap. We let $r \to 0$ in (4.16), keeping λ fixed; from (4.15), we see that R must $\to \infty$ The functions H and K become simple rational functions of s, and the characteristic equation (4.12) reduces to

$$s^4 + (4+ge^{-\lambda})s^3 + (6+4ge^{-\lambda})s^2$$

$$+ (4+6ge^{-\lambda})s + 1+3ge^{-\lambda} + (b+\lambda g)e^{-\lambda} = 0 \qquad (4.17)$$

The polynomial character of (4.17) makes matters especially simple, and a straightforward application of the Routh-Hurwitz criterion shows that the system will be stable provided only that

$$g > -4e^{\lambda}$$

(which will of course always be satisfied), and further that

$$b < \frac{(21-\lambda)g^3+(87-8\lambda)e^{\lambda}g^2+(128-16\lambda)e^{2\lambda}g+64e^{3\lambda}}{(g+4e^{\lambda})^2} \qquad (4.18)$$

By introducing a function σ to represent the stable limit

$$\sigma(g) = \frac{21g^3+87g^2+128g+64}{(g+4)^2} \qquad (4.19)$$

we may rewrite the stability condition (4.18) in a form that shows more clearly the natural groupings of the crystallizer

parameters

$$(b+\lambda g)e^{-\lambda} < \sigma(ge^{-\lambda}) \tag{4.20}$$

The stability condition (4.20) is shown graphically in fig. 8. We may note that on setting $\lambda = 0$ we recover the stability condition for a mixed crystallizer without fines trap, since in (4.16), setting $\lambda = 0$ is entirely equivalent to setting h, that is η, identically = 0. While fig. 8 embodies the general stability condition for a crystallizer with point fines trap, it may be useful for certain working purposes to replot it in a somewhat more explicit form. We see from (4.18) that just on the verge of instability, b/g has a limiting value = $21 - \lambda$ as $g \uparrow \infty$, so that the larger we take λ (the more fines we destroy), the smaller we must take b/g to ensure stable operation. The approach to this limiting value is not uniform; that is, the larger we take λ, the larger we must take g to approximate the limiting behavior of b/g. This whole state of affairs is shown graphically in fig. 9.

The stability curves overlying the steady-state characteristic curves of figs. 4,5 and 7 for a crystallizer with point fines trap may be developed directly from the foregoing stability conditions. In plotting the curves of (3.14) to give

fig. 4, or those of (3.17) to give fig. 5, it is only necessary, for each value of the parameter G, to compute the sensitivity parameters b and g of (4.10), and consult the stability condition of (4.18) or (4.20). These sensitivitly parameters can be directly expressed in terms of the dimensionless quantities of the preceding section. For the Mier nucleation kinetics of (3.15), we have

$$\begin{cases} b = 6\left(\frac{G-M}{1-M}\right)^n G^3 \theta^4 \left(1+n \frac{L-G}{G-M}\right) \\ g = 6\left(\frac{G-M}{1-M}\right)^n G^3 \theta^4 \frac{L-G}{G} \end{cases}$$

where G and θ are the dimensionless quantities of (3.11), and L is the dimensionless parameter introduced in (3.12). In the curves of equation (3.14) that lead to fig. 4, λ must be computed as $r_o/\theta_o G$ for each choice of G in order to enter the stability condition. In the curves of equation (3.17) that lead to fig. 5, λ already appears explicitly. Similar considerations apply for the Volmer kinetics on which the curves of fig. 7 are based.

Re-examining the steady-state curves of figs. 4 and 5 in the light of these superimposed stability conditions shows how a fines trap may permit the stabilizing of a crystallizer operation without sacrificing product quality.

Figure 8 General Stability Condition For A Crystallizer With Point Fines Trap

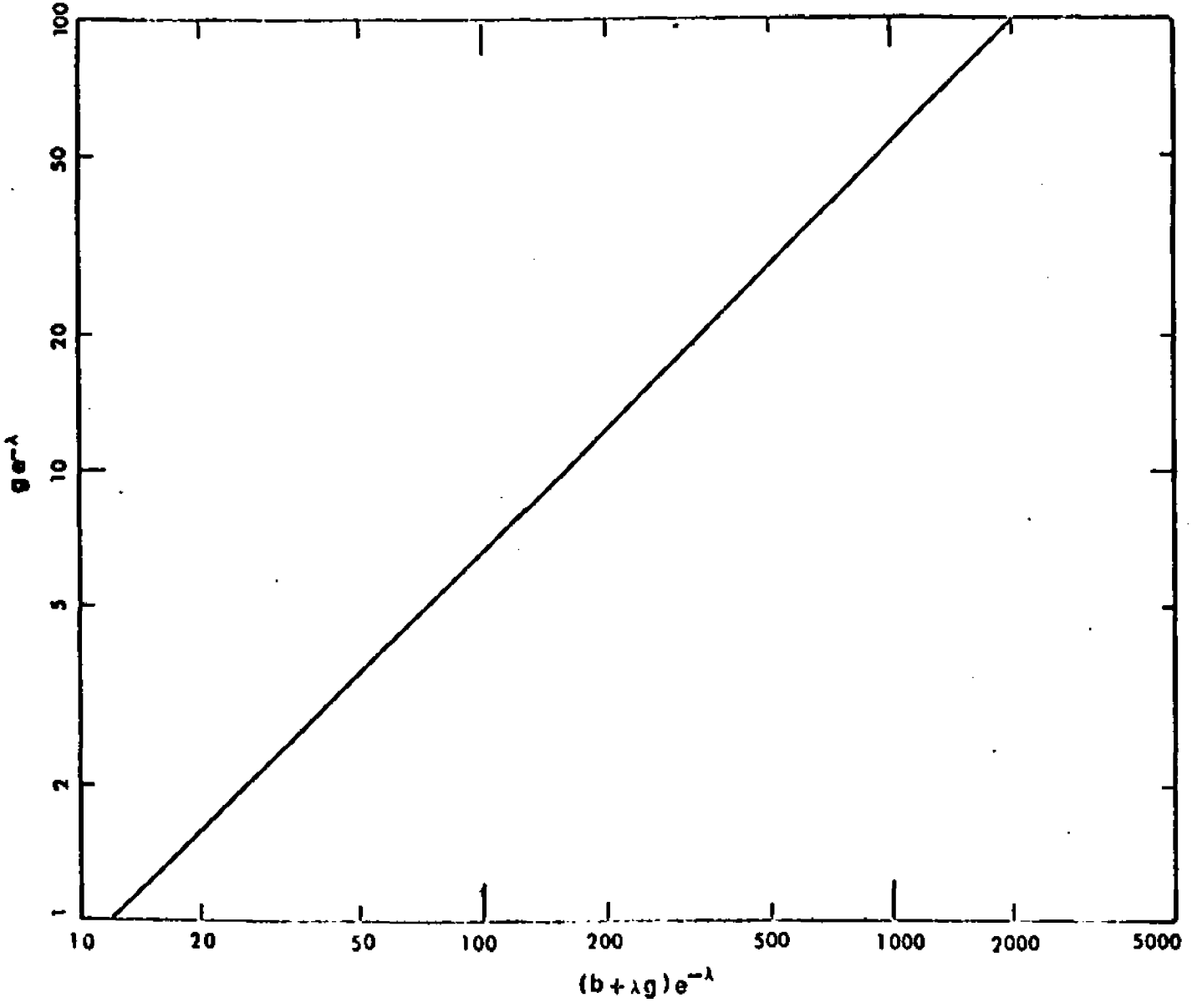

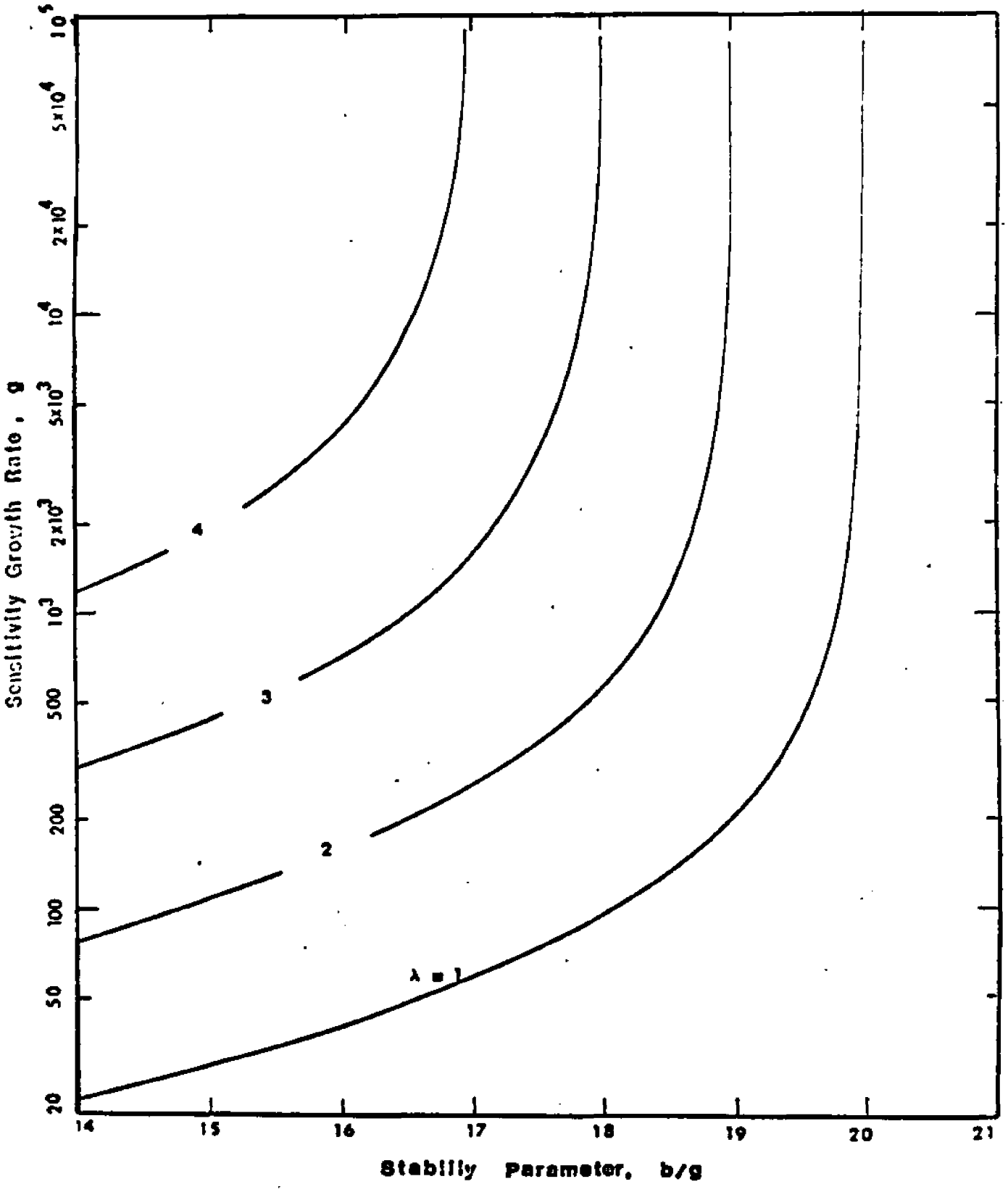

Figure 9 Working Stability Curves For A Crystallizer With Point Fines Trap

From the design curves of fig. 5, for example, we may see that when a desired product size $\bar{r}$ leads to unstable operation in a crystallizer without fines trap ($\lambda = 0$), a crystallizer with fines trap may be designed to give stable operation with the some $\bar{r}$. The required mean residence time θ will be shorter in the crystallizer with fines trap, and the design value of the crystallizer volume correspondingly smaller for a desired production rate. Corresponding conclusions about the operation of an existing fines trap may be drawn from fig. 4; here $r_o/\theta_o = 0$ represents operation without the fines trap.

We turn now to a consideration of how the character of the stability curves of fig. 9 is modified on relaxing the condition $r^* = 0$ that leads to a point fines trap. Our starting point is the characteristic equation (4.12) with the general H and K of (4.16) for a finite fines trap. With h given by (4.14), the functions H and K are no longer simply rational functions of s, but involve as well delay terms e^{-sr^*}. The details are shown in Appendix II, and the upshot is that the characteristic equation for a finite fines trap takes the form

$$P(s) + Q(s)e^{-sr^*} = 0 \qquad (4.21)$$

where P and Q are polynomials in s, with coefficients depending on b, g, r* and λ (or R). There are of course various ways of extracting stability conditions from characteristic equations like (4.21). We used primarily the method of finding those relations among the parameters b, g, r*, λ for which (4.21) has purely imaginary roots s, and interpreting these relations as stability limits. For fixed r* and λ, this leads to curves in the b-g plane which may be compared with the point fines trap curves, and with curves obtained by various approximative methods. All the curves so obtained showed limiting values of b/g for large g; we recall that for the point fines trap, r* = 0, the limiting value is $(b/g)_\infty = 21-\lambda$. Fig. 10 summarizes our numerical results in this area by showing how this limiting value $(b/g)_\infty$ depends on the fines trap parameters λ and r*.

Typical shapes of the full b-g stability curves are shown in figs. 11 and 12. Fig. 11 illustrates the orderly progress of these curves as the parameter λ; and hence the recirculation ratio R, are raised for fixed r*. The limiting value $(b/g)_\infty$ goes steadily down as λ goes up. Fig. 12 illustrates the more complicated advance and retreat of the curves with r* for fixed λ. Here $(b/g)_\infty$ rises to a maximum

as r* goes up from 0, and then decreases; the behavior as r* nears unity (not shown here) becomes very complicated. The stability curve superimposed on the steady-state curves of fig. 6 was taken from fig. 12 in the manner described earlier for the point fines trap curves. Its shape opens up the interesting possibility that, with λ chosen, perhaps from the considerations mentioned earlier, there is a value of r* which gives the largest stable margin for the operation of the fines trap.

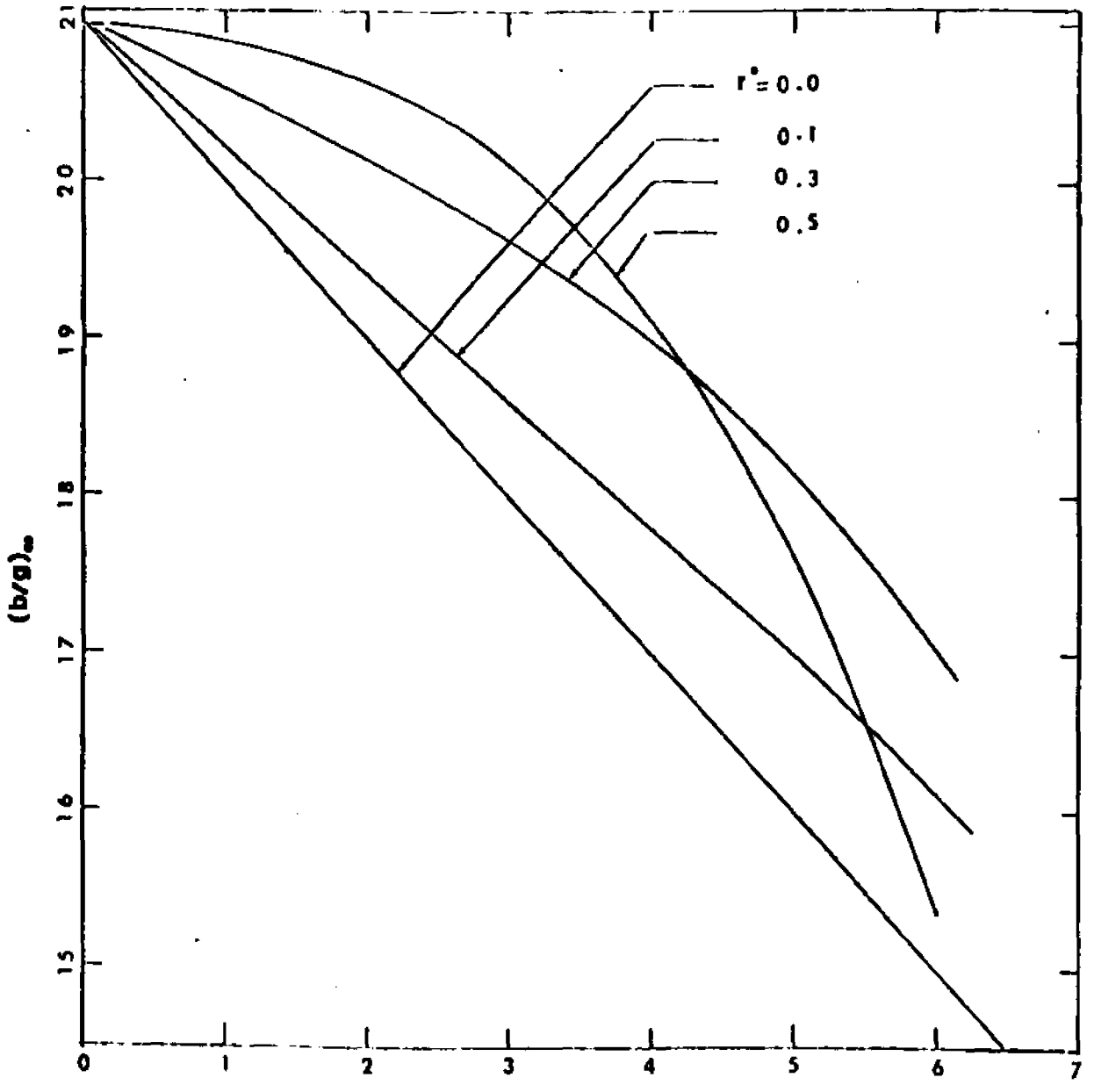

Figure 10 Limiting Stability Curves For A Crystallizer With Finite Fines Trap

Figure 11-1 Illustrations Of The Effect Of Fines Destruction Rate On The Stability Curves For A Crystalliser With Finite Fines Trap

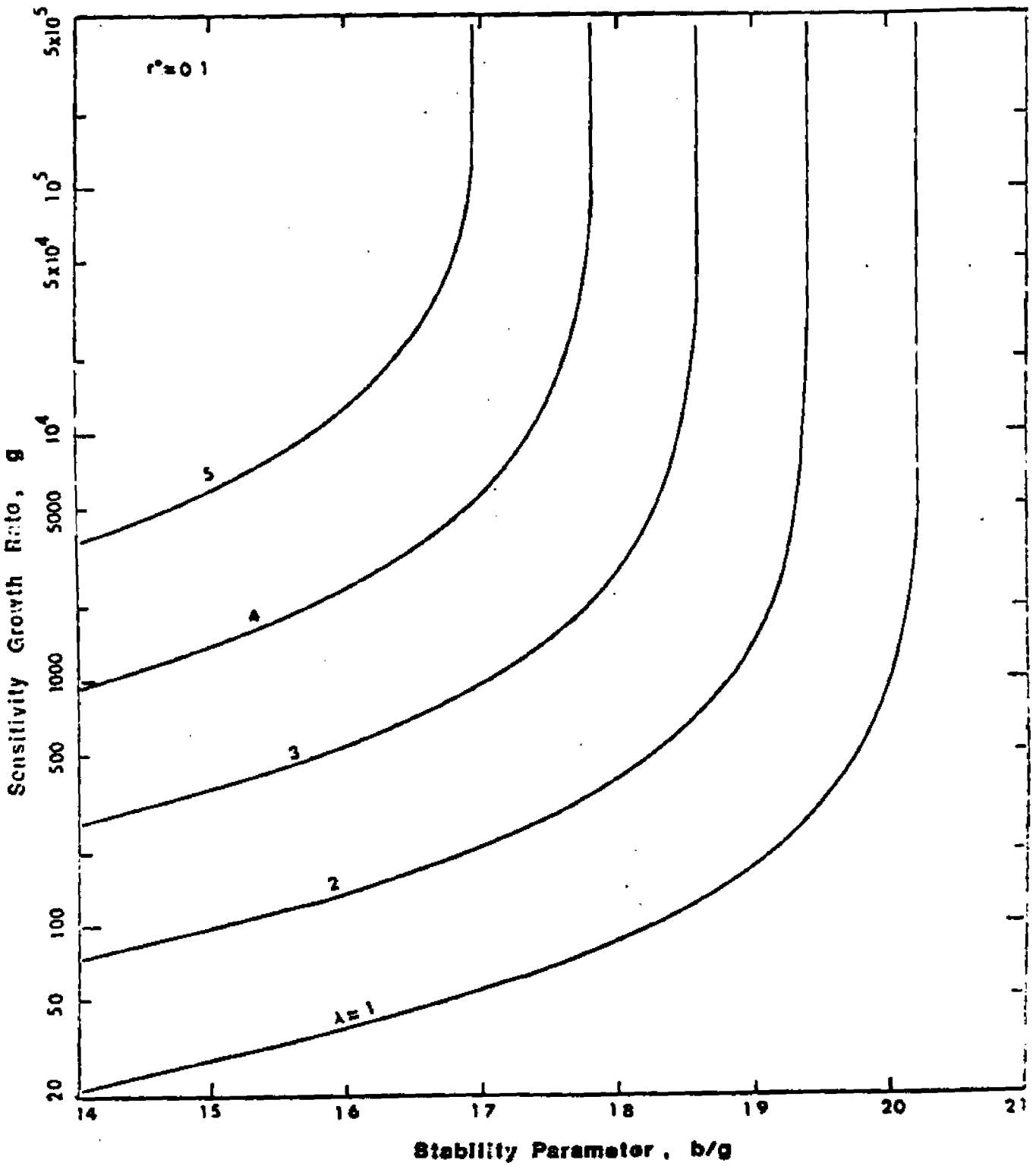

Figure 11-2 Illustrations Of The Effect Of Fines Destruction Rate On The Stability Curves For A Crystalliser With Finite Fines Trap

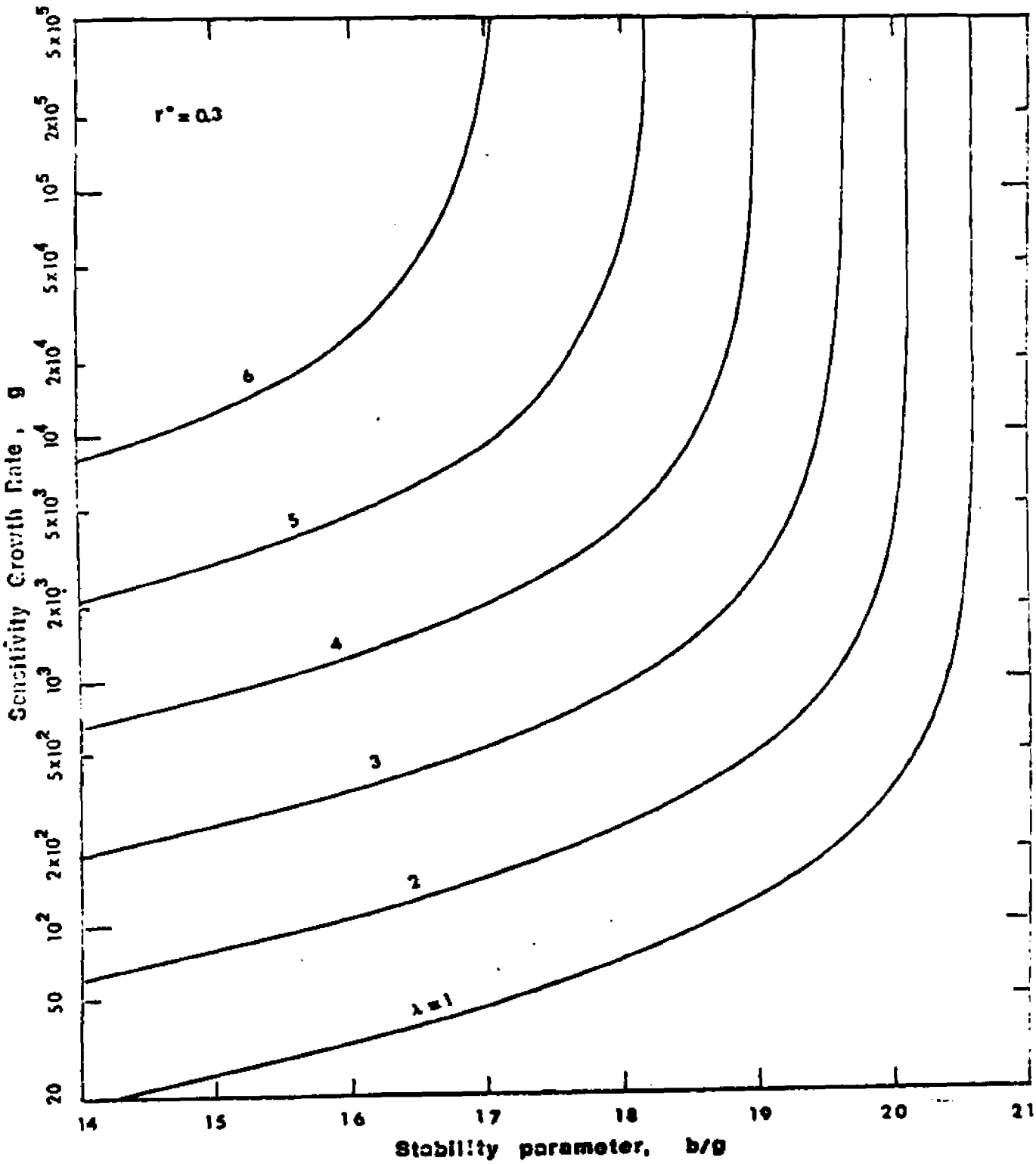

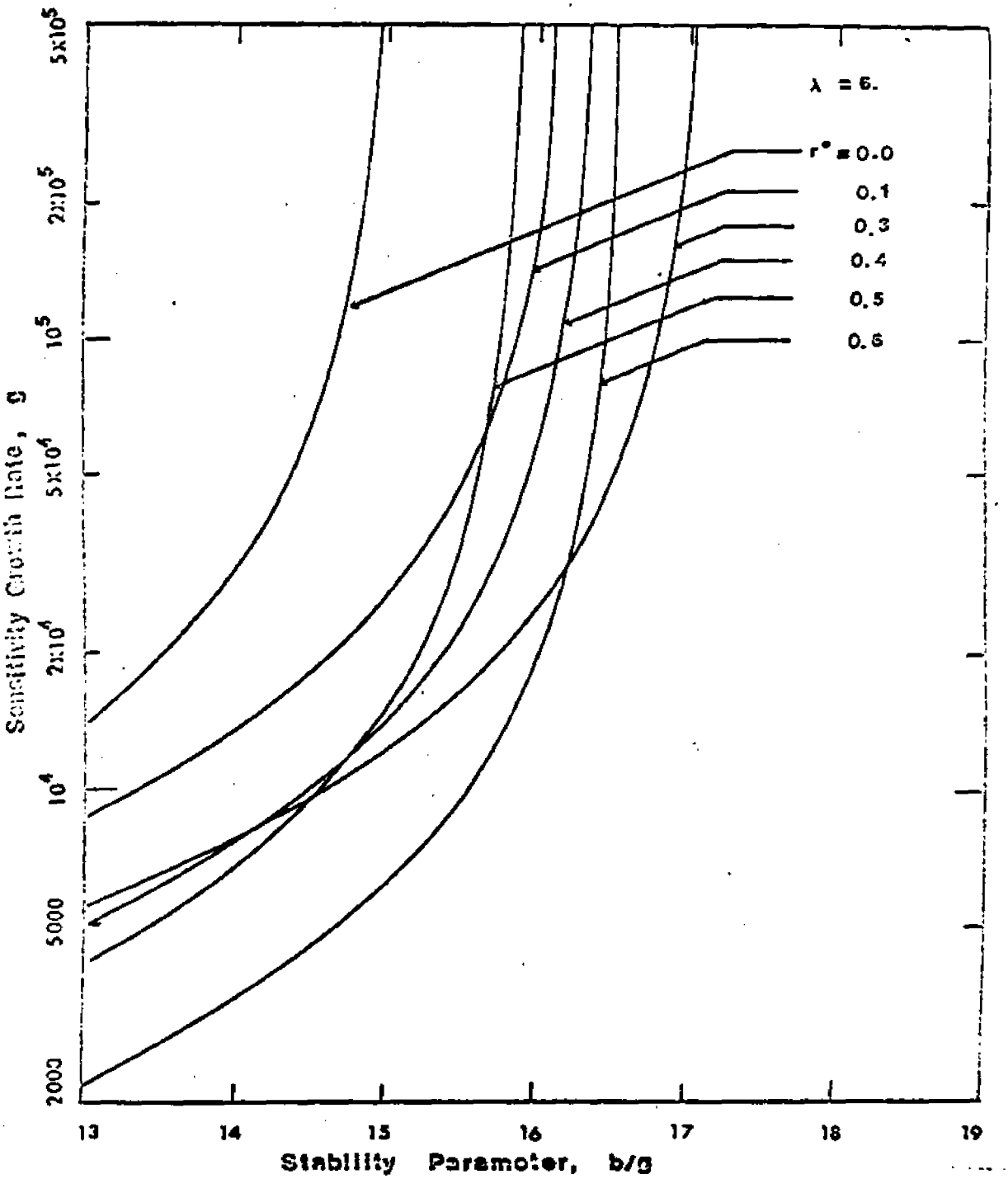

Figure 12 Illustrations Of The Effect Of Fines Destruction Size On The Stability Curves For A Crystalliser With Finite Fines Trap

CHAPTER 5

Nonlinear Dynamic Behavior

In this chapter, we present the results of some numerical solutions of the full nonlinear dynamic equations (3.1-3.3). The numerical procedures are shown in Appendix III. All calculations are made about same steady-state operating point. Their purpose is primarily to verify the linearized stability analysis of the preciding section, by following the propagation of finite perturbations from various steady-state solutions. From these numerical investigations we conclude that a linearly stable operating point is stable in the large and that a linearly unstable operating point has associated with it a stable limit cycle.

The calculations have also another purpose: to follow the stabilizing effect of fines destruction noted earlier, under comparable feed and product conditions for the system as a whole. To this end, cases for presentation are not chosen at random, but rather to have the same inlet conditions and the same mean product size. The precise form in which the equations are taken for solution, and the details of the numerical procedures, are for brevity omitted here.

We present here a number of cases, all with the same dimensionless steady-state mean crystal size of (3.11), $\bar{r}=5$, and all with the parameter L of (3.12) equal to 5. These

cases are all calculated for the kinetics of (3.15), with $K = 0.0025$, $n = 1$. Since the zeroth moment of f(r,t) shows the effects we are looking for most sensitively, we present only plots of its perturbation $\delta\mu_o$ (taken in units of the steady-state zeroth moment) against the time t (taken in units of the mean residence time). The curves presented here are for initial perturbations from steady-state values in supersaturation, and certain corresponding perturbations in the size distribution made to give a smoother mathematical response.

Under these conditions, $\bar{\tau} = 5$ gives unstable operation for a crystallizer without fines trap, and the curves of fig. (13-1) show how the instability leads to continued stable cycling in the absence of enough fines trap action, and how the cycling is damped and finally removed completely by suitable fines trap action (figs. 13-2, 13-3).

It is particularly interesting to observe how the behavior of the nonlinear system is correctly predicted by the linear stability analysis, and how the behavior of the nonlinear system calculated by the finite fines trap model can be represented by the calculation based on the point fines trap (when the critical size r* is small). It is also important to note that the r* which lead to the largest

stable margin for fixed λ gives the best response in the nonlinear calculation (fig. 13-4).

CHAPTER 6

Discussion of Open-Loop Operation

In the previous chapters some typical general examples were given of the effect of a fines trap on the operation of a continuous stirred crystallizer. As stated in the Introduction, any such analysis depends on the exact kinetics of both nucleation and growth. Now such data are hard to obtain. Most published data are obtained under conditions of relatively high supersaturation and high nucleation rates, whereas in industrial crystallizers one is very often interested in large particle sizes and low nucleation rates. It is therefore difficult to compare the industrial results directly with published data. On the other hand our results show some basic trends which are not very sensitive to the exact form of the nucleation rate, and we can compare these with general experience in industrial practice.

First of all it is well known that cycling in crystallizers can be reduced or eliminated by adjusting the operation of the fines trap. The results in fig.4-6 explain this by a quantitative model. The physical explanation for this stabilization is that the operation of the fines trap increases the supersaturation, and therefore decreases the sensitivity parameter of the nucleation rate. This stabilization is due to the increase in the fraction of nuclei de-

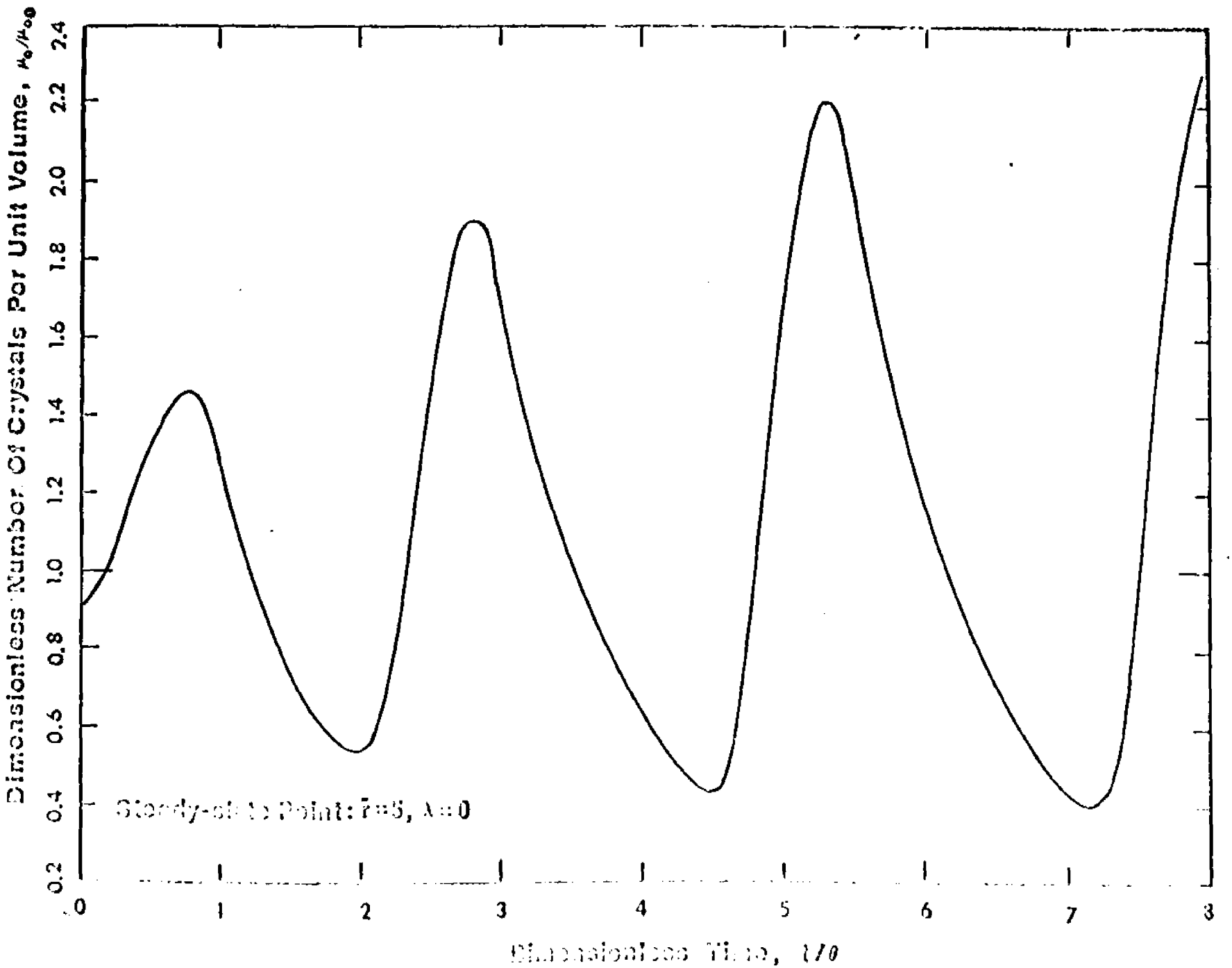

Figure 13-1 Illustrative Dynamics Of A Crystallizer [illegible] Fines Trap

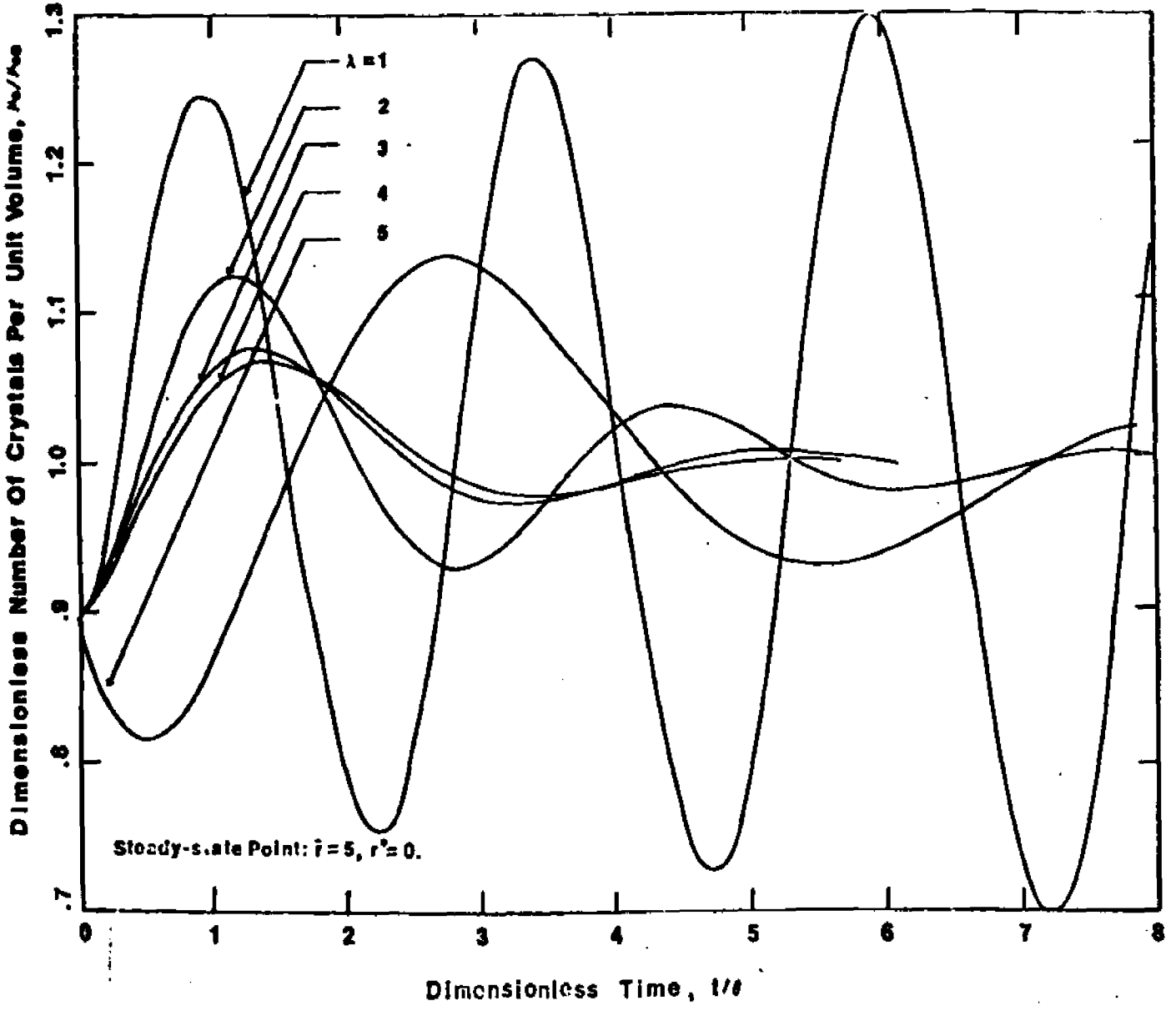

Figure 13-2 Illustrative Dynamics Of A Crystallizer With Finite Fines Trap

Figure 13-3 Illustrative Dynamic Of A Continuous Crystallizer With Finite Fines Trap

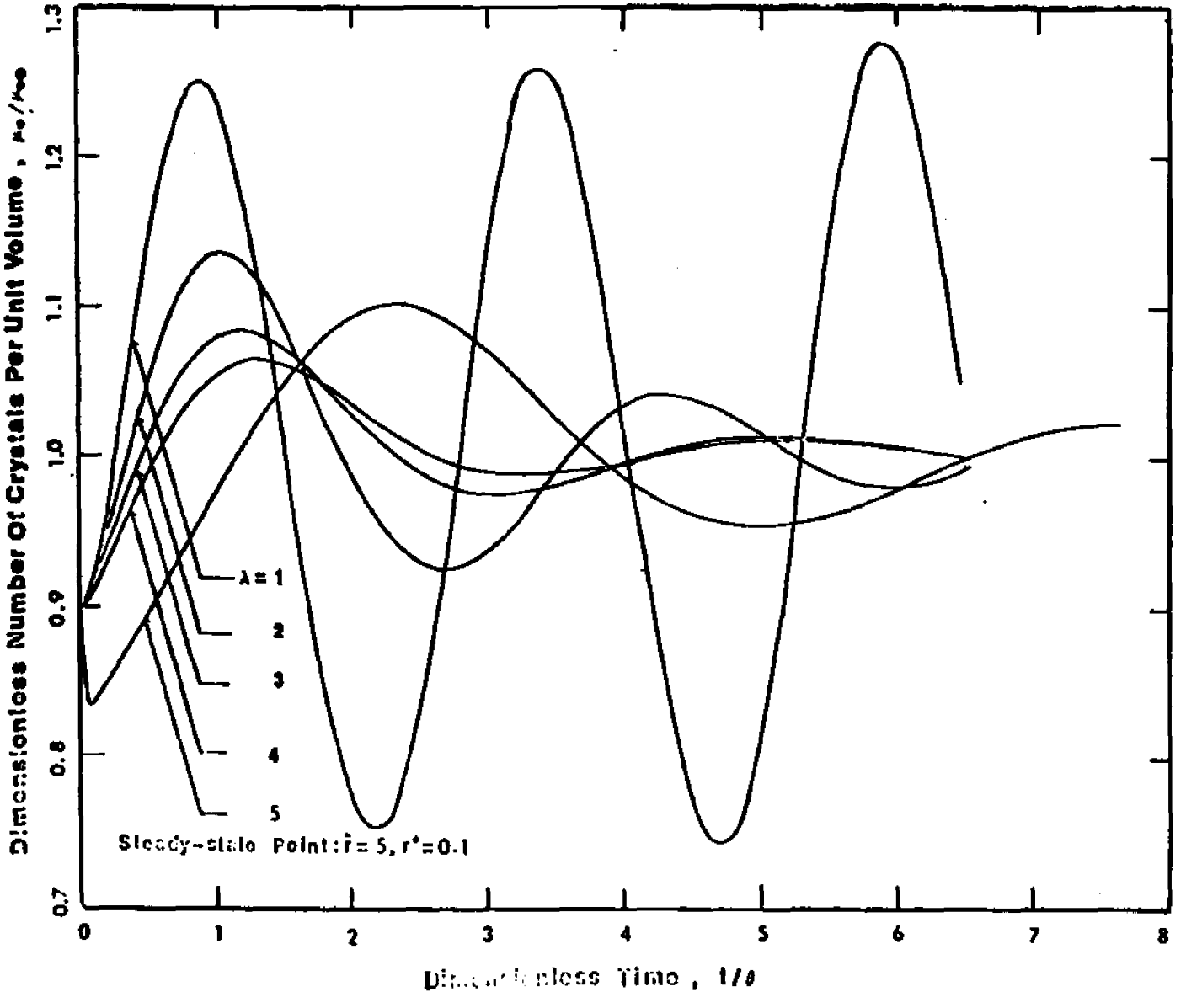

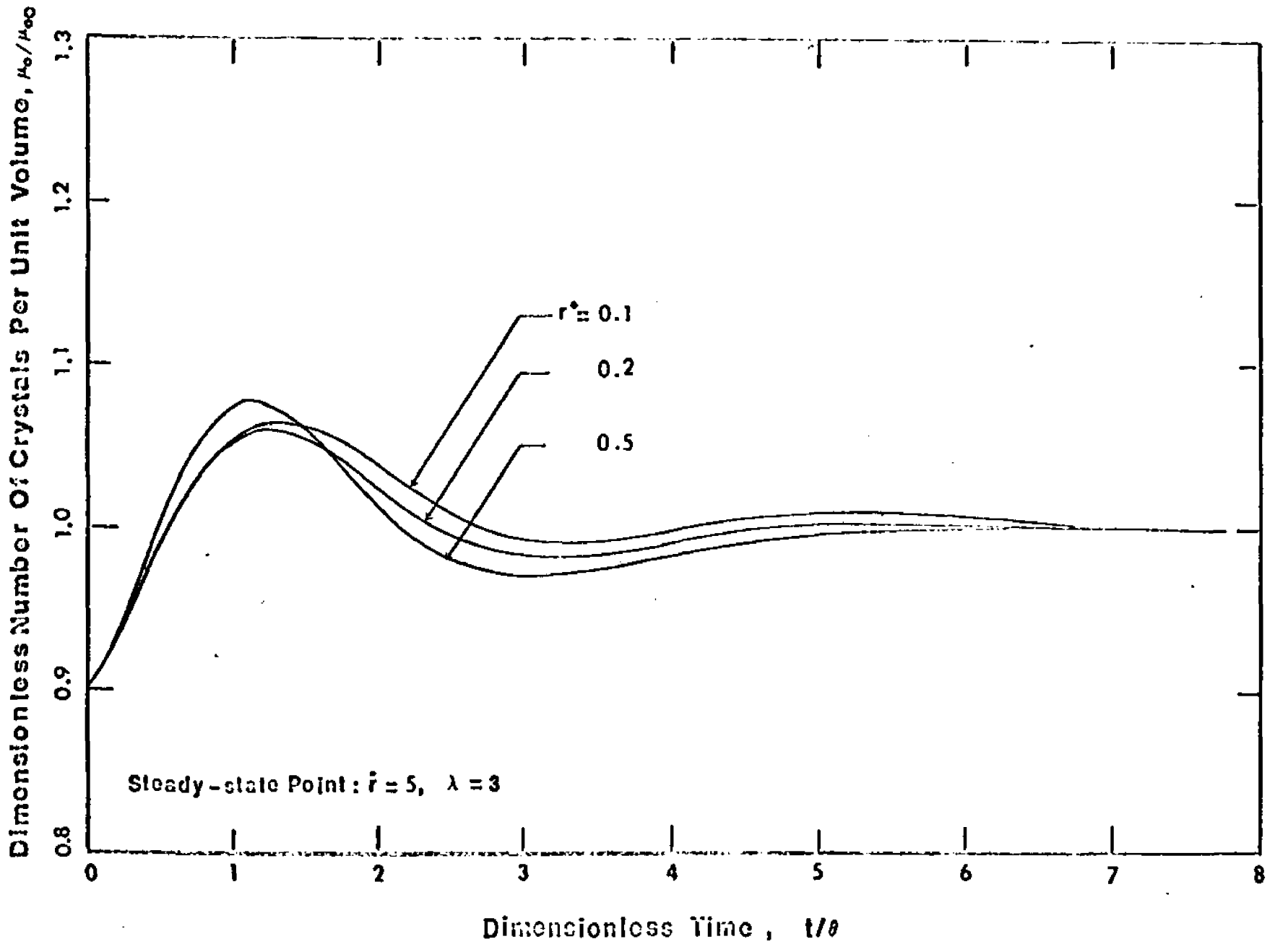

Figure 13-4 Illustrative Dynamic Of A Continuous Crystallizer With Finite Fines Trap

stroyed, and occurs both at constant residence time and at constant mean particle size.

Under some conditions the value of λ (or the fraction destroyed, $1-e^{-\lambda}$) necessary to stabilize is quite reasonable ($\lambda \approx 3$ or $1-e^{-\lambda} \approx .95$). In other cases it is quite high and the total mass of nuclei destroyed is not negligible at all, but a significant fraction (up to 30%) of the production rate. This can be seen from the general form of figs. 5 and 6 which should have the correct shape for the majority of systems though in some special cases there could be strong deviations.

We also note that, depending on conditions, increase of the fraction of nuclei destroyed might destabilize. In fact, we should be able, by strong increases in λ, to bring any stable crystallizer to a cycling condition. Such destabilizing effects have also been observed. In practice destabilization due to such traps is even more common than one would expect from the results. A possible explanation might be the fact that even in mixed crystallizers some classification at the outlet occurs.

As shown in [16], classification reduces the stability limit for the nucleation sensitivity. Thus instabilities

might occur at much lower values of $\lambda+b/g$, than would be predicted from an ideally mixed crystallizer.

For a point fines trap at high values of b and g the results can be given in a very simple form. If instead of b/g one uses $d\ln B_{eff}/d\ln G$, one can use the stability analysis of [8,15,16] without a fines trap. Thus the results of the classified case can also be applied to the point fines trap.

For an ideally classified crystallizer [16], b/g must be less than 2. In this case stabilization by the fines trap is impractical and the fines trap would always tend to destabilize.

In a real stirred crystallizer some classification occurs and the initial value of $(b/g+\lambda)$ should be somewhere between 21 and 2. Its exact value can be experimentally determined. The above analysis for an ideally mixed crystallizer while not applying quantitatively to a partially classified crystallizer, should still provide some useful guidelines in the effect of the different design parameters on the stability of the operation.

Now reversing the argument, the sensitivity of the system to cycling and the dependence of cycling on the operation of the fines trap could be a very important tool in

gaining some information about B and G at low supersaturations, just as the dependence of $\bar{r}$ on θ gives us at least some partial information at lower residence times.

In addition to explaining the observed behavior of fines traps, the results presented have provided some useful guidelines for their design. In designing such traps, r_o and θ_o are related by the design parameters of the baffle. The curves of figs. 4 and 5 show that for small values of r_o, $r_o/\bar{r} < 0.05$, the individual values of r_o and θ_o are unimportant as long as r_o/θ_o, or, equivalently, the design parameter λ, has the desired value. The designer is free to choose the optimal combination based on cost considerations.

However, in many cases low values of r_o are expensive to obtain and one asks oneself what value of r_o can one tolerate. Increasing r_o increases the load on the heat exchanger in the fines trap, but on the other hand a slight increase in r_o might have beneficial effects on stability as long as the optimum value of r_o is not exceeded. The final design choice is again an economic question. The above considerations should provide some quidelines as the proper mechanical design of the fines trap.

The actual design of the fines trap strongly depends

on the viscosity of the solution and its density, as these give the relation between r_o and w_o. Our above considerations indicate that in the absence of other information, it is desirable to design for a range of λ between 3 and 7.

There are basically two ways in which such fines traps are designed. One can either have a large fixed recirculation through the settling zone, which keeps r_o fixed, and adjust w_o by changing the rate of withdrawal through the trap. Alternatively, one can withdraw directly through a settling zone; here r_o is related to the withdrawal rate w_o, being of the order of $w_o^{1/2}$. Our above relations indicate that as long as r_o over the whole design range remains less than $0.3\bar{r}$, this dependence of r_o on the withdrawal rate has no detrimental effect on the control and stabilizing action of the fines trap.

CHAPTER 7

Open Loop Transfer Functions

We develop in this chapter the open loop transfer functions that will be needed in the control studies that follow. The development will be all for a crystallizer with point fines trap, that is, one in which the fines destruction size and the fines retention time are both very small, their ratio however being finite.

Following prior work [15], and our own open loop analysis, from which we take also the general notation and the plan of the working equations, point fines trap operation can be represented by a suitable reduction in nucleation rate, so that the working equations for the crystal size distribution f(r,t) become

$$\begin{cases} G(c)\cdot f = \epsilon B(c) e^{-r_o/\theta_o G(c)} & ; \quad r = 0 \\ \dfrac{\partial f}{\partial t} + G(c)\dfrac{\partial f}{\partial r} = -\dfrac{1}{\theta} f & ; \quad r > 0 \end{cases} \tag{7.1}$$

where ϵ is the liquid volume fraction in the crystallizer

$$\epsilon = 1 - k\int_o^\infty r^3 f \, dr \tag{7.2}$$

here r_o is the fines destruction size, θ_o the fines retention time (the ratio of crystallizer volume v to fines recirculation rate w_o) in the system and θ the overall holdup time (the ratio of v to the volumetric throughput rate w). The equations (7.1,7.2) must be completed by an overall material balance

on solute-crystal material in the system, and this takes the form of an ordinary differential equation in the solute concentration C

$$\frac{d}{dt}\left(\epsilon \cdot C + (1-\epsilon)\cdot\rho\right) = \frac{C_i}{\theta} - \frac{1}{\theta}\left(\epsilon \cdot C + (1-\epsilon)\cdot\rho\right) \tag{7.3}$$

Now many of the quantities of interest in the crystallizer operation can be expressed in terms the moments of distribution f(r,t)

$$\mu_n(t) = \int_o^{\infty} r^n f(r,t)\, dr \tag{7.4}$$

Thus the number of crystals per unit volume is

$$n = \mu_o \tag{7.5}$$

The total crystal surface per unit volume is

$$\sigma = 3k\mu_2 \tag{7.6}$$

The volume fraction liquid in the system is

$$\epsilon = 1 - k\mu_3 \tag{7.7}$$

and the weight average crystal size is

$$\bar{r} = \mu_4/\mu_3 \tag{7.8}$$

Indeed, the equations (7.1-7.3) can be represented in moment form:

$$\begin{cases} \dfrac{d}{dt}\left\{(1-k\mu_3)c + k\mu_3\rho\right\} = \dfrac{C_i}{\theta} - \dfrac{1}{\theta}\left\{(1-k\mu_3)c + k\mu_3\rho\right\} \\ \dfrac{d\mu_o}{dt} = (1-k\mu_3)B(c)e^{-r_o/\theta_o G(c)} - \dfrac{1}{\theta}\mu_o \\ \dfrac{d\mu_n}{dt} = nG(c)\,\mu_{n-1} - \dfrac{1}{\theta}\mu_n \qquad ;\quad n = 1, 2, \ldots \end{cases} \tag{7.9}$$

and the quantities (7.5-7.8) recovered from their solution.

However, the corredsponding properties for the population of fines cannot be developed so readily from the point fines trap equations, since, taken literally, these equations put all the fines at zero size, and hence with zero surface and so on. To arrive at working expressions for these properties, we consult the steady state solution for the finite fines trap, in the form

$$f(r) = (1-k_v)\frac{B(c)}{G(c)}\, e^{-\frac{r}{\theta G(c)} - \frac{1}{\theta_o G(c)}\int_o^r \eta(s)ds} \quad ; \quad r > 0 \qquad (7.10)$$

where η is the fines selection function

$$\eta(r) = \begin{cases} 1 & ; \quad r < r_o \\ 0 & ; \quad r > r_o \end{cases} \qquad (7.11)$$

In terms of (7.10), we may express the number of fines per unit crystallizer volume as

$$n_o = \int_o^{\infty} \eta \cdot f(r)dr \qquad (7.12)$$

and the fines surface per unit crystallizer volume as

$$\sigma_o = 3k\int_o^{\infty} r^2 \eta \cdot f(r)dr \qquad (7.13)$$

Evaluating the integral (7.12) with the selection curve (7.11) gives

$$n_o = r_o(1-k\mu_3)\frac{B(c)}{G(c)}\ \frac{1 - e^{-\frac{r_o}{\theta G(c)} - \frac{r_o}{\theta_o G(c)}}}{\frac{r_o}{\theta G(c)} + \frac{r_o}{\theta_o G(c)}}$$

and in the point fines trap approximation, where r_o/θ is negligibly small compared to r_o/θ_o, we may write

$$n_o = r_o\ (1-k\mu_3)\frac{B(c)}{G(c)}\ \frac{1 - e^{-r_o/\theta_o G(c)}}{r_o\ /\theta_o G(c)} \qquad (7.14)$$

A similar calculation for the fines surface integral (7.13) gives

$$\sigma_o = kr_o^3\ (1-k\mu_3)\frac{B(c)}{G(c)}\ \frac{1-\left\{1+\left(r_o/\theta_o G(c)\right)+\frac{1}{2}\left(r_o/\theta_o G(c)\right)^2\right\}e^{-r_o/\theta_o G(c)}}{\frac{1}{6}\left(r_o/\theta_o G(c)\right)^3} \qquad (7.15)$$

In developing the transfer functions below, and in making the control studies that follow, the equations (7.14,7.15) are appended to the moment equations (7.9) and taken to hold dynamically at every instant of time. This does not seem to be a

bad assumption physically, and we shall have the occasion to use only the fines surface expression (7.15).

We now proceed to linearize the moment equations (7.9) about a steady state, taking into account as driving forces fluctuations both in the bulk throughput rate w and in the fines recirculation rate w_o, that is, both in θ and in θ_o. It is convenient to introduce a crystal-solute resource function

$$\varphi = (1-k\mu_3)C + k\mu_3\rho$$

and the moment equations (7.9) give linear equations in the perturbations $\delta\varphi$, $\delta\mu_n$ in the form

$$\frac{d\delta\varphi}{dt} + \frac{1}{\theta}\,\delta\varphi = 0$$

$$\begin{cases} \dfrac{d\delta\mu_o}{dt} + \dfrac{1}{\theta}\,\delta\mu_o + kB\, e^{-r/\theta_o G}\left\{1 + (\rho-C)\left(\dfrac{B'}{B} + \dfrac{r_o}{\theta_o G}\,\dfrac{G'}{G}\right)\right\}\delta\mu_3 \\ \quad - B\, e^{-r_o/\theta_o G}\left(\dfrac{B'}{B} + \dfrac{r_o}{\theta_o G}\,\dfrac{G'}{G}\right)\delta\varphi = -\dfrac{\mu_o}{\theta}\dfrac{\delta(1/\theta)}{1/\theta} - (1-k\mu_3)B\dfrac{r_o}{\theta_o G}\, e^{-r_o/\theta_o G}\cdot\dfrac{\delta\left(\frac{1}{\theta_o}\right)}{1/\theta_o} \\ \dfrac{d\delta_n}{dt} + \dfrac{1}{\theta}\,\delta\mu_n - nG\cdot\delta\mu_{n-1} + \dfrac{knG'\mu_{n-1}(\rho-C)}{1-k\mu_3}\,\delta\mu_3 - \dfrac{nG'\mu_{n-1}}{1-\mu_3}\,\delta\varphi \\ \qquad = -\dfrac{\mu_n}{\theta}\dfrac{\delta(1/\theta)}{1/\theta} \qquad ; \quad n = 1,2,\cdots\cdots \end{cases} \tag{7.16}$$

Here B' and G' are derivatives with respect to the solute concentration C, and the perturbation in this concentration can readily be expressed in terms of $\delta\varphi$ and the $\delta\mu_n$.

$$\delta C = \frac{\delta\varphi - k(\rho-c)\delta\mu_3}{1 - k\mu_3}$$

as can the perturbations in any of the quantities (7.5-7.8, 7.14, 7.15). We are concerned here primarily with the mean crystal size $\bar{r}$, the total crystal surface σ per unit volume, and the corresponding fines surface σ_o. We find accordingly from (7.6, 7.8, 7.15)

$$\frac{\delta\bar{r}}{\bar{r}} = \frac{\delta\mu_4}{\mu_4} - \frac{\delta\mu_3}{\mu_3} \tag{7.17}$$

$$\frac{\delta\sigma}{\sigma} = \frac{\delta\mu_2}{\mu_2} \tag{7.18}$$

$$\frac{\delta\sigma_o}{\sigma_o} = -\left\{ \frac{B'}{B} - \frac{G'}{G} + 3\frac{1-\left[1+(r_o/\theta_oG)+\frac{1}{2}(r_o/\theta_oG)^2+\frac{1}{6}(\frac{r_o}{\theta_oG})^3\right]e^{-\frac{r_o}{\theta_oG}}}{1-\left[1+(r_o/\theta_oG)+\frac{1}{2}(r_o/\theta_oG)^2\right]e^{-r_o/\theta_oG}} \right\} \frac{\delta\varphi}{1-k\cdot\mu_3}$$

$$-3\,\frac{1-\left[1+(r_o/\theta_oG)+\frac{1}{2}(r_o/\theta_oG)^2+\frac{1}{6}(r_o/\theta_oG)^3\right]e^{-r_o/\theta_oG}}{1-\left[1+(r_o/\theta_oG)+\frac{1}{2}(r_o/\theta_oG)^2\right]e^{-r_o/\theta_oG}}\,\frac{\delta(1/\theta_o)}{1/\theta_o}$$

$$-\left\{1+(\rho-C)\left(\frac{B'}{B}-\frac{G'}{G}+3\frac{G'}{G}\,\frac{1-\left[1+(r_o/\theta_oG)+\frac{1}{2}(r_o/\theta_oG)^2+\frac{1}{6}(\frac{r_o}{\theta_oG})^3\right]e^{-(\frac{r_o}{\theta_oG})}}{1-\left[1+(r_o/\theta_oG)+\frac{1}{2}(r_o/\theta_oG)^2\,e^{-(r_o/\theta_oG)}\right]}\right)\right\}\frac{k\cdot\delta\mu_3}{1-k\cdot\mu_3}$$

(7.19)

We are now in a position to assemble the transfer functions of $\bar{r}$, σ, σ_o with respect to w and w_o. We note first that, the crystallizer volume being constant, we already have $\delta w/w$ and $\delta w_o/w_o$ at hand in the form

$$\frac{\delta w}{w} = \frac{\delta(1/\theta)}{1/\theta}$$

$$\frac{\delta w_o}{w_o} = \frac{\delta(1/\theta_o)}{1/\theta_o} \tag{7.20}$$

Next, we carry

$$t \rightarrow \theta t$$

referring all times to the mean residence time in the crystallizer. Finally, we introduce Laplace transforms

$$\begin{cases} \hat{\delta\varphi}(s) = \int_o^\infty e^{-st}\,\delta\varphi(t)dt \\ \hat{\delta\mu}_n(s) = \int_o^\infty e^{-st}\delta\mu_n(t)dt \\ \hat{\delta r}(s) = \int_o^\infty e^{-st}\delta r(t)dt \\ \hat{\delta\sigma}(s) = \int_o^\infty e^{-st}\,\delta\sigma(t)dt \\ \hat{\delta\sigma}_o(s) = \int_o^\infty e^{-st}\delta\sigma_o(t)dt \\ \hat{\delta w}(s) = \int_o^\infty e^{-st}\delta w(t)dt \\ \hat{\delta w}_o(s) = \int_o^\infty e^{-st}\delta w_o(t)dt \end{cases}$$

in the equations (7.16-7.19), taking initial conditions zero, so

that the system is initially in its steady state. The solution of the resulting algebraic equations in the transforms is tedious, but straightforward. We omit the details and simply quote the results.

$$\frac{\hat{\delta r}}{\bar{r}} = -\left\{ \frac{(b+\lambda g)e^{-\lambda} - ge^{-\lambda} + 1}{(s+1)\left[(b+\lambda g)e^{-\lambda} + ge^{-\lambda}\sum_{i=1}^{3}(s+1)^i + (s+1)^4\right]} \right\} \frac{\hat{\delta w}}{w}$$

$$+\left\{ \frac{\lambda(ge^{-\lambda}+s)}{(s+1)\left[(b+\lambda g)e^{-\lambda} + ge^{-\lambda}\sum_{i=1}^{3}(s+1)^2 + (s+1)^4\right]} \right\} \frac{\hat{\delta w}_o}{w_o} \qquad (7.21)$$

$$\frac{\hat{\delta\sigma}}{\sigma} = \left\{ \frac{(b+\lambda g)e^{-\lambda} - ge^{-\lambda} - \sum_{i=1}^{3}(s+1)^i}{(b+\lambda g)e^{-\lambda} + ge^{-\lambda}\sum_{i=1}^{3}(s+1)^i + (s+1)^4} \right\} \frac{\hat{\delta w}}{w}$$

$$-\left\{ \frac{\lambda(ge^{-\lambda} + s + 1)}{(b+\lambda g)e^{-\lambda} + ge^{-\lambda}\sum_{i=1}^{3}(s+1)^i + (s+1)^4} \right\} \frac{\hat{\delta w}_o}{w_o} \qquad (7.22)$$

$$\frac{\hat{\delta\sigma}_o}{\sigma_o} = \left\{ \frac{(b+ag-g)e^{-\lambda}\sum_{i=0}^{3}(s+1)^i}{(b+\lambda g)e^{-\lambda} + ge^{-\lambda}\sum_{i=1}^{3}(s+1)^i + (s+1)^4} \right\} \frac{\hat{\delta w}}{w}$$

$$+\left\{ \frac{\lambda(b-g)e^{-\lambda} - abe^{-\lambda} - age^{-\lambda}\sum_{i=1}^{3}(s+1)^i - a(s+1)^4}{(b+\lambda g)e^{-\lambda} + ge^{-\lambda}\sum_{i=1}^{3}(s+1)^i + (s+1)^4} \right\} \frac{\hat{\delta w}_o}{w_o} \qquad (7.23)$$

The coefficients of $\delta w/w$ and of $\delta w_o/w_o$ in the equations above are, in dimensionless form, the transfer functions in question. The parameters

$$\begin{cases} g = 6kBG^3\theta^4(\rho-c)\,\dfrac{G'}{G} \\ b = 6kBG^3\theta^4\left\{1+(\rho-c)\,\dfrac{B'}{B}\right\} \\ \lambda = r_o/\theta_o G \end{cases} \tag{7.24}$$

are familiar from prior open loop stability analyses, and the parameter a is

$$a = 3\,\frac{1-(1+\lambda+\lambda^2/2+\lambda^3/6)\,e^{-\lambda}}{1-(1+\lambda+\lambda^2/2)\,e^{-\lambda}} \tag{7.25}$$

It should be noted that s is a dimensionless transform variable, corresponding to the time measured in units of the overall residence time.

Figure 14 Feedback Control Schematics

A. When x is an increasing function of u

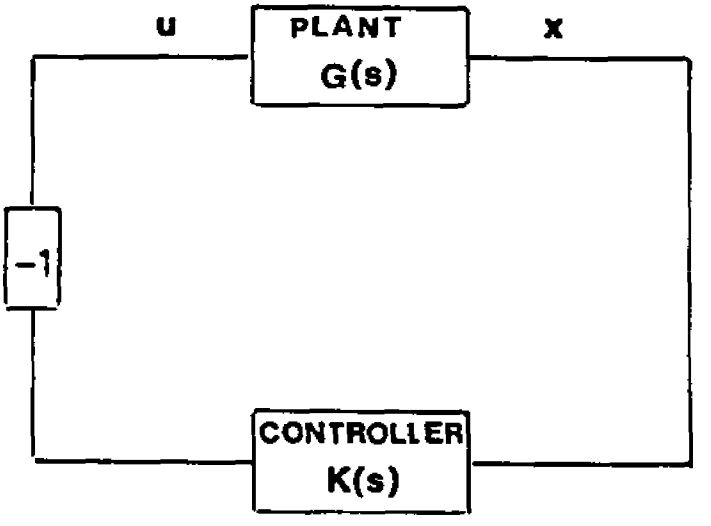

STABILITY CHARACTERISTIC :

$$1 + G(s)K(s) = 0$$

B. When x is a decreasing function of u

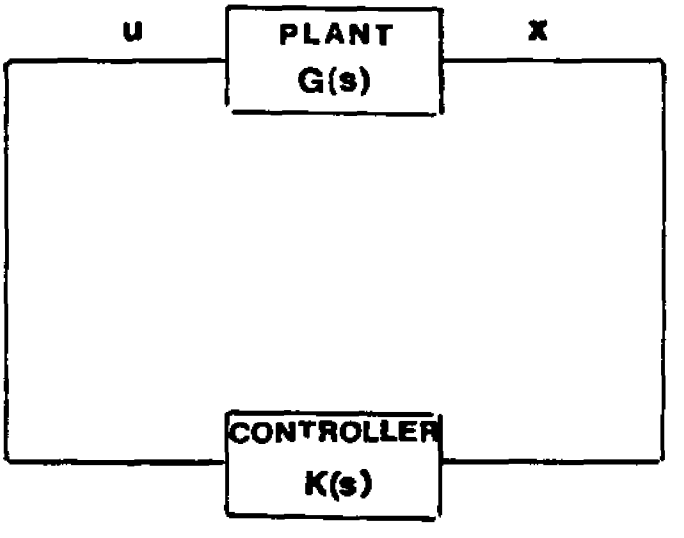

STABILITY CHARACTERISTIC :

$$1 - G(s)K(s) = 0$$

CHAPTER 8

Control On Mean Crystal Size

We analyze here a control system based on measurement of the mean crystal size $\bar{r}$ and manipulation of the bulk flow rate w. Such a control system would likely be applied in practice on a sampled data basis, $\bar{r}$ being measured periodically by screen analysis. It could of course be applied equally to a crystallizer with or without fines trap. Our development is carried out on a continuous basis, and aims to show the limits of stability for a proportional controller.

The plan of the control systems we study in this work is shown in Fig. 14, which shows also our negative feedback convention. In the present system, the response δx is

$$\delta x = \frac{\delta \bar{r}}{\bar{r}}$$

and the control action δu is

$$\delta u = \frac{\delta w}{w}$$

That is to say, formally,

$$x = \ln r$$

$$u = \ln w$$

and since we know from prior work that $\bar{r}$ is a decreasing function of w (an increasing function of the mean residence time θ), we adopt the convention B of Fig. 14 for our controller.

Accordingly, we take

$$\hat{\delta u}(s) = K(s)\ \hat{\delta x}(s)$$

(the caret denoting Laplace transform), that is

$$\frac{\hat{\delta w}(s)}{w} = K(s)\ \frac{\hat{\delta \bar{r}}(s)}{\bar{r}} \tag{8.1}$$

where K(s) is the transfer function of the controller. The plant (crystallizer) transfer function G(s) for this configuration

$$\frac{\hat{\delta \bar{r}}(s)}{\bar{r}} = G(s)\ \frac{\hat{\delta w}(s)}{w} \tag{8.2}$$

is given from (7.21) as

$$G(s) = -\ \frac{(b+\lambda g-g)e^{-\lambda} + 1}{(s+1)\left\{(b+\lambda g)\ e^{-\lambda}+ge^{-\lambda}-\sum_{i=1}^{3}(s+1)^i+(s+1)^4\right\}} \tag{8.3}$$

and the stability characteristic of the controlled system

$$1 - G(s)K(s) = 0$$

become

$$(s+1)^5+ ge^{-\lambda}\ \sum_{i=2}^{4}(s+1)^i\ +\ (b+\lambda g)e^{-\lambda}(s+1)$$
$$+k(s)\left\{(b+\lambda g-g)e^{-\lambda}+ 1\right\} = 0 \tag{8.4}$$

The controlled system is stable according as the characteristic equation (8.3) has all its roots with negative real part. For a proportional controller, the transfer function

K(s) is simply a constant K, and we have a polynomial equation whoe stability we can test by the Routh-Hurwitz criterion. The condition that the system be stable is

$$\left\{\begin{array}{l} ge^{-\lambda} + 5 > 0 \\ \left|\begin{array}{ll} 5 + ge^{-\lambda} & 1 \\ 10 + 10ge^{-\lambda} & 10 + 5ge^{-\lambda} \end{array}\right| > 0 \end{array}\right. \qquad (8.5)$$

$$\left\{\begin{array}{l} \left|\begin{array}{lll} 5 + ge^{-\lambda} & 1 & 0 \\ 10 + 10\,ge^{-\lambda} & 10 + 5ge^{-\lambda} & 5 + ge^{-\lambda} \\ 1 + be^{-\lambda} + k\left\{(b+\lambda g - g)e^{-\lambda} + 4\right\} & 5 + (g+\lambda)ge^{-\lambda} & 10 + 10ge^{-\lambda} \\ \quad + (3+\lambda)ge^{-\lambda} & + be^{-\lambda} & \end{array}\right| > 0 \end{array}\right.$$

This gives in the region of practical interest a rather narrow stable range for k. For example, in a typical crystallizer without fines trap, $\lambda = 0$, with $g = 500$, $b/g = 20$, the operation will be stable only in the range $-1.2 < K < 0.072$.

The nature of the stable range can be seen somewhat more clearly by going to the limit of large b and g, keeping b/g finite. This is anyway the region of practical interest, and the stability conditions (8.5) reduce in this limit to

$$-\left(3+\frac{b}{g}+\lambda\right) < \left(\frac{b}{g} + \lambda - 1\right) K < \frac{1}{25}\left(21 - \frac{b}{g} - \lambda\right)\left(\frac{b}{g} + \lambda + 14\right) \qquad (8.6)$$

A plot showing these stable limits is given Fig. 15. To furnish a standard against which to set the size of the con-

troller gain k_1, Fig. 15 shows as well a plot of the static sensitivity of the system in the form

$$\frac{d \ln \bar{w}}{d \ln \bar{r}} = \frac{\bar{r}}{\bar{w}} \frac{d\bar{w}}{d\bar{r}} = \frac{-1}{G(o)}$$

where from (8.3)

$$\frac{-1}{G(o)} = \frac{\frac{b}{g} + \lambda + 3}{\frac{b}{g} + \lambda - 1} \tag{8.7}$$

As the sensitivity of the controller depends on λ and b/g, the numerical value of K as defined here does not immediately give a clear indication of the quality of the control. For two cases with different λ and b/g, the steady state deviations are equal if the values of K are inversely proportional to the values of G(o). Taking $K = -1/G(o)$ halves the steady state devition for a step perturbation. Plotting $-1/G(o)$ along with K accordingly allows one to compare the stable range of K for different b/g and λ with the desired value for control, which should be at least $-1/G(o)$ and probably less than $-5/G(o)$.

Now we know from prior work that in the limit of large g, the uncontrolled system is stable only when

$$\frac{b}{g} + \lambda < 21$$

It may be seen from Fig. 15 that this control system cannot, then, for a positive K, stabilize an operation that is open loop unstable. A limited amount of stabilization is possible if one permits negative K, but the stable regions become very narrow, and shrink to nothing when $b/g + \lambda$ exceeds 41. Besides negative K introudces the possibility that new steady-state solutions will be introduced into the system, uncontemplated in the original design. This situation is discussed in general in the Appendix IV, and numerical calculations show the existence of such solutions in our case. We also note that for b/g less than unity $-(1/G(0))$ changes sign and becomes negative. Now for $b/g < 1$, the particle size increases with increasing flow rate and $(1/G(0))$ is positive (Control scheme A of figure 14). We adopted convention B for figure 15, as values of $b/g > 1$ are more frequently encountered. For b/g less than unity, the useful range of K is therefore negative.

For $(b/g + \lambda) = 1$, particle size is independent of flow rate, and it is therefore not surprising that one cannot control the particle size by changing the flow rate. The practical range of such a control is therefore limited to $0 < b/g < 1/3$ and $3 < b/g < 7$. In these ranges we can find a stable and reasonable value of K which is sufficiently large

for control. Very high values of K are normally impractical even if stable, as they lead to excessive control efforts and also to amplification of high frequency disturbance.

We conclude our discussion of this control system by seeing how the nonlinear system responds to this controller. Our illustrative calculations for this case will be for the mixed crystallizer without fines trap. We develop the closed loop equations by first solving the open loop equations (7.9) in steady state and calculating the corresponding steady state $\bar{r}$ from (7.8). Identifying these steady state values by the subscript e, we may represent the controller shown differentially in (8.1) as, for proportional control

$$\frac{w - w_e}{w_e} = K \frac{\bar{r} - \bar{r}_e}{\bar{r}_e}$$

Equivalently, since $\theta = v/w$, we may write

$$\frac{\theta_e}{\theta} - 1 = K \left(\frac{\bar{r}}{\bar{r}_e} - 1 \right) \qquad (8.8)$$

and solve (8.8) together with the open loop equations (7.8,7.9). These are ordinary differential equations and their numerical solution presents no expected difficulties.

Two numerical cases are given here, both having Mier

nucleation kinetics with exponent unity, and linear growth kinetics. In both cases, an initial disturbance is put on the system, and number density μ_o (normalized on μ_{oe}) is plotted against time t (normalized on θ_c). In Fig.16, we show a controllable case with

$$b/g = 14., \quad g = 460.$$

The stable range of K here is

$$-1.4 < K < 0.52$$

and we may see from Fig. 16 how a positive K outside this range seems to go into a limit cycle, while a negative K outside the range approaches numerically a second steady state solution. Inside the stable range, the numerical solution behave stably. In Fig. 17, we show an uncontrollable case, with

$$b/g = 63, \quad g = 490.$$

All the numerical cases here show limit cycle behavior.

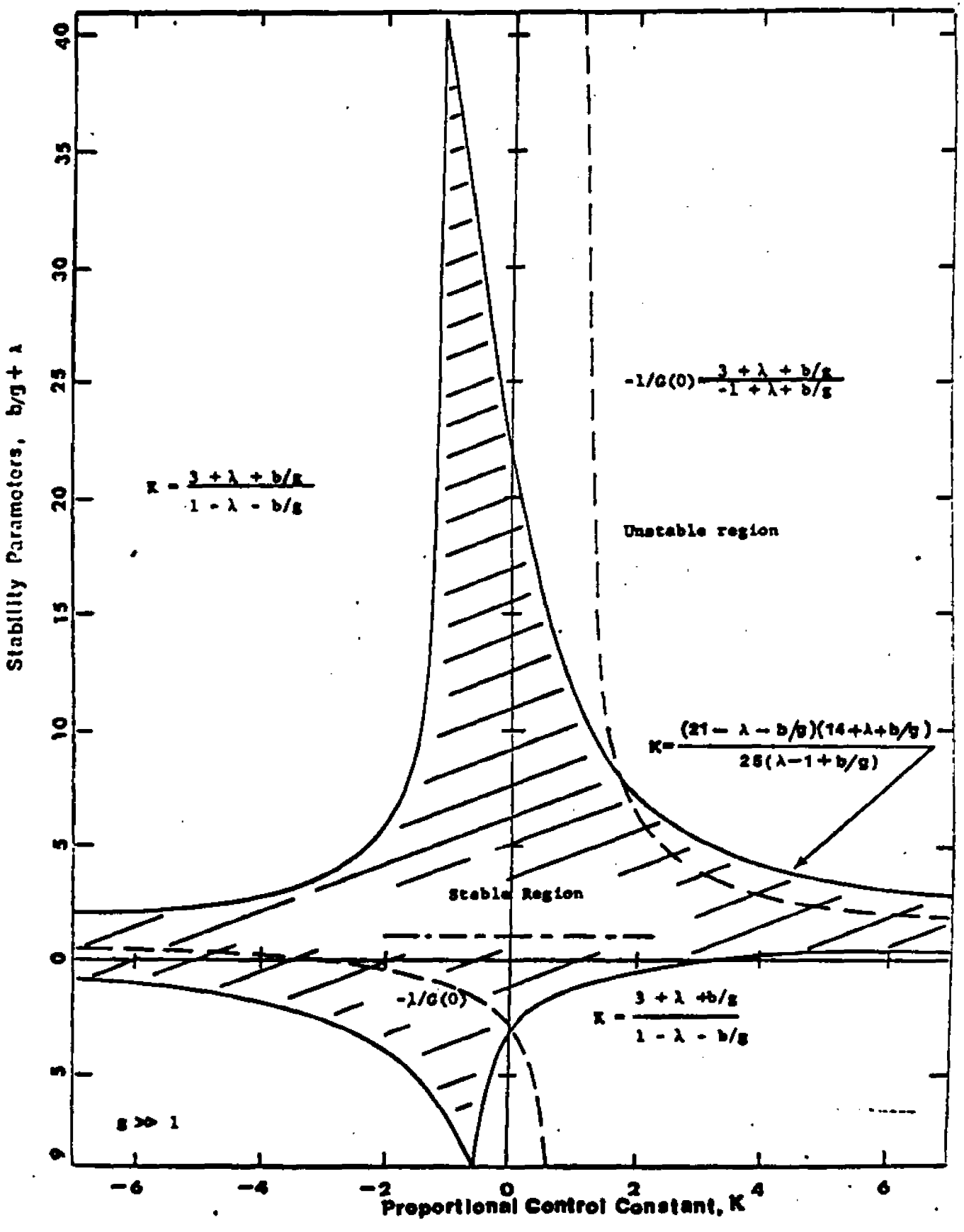

Figure 15 Stable Limits For Proportional Mean Size Controller

Figure 16 Illustrative Dynamics of A Mixed Crystallizer With Mean Size Controller: Controllable Case

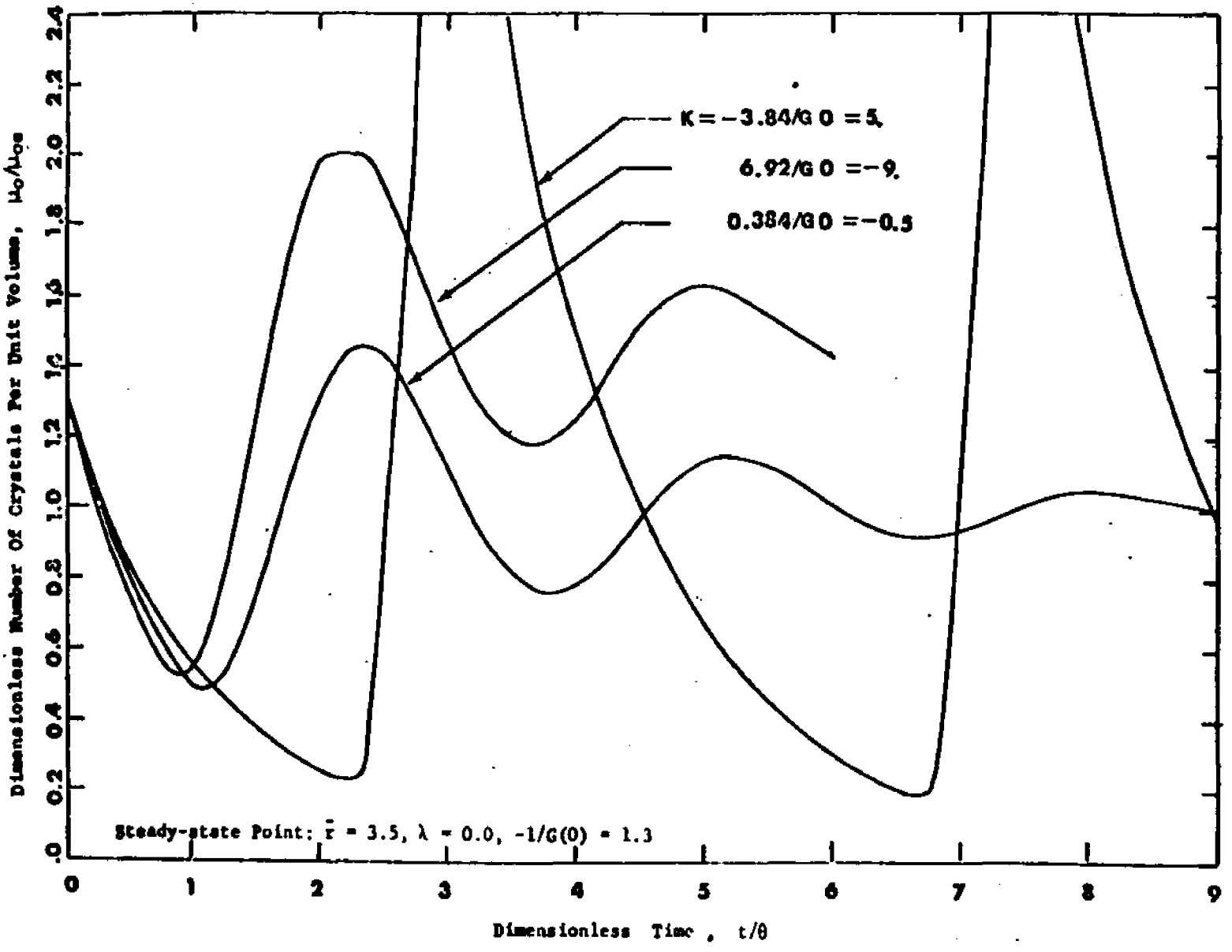

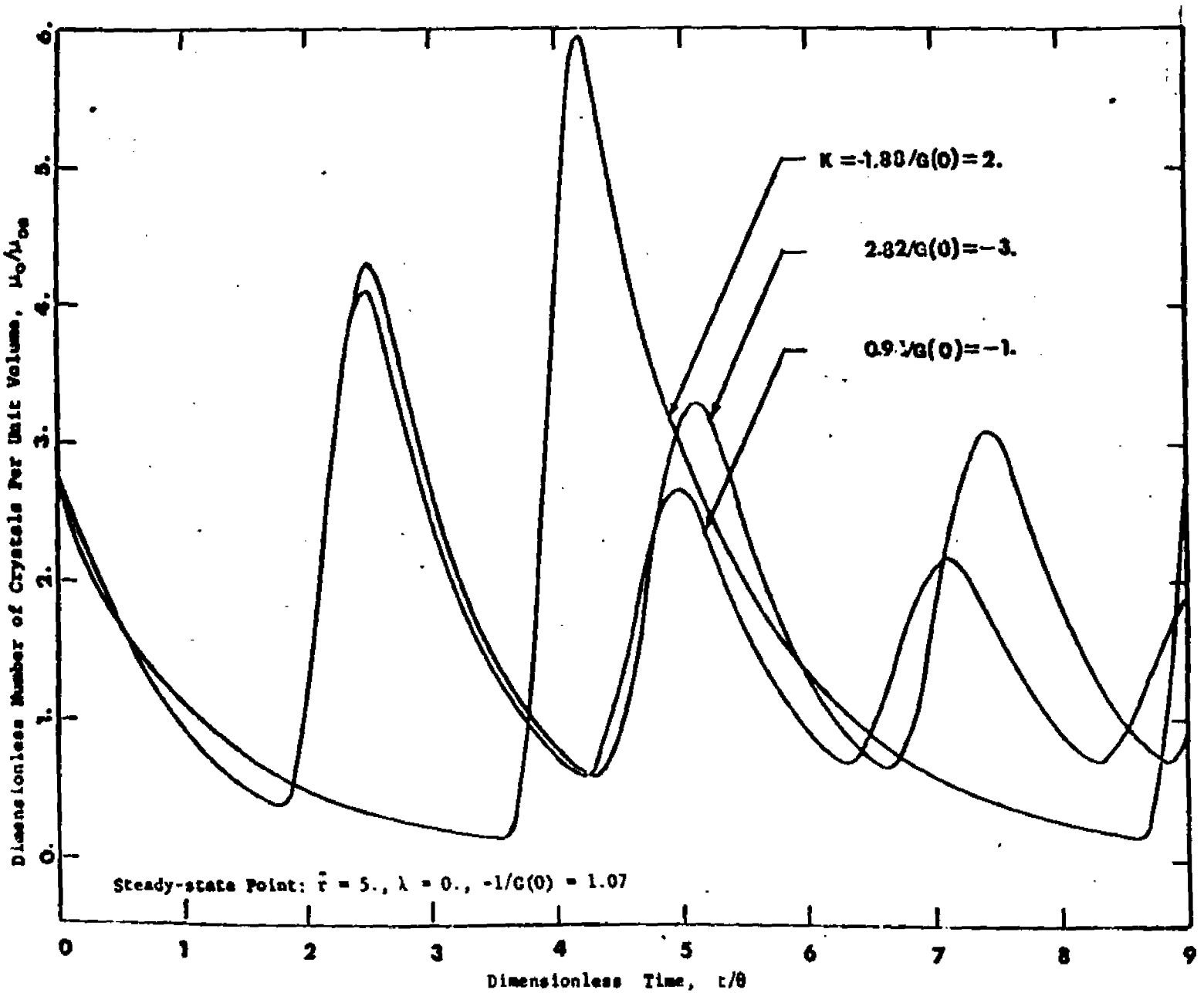

Figure 17 Illustrative Dynamics of A Mixed Crystallizer With Mean Size Controller: Uncontrollable Case

CHAPTER 9

Control On Crystal Surface

We analyze here a number of control systems based on measurement of a suitable crystal surface per unit volume, and manipulation of a flow rate. There are two directly measurable crystal surfaces at hand: σ, for the population of crystals overall; and σ_o for the fines only. There are as well two accessible flow rates: w, the bulk throughput; and w_o, the circulation rate through the fines trap. There are accordingly four different control configurations to be analyzed, and while stability conditions are given for all of them, our primary interest focuses on the two in which the fines surface σ_o is measured.

Before taking up the stability analyses proper, we show the form of the steady-state dependencies between the surfaces σ, σ_o on the one hand, and the flow rates w, w_o on the other. For a point fines trap, these relationships are all given by the steady-state form of eqns (7.5-7.9,7.14,7.15). Illustrative cases have been calculated, normalized on typical base values denoted by the subscript e. The calculations are all for linear growth kinetics, and for Mier nucleation kinetics with exponent 1. Fig.18 shows the relation between σ_o and w_o, and we see this to be a fairly complicated relationship. Not only does the slope of the curve through the base point

change sign as λ varies, but we see that the curves for a fixed θ are not monotone over their whole extent. The shape of these curves is of course slightly different for the finite fines trap, and Fig. 19 illustrates the order of this difference by showing how a typical curve of Fig. 18 is broadened in finite fines trap operation. Fig. 20 shows the relationship between σ and w_o, and we see that σ is a decreasing function of w_o. Figs. 21 and 23 show the dependencies of σ_o and σ on the bulk flow rate w for constant θ_o. We see that σ_o and σ are both increasing functions of w. Fig. 22 shows the broadening of a typical σ_o-w curve with finite fines trap operations.

We begin now an analysis of the σ_o - w_o controller, where the fines surface σ_o is measured and the recycle flow rate w_o manipulated. The instantaneous effect of increasing w_o is always to decrease σ_o. If we continue to operate with an increased w_o the supersaturation will increase. Depending on the value of b/g the new steady state will show either an increase or decrease in σ_o. Intuitively one would expect that a control scheme in which the instantaneous response has a different direction from the final steady state response cannot be successfully operated with a simple feed back controller. As will be later shown, one of the necessary condi-

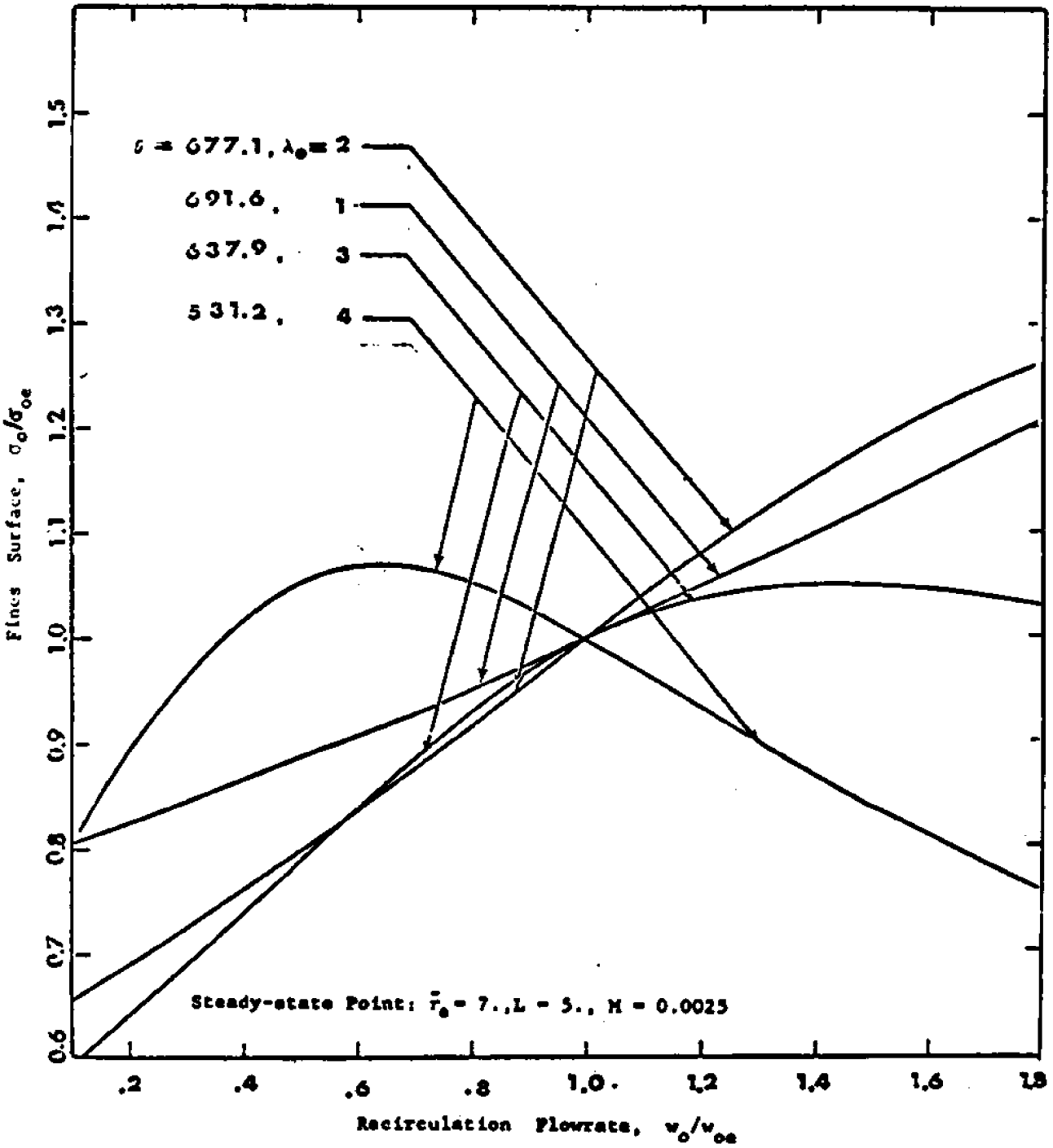

Figure 18 Illustrative σ_o - w_o Curves For A Crystallizer With Point Fines Trap

Figure 19 Broadening of The σ_o- w_o Curves for A Crystalliser With Finite Fines Trap

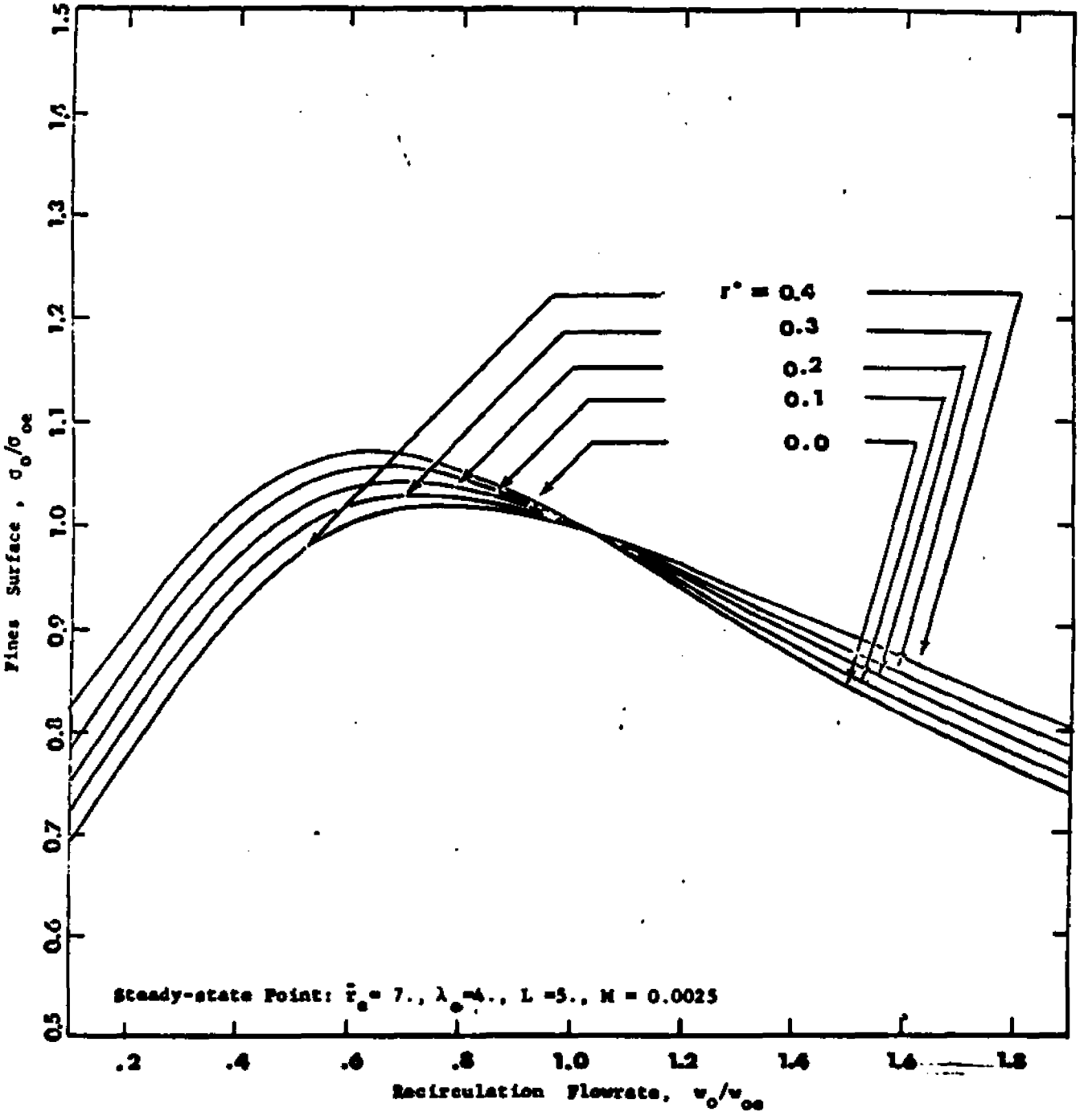

Figure 20 Illustrative - w_D Curves For A Crystallizer With Point Fines Trap

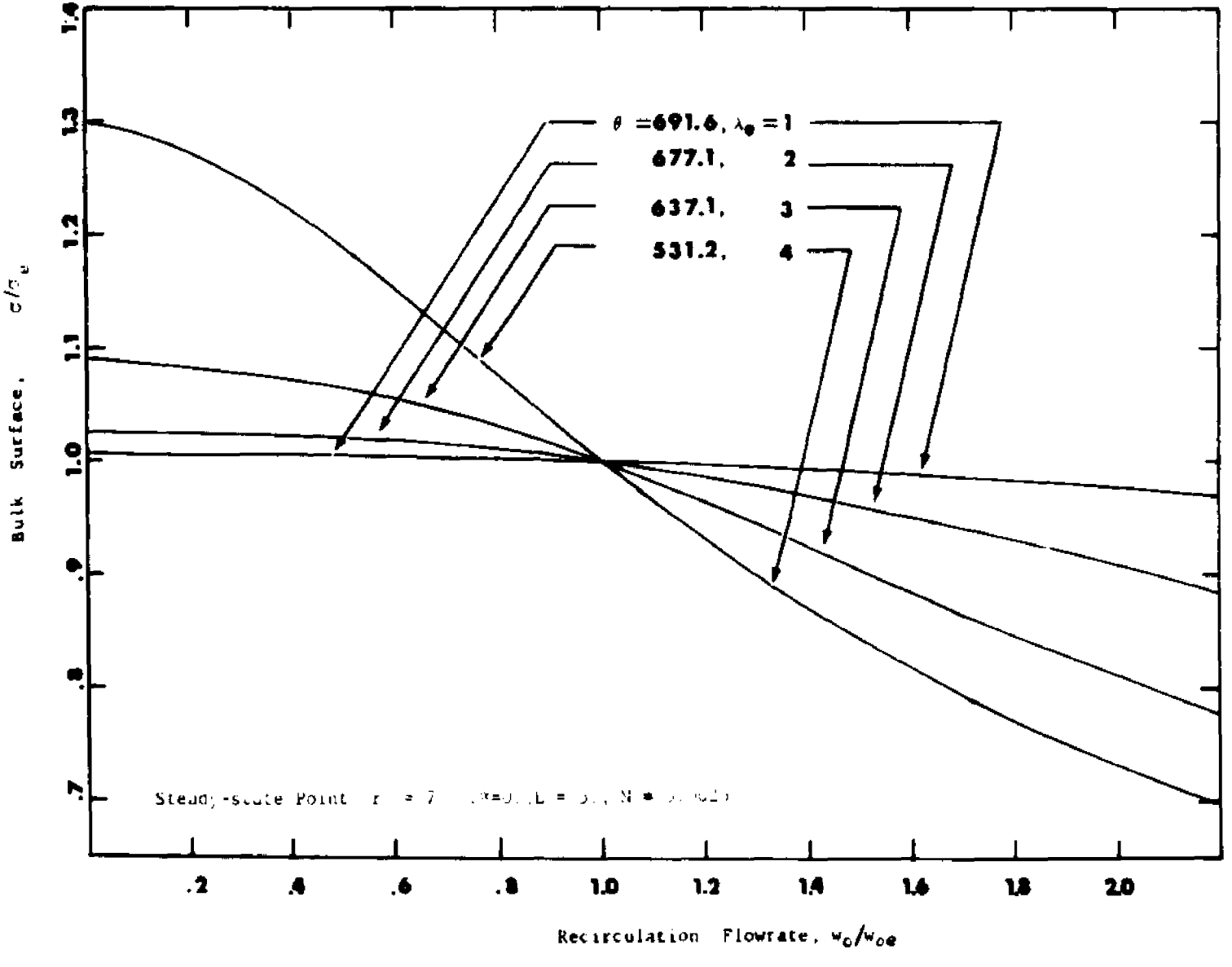

Figure 21 Illustrative σ_0 - w Curves for A Crystallizer With Point Fines Trap

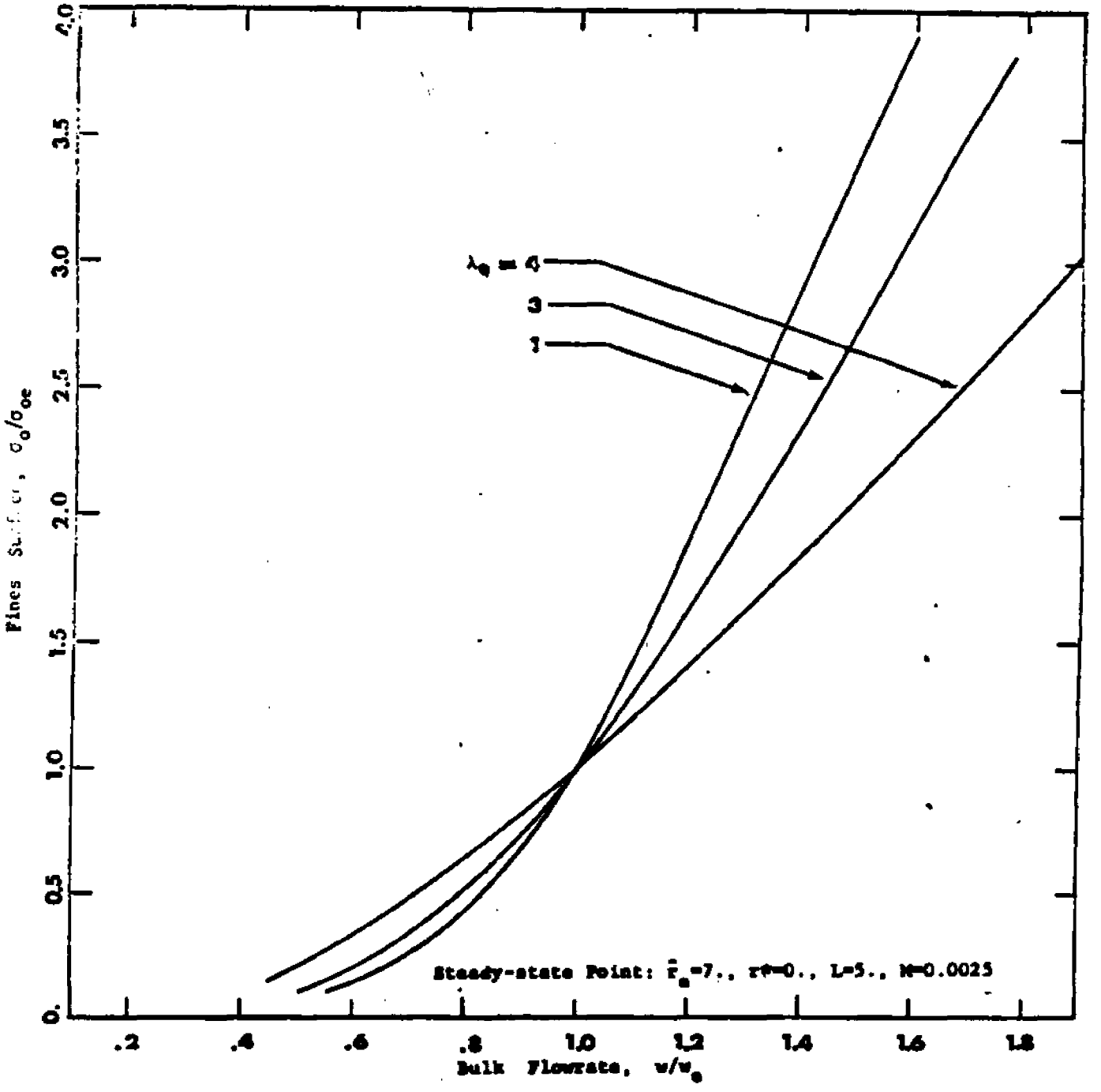

Figure 22 Broadening of The σ_o - w Curves for A Crystallizer With Finite Fines Trap

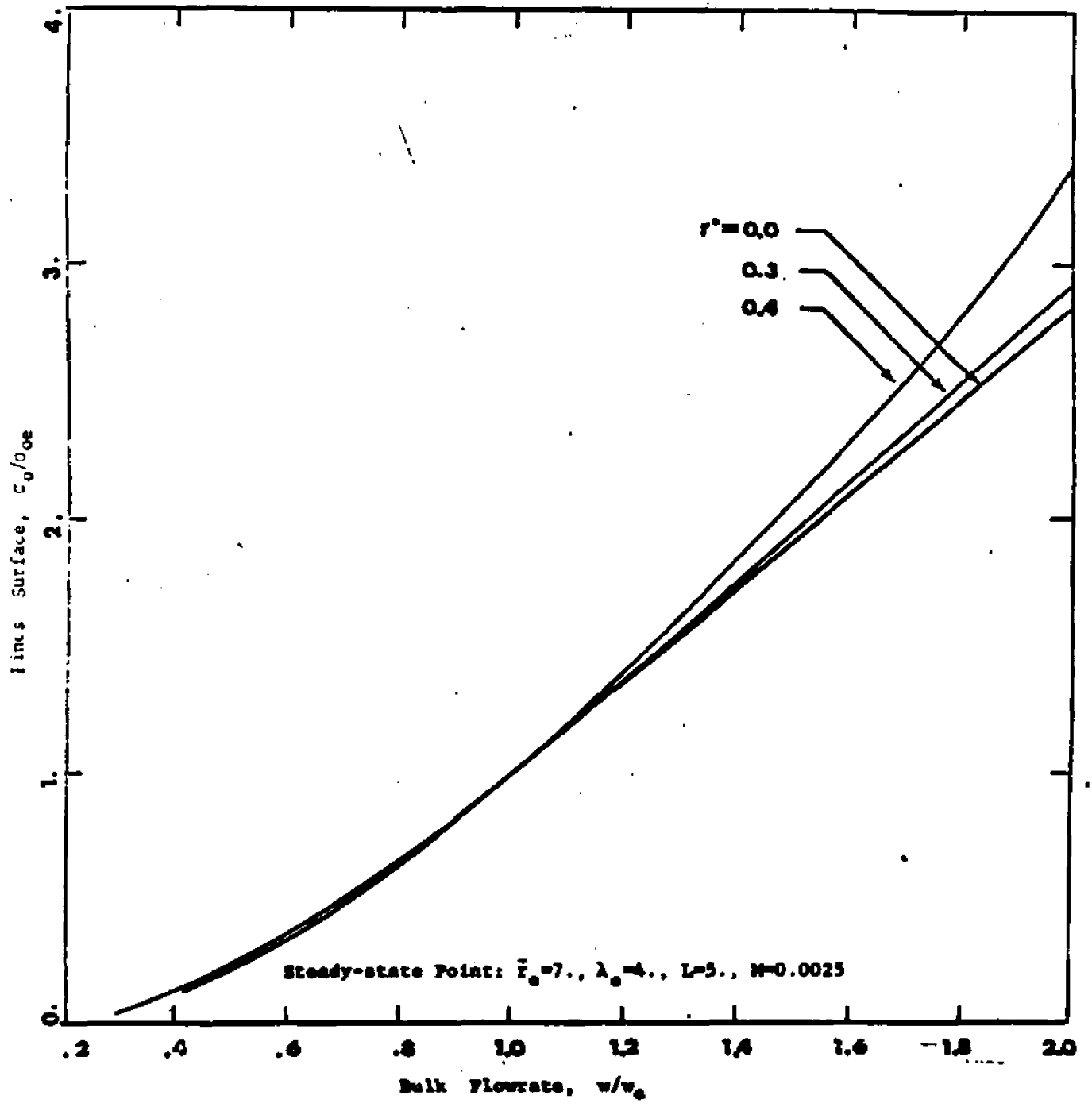

Figure 23 Illustrative σ - w Curves for A Crystalliser With Point Fines Trap

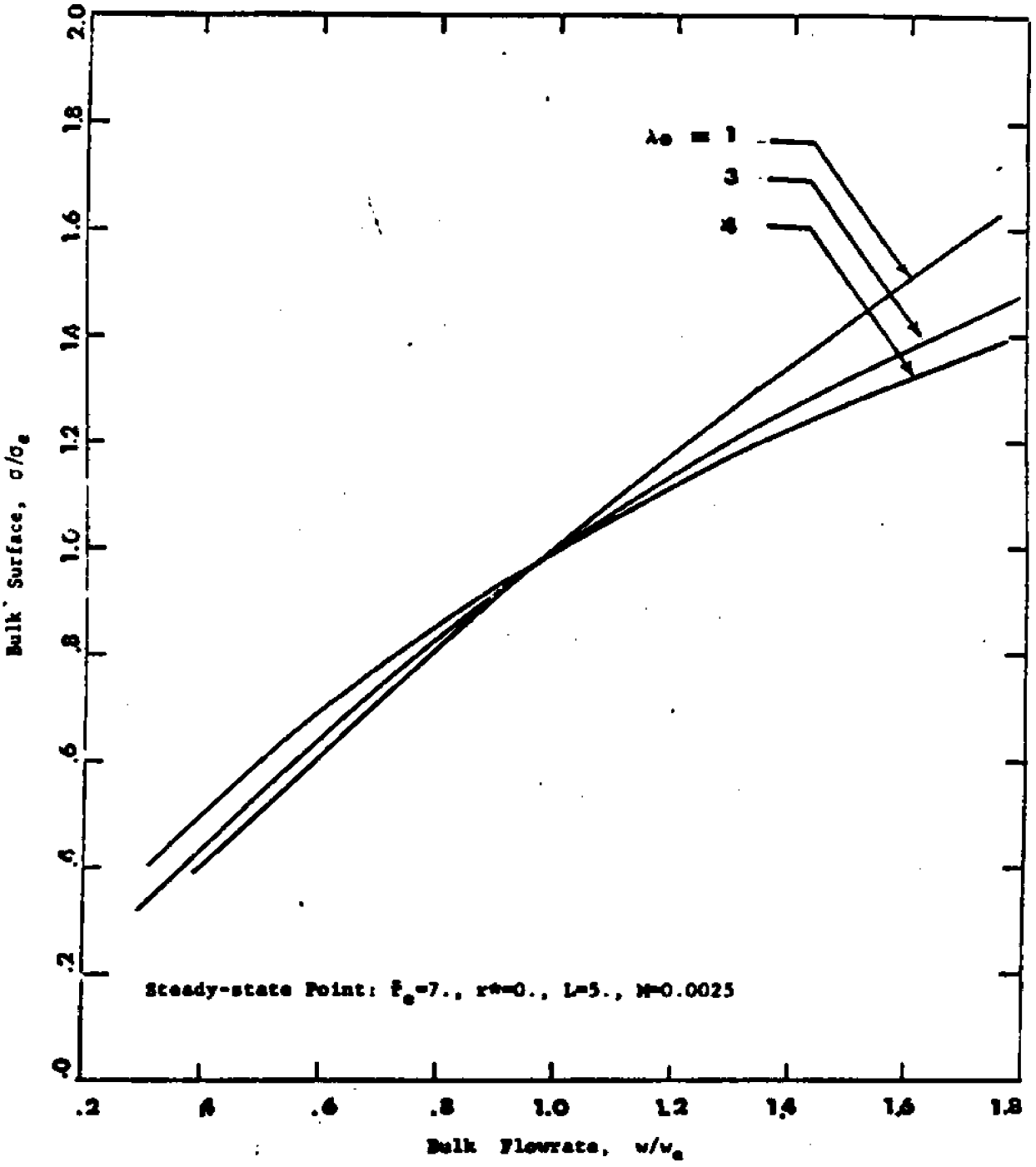

tions for a practical feed back controller case is that σ_o is a decreasing function of w_o. In Fig. 18 the operating lines are for a given explicit dependence of B and G on c. The slope of the dependence of σ_o on w_o is, however, a function of b/g only. The condition that this slope is negative , which is a necessary condition for control, can, therefore, be expressed in a model free way, and this we turn to next.

Now in the steady state operating lines of Fig. 18, we see that there is a locus of points where σ_o is a maximum. We can identify this locus in a model-free way by setting down the condition that the $\sigma_o - w_o$ transfer function of (7.23) vanish. This condition is:

$$\left(\frac{b}{g}\right)_{max} = \frac{3a + \lambda + a/ge^{-\lambda}}{\lambda - a}$$

For large b and g, with b/g finite, it reduces to

$$\left(\frac{b}{g}\right)_{max} = \frac{3a + \lambda}{\lambda - a}$$

and is shown as a b/g vs. λ plot in Fig. 24. For operating points below this curve, σ_o is a monotone decreasing function of w_o, above the curve, a monotone increasing function. The operating curves of Fig. 18 can be replotted in the (b/g) - λ plane of Fig. 24, and some typical cases are shown there.

We see that these operating curves are in general steeper than the locus of maximum σ_o, and lie below this locus for a considerable part or all of their range.

Accordingly, in carrying out the stability analysis for the σ_o - w_o controller, we adopt the feed back convention B of Fig. 14, associated with σ_o a decreasing function of w_o. That is, we take

$$\frac{\hat{\delta w}_o(s)}{w_o} = K(s) \frac{\hat{\delta \sigma}_o(s)}{\sigma_o} \tag{9.1}$$

where K(s) is the transfer function of the controller. The crystallizer transfer function G for this configuration

$$\frac{\hat{\delta \sigma}_o(s)}{\sigma_o} = G(s) \frac{\hat{\delta w}_o(s)}{w_o} \tag{9.2}$$

is given from (7.23) as

$$G(s) = \frac{\lambda(b-g)e^{-\lambda} - abe^{-\lambda} - age^{-\lambda} \sum_{i=1}^{3}(s+1)^i - a(s+1)^4}{(b+\lambda g)e^{-\lambda} + ge^{-\lambda} \sum_{i=1}^{3}(s+1)^i + (s+1)^4} \tag{9.3}$$

and the stability characteristic of the controlled system

$$1 - G(s)\, K(s) = 0$$

becomes

$$(1+aK(s))\left\{(S+1)^4 + ge^{-\lambda} \sum_{i=1}^{3}(s+1)^i\right\} + (b+\lambda g)e^{-\lambda} + K(s)\left\{(a-\lambda)be^{-\lambda} + \lambda ge^{-\lambda}\right\} = 0 \tag{9.4}$$

Figure 24 Locus of Maxima of $\sigma_o - w_o$ Curves for a Crystalliser with Point Fines Trap Together with Illustrative Operating Curves

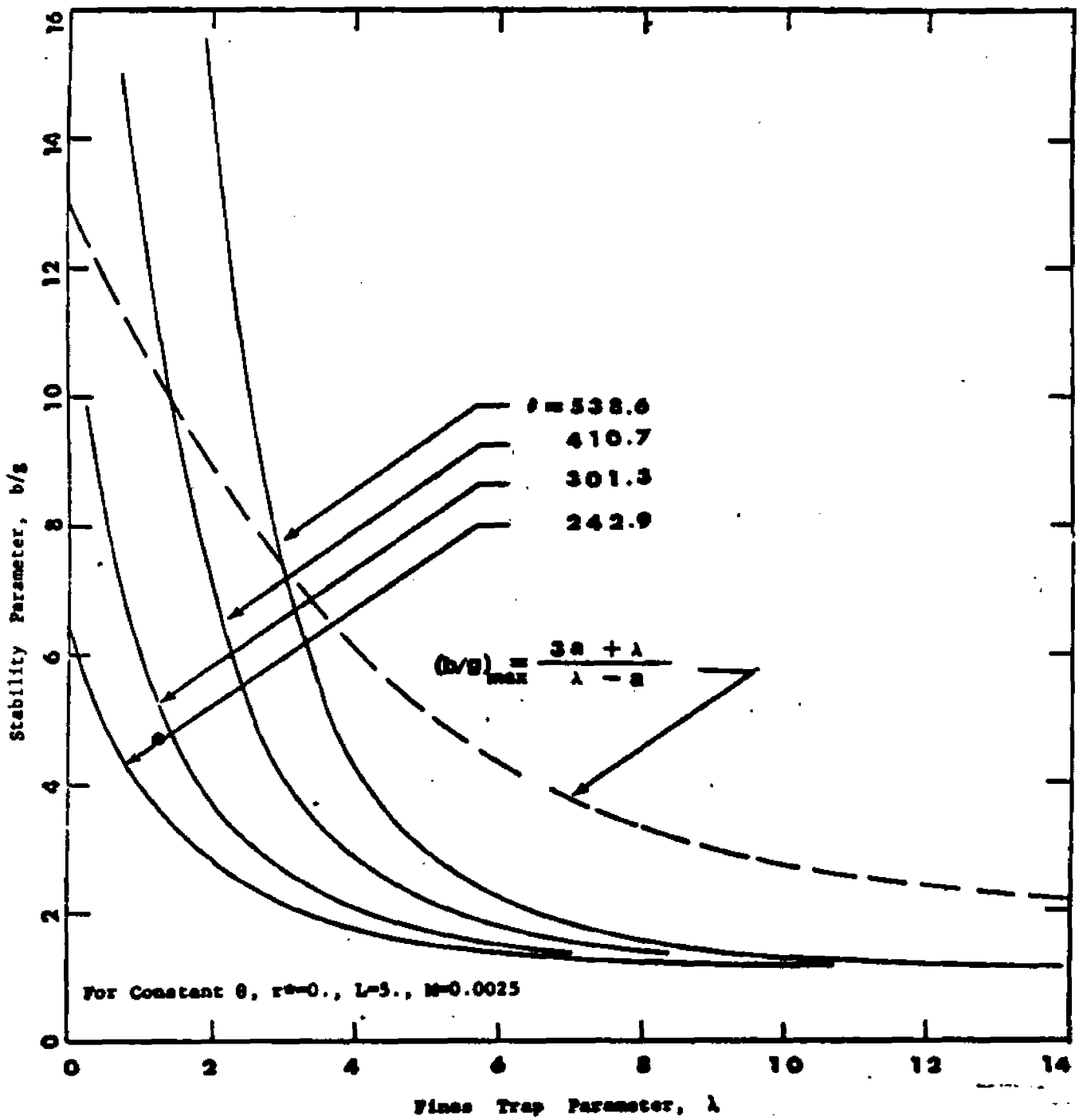

The controlled system is stable according as the characteristic equation (9.4) has all its roots with negative real part. For a proportional controller, where the transfer function K(s) is simply a constant K, we have a polynomial equation where stability can be tested by the Routh-Hurwitz criterion. We find that the condition that the $\sigma_o - w_o$ controller be stable is

$$-3-\frac{1}{ge^{-\lambda}} < \frac{\frac{b}{g}+\lambda+\left\{\lambda+(a-\lambda)\frac{b}{g}\right\}K}{1+aK} < \frac{21(ge^{-\lambda})^3+87(ge^{-\lambda})^2+128(ge^{-\lambda})+64}{ge^{-\lambda}(4+ge^{-\lambda})^2} \tag{9.5}$$

For large b and g, with b/g remaining finite, this simplifies to

$$-3 < \frac{\frac{b}{g}+\lambda+\lambda+(a-\lambda)\frac{b}{g}K}{1+aK} < 21 \tag{9.6}$$

The stable region described by (9.6) actually breaks up into two parts, as shown in Fig. 25. Shown as well in Fig. 25 is a plot of the static sensitivity of the system in the form

$$-\frac{\sigma_o}{w_o}\frac{dw_o}{d\sigma_o} = -\frac{1}{G(o)}$$

where, from (9.3)

$$\frac{-1}{G(o)} = \frac{\frac{b}{g}+\lambda+3}{(a-\lambda)\frac{b}{g}+\lambda+3a} \tag{9.7}$$

The practical operating portion of Fig. 25 is the shaded stable zone in the lower right hand corner lying above the positive K-axis, and below the asymptote of $-1/G(0)$. (This asymptote is also the locus of maxima of steady state $\sigma_o - w_o$ curves). The other stable zones shown are not practically useful, since in them K has the same sign as G(0), the controllers are in effect amplifiers (albeit stable amplifiers), and there is the possibility that they introduce extra steady-state solutions. The practical operating zone corresponds as we see to a mode of operation where σ_o is a decreasing function of w_o, and the operation is open loop stable. We see further from Fig. 25 that it is possible to stabilize unstable modes of operation with arbitrarily large values of b/g, but only by going into the amplifying range of K, and even then working in increasingly narrow bands around $K = 1/(\lambda-a)$. We note, therefore, that this control mode cannot be used to stabilize a system which is unstable due to kinetic reasons (b/g large). It can, however, stabilize a system which is unstable due to a high value of λ, if b/g is small.

We turn next to the σ_o-w controller, where the fines surface σ_o is measured and the bulk flow rate w manipulated. We see from Fig. 21 that σ_o is an increasing function of w. Accord-

ingly, we adopt the feedback convention A of Fig.14 and take

$$\frac{\delta\hat{w}(s)}{w} = - K(s) \frac{\delta\hat{\sigma}_o(s)}{\sigma_o} \tag{9.8}$$

where K(s) is the transfer function of the controller. The crystallizer transfer function G for this configuration

$$\frac{\delta\hat{\sigma}_o(s)}{\sigma_o} = G(s) \frac{\delta\hat{w}(s)}{w} \tag{9.9}$$

is given from (7.23) as

$$G(s) = \frac{(b+ag-g)\, e^{-\lambda} \sum_{i=o}^{3} (s+1)^i}{(b+\lambda g)e^{-\lambda} + ge^{-\lambda} \sum_{i=1}^{3} (s+1)^i + (s+1)^4} \tag{9.10}$$

and the stability characteristic of the controlled system

$$1 + G(s)K(s) = 0$$

becomes

$$(s+1)^4 + ge^{-\lambda} \sum_{i=1}^{3} (s+1)^i + (b+\lambda g)e^{-\lambda} + K(s)(b+ag-g)e^{-\lambda} \sum_{i=o}^{3} (s+1)^i$$

$$= 0 \tag{9.11}$$

For simple proportional control, K(s) = K, a constant, the stability characteristic (9.11) is simply a polynomial, and the Routh-Hurwitz criterion gives us directly the stability conditions for the σ_o-w controller. We have

Figure 25 Illustrative Stable Limits For A Proportional $\sigma_o - w_o$ Controller

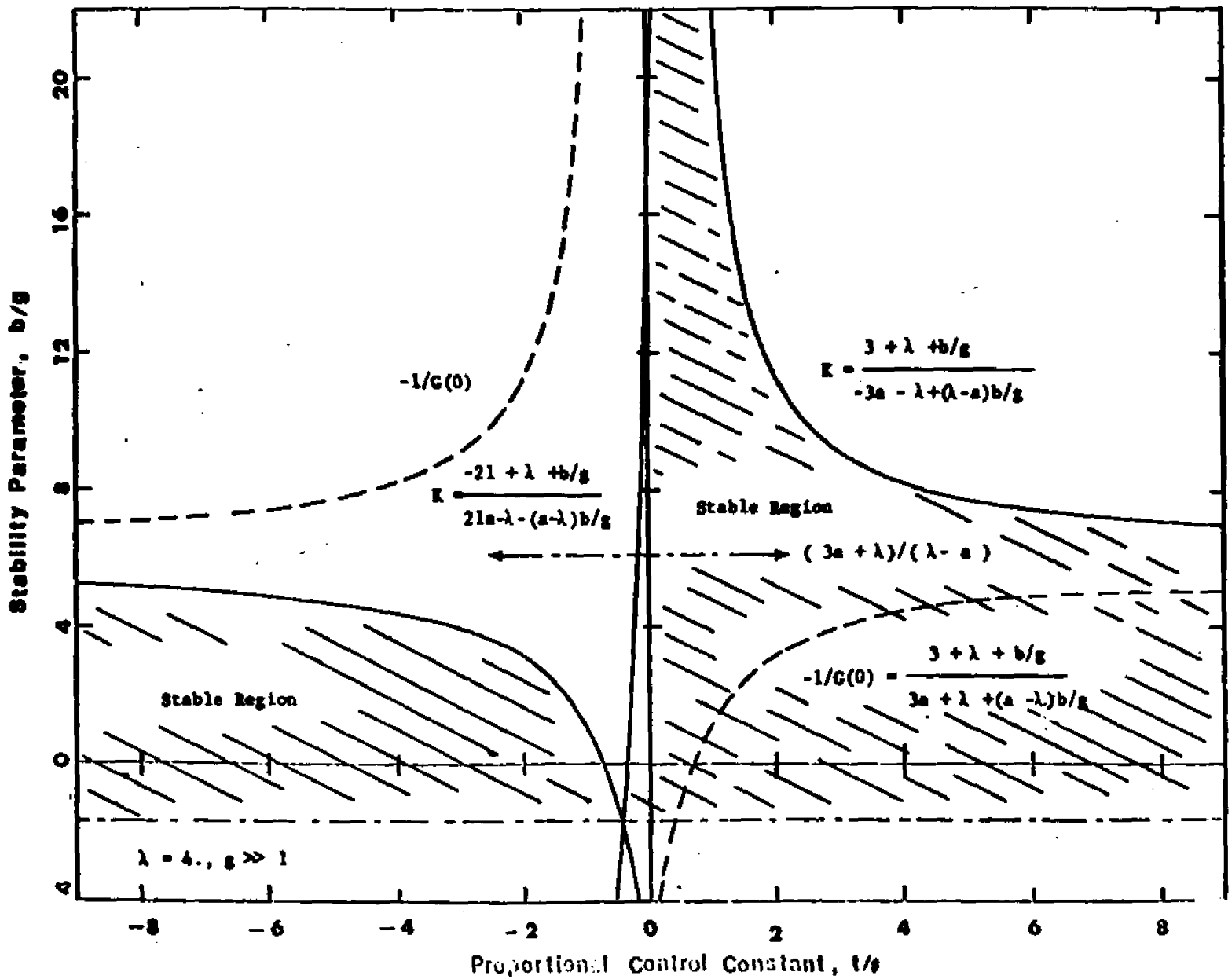

$$\frac{21x^3 + 87x^2 + 128x + 64}{x(x+4)^2} > \frac{\frac{b}{g} + \lambda + K\left(\frac{b}{g} + a - 1\right)}{1 + K\left(\frac{b}{g} + a - 1\right)} \qquad (9.12)$$

$$x = ge^{-\lambda} + K(b+ag-g)\, e^{-\lambda}$$

The stability condition can be seen a little more intuitively for large b, g with b/g finite. The condition (9.12) reduces in this limiting case to

$$k > \frac{1}{20} \quad \frac{\frac{b}{g} + \lambda - 21}{\frac{b}{g} + a - 1} \qquad (9.13)$$

and Fig. 26 shows the stable region described by (9.13). Fig.26 shows as well a plot of the static sensitivity of the system to serve as a standard against which to measure K. The sensitivity is in the form

$$\frac{\sigma_o}{w} \quad \frac{dw}{d\sigma_o} = \frac{1}{G(o)}$$

where, from (9.10)

$$\frac{1}{G(o)} = \frac{\frac{b}{g} + \lambda + 3}{4\left(\frac{b}{g} + a - 1\right)} \qquad (9.14)$$

The most striking feature of the σ_o - w controller is that every mode of operation can readily be stabilized by taking a proportional controller with gain K in a suitable range. We see from Fig. 26 that K > 1/20 gives stable operation for every

b/g. This is a very small value compared with the sensitivity index $1/G(0)$. Further, the stable range is positive, and hence can lead to no extraneous solutions.

We conclude the stability analyses with a brief discussion of the controllers in which the overall fines surface σ is measured and one of the flow rates w_o or w is manipulated. For the σ - w_o controller, we see from Fig. 20 that σ is a decreasing function of w_o. Accordingly we adopt the feedback convection B of Fig. 14 and write

$$\frac{\hat{\delta w}_o}{w_o} = K \frac{\hat{\delta\sigma}}{\sigma} \tag{9.15}$$

With the transfer function $G(s)$

$$\frac{\hat{\delta\sigma}}{\sigma} = G \frac{\hat{\delta w}_o}{w_o} \tag{9.16}$$

given from (7.22), the stqbility characteristic

$$1 - GK = 0$$

becomes

$$(s+1)^4 + ge^{-\lambda} \sum_{i=1}^{3} (s+1)^i + (b+\lambda g)e^{-\lambda} + \lambda K(s+1+ge^{-\lambda}) = 0 \tag{9.17}$$

and an application of the Routh-Hurwitz criterion gives for the stability condition with proportional control and large b, g with b/g finite,

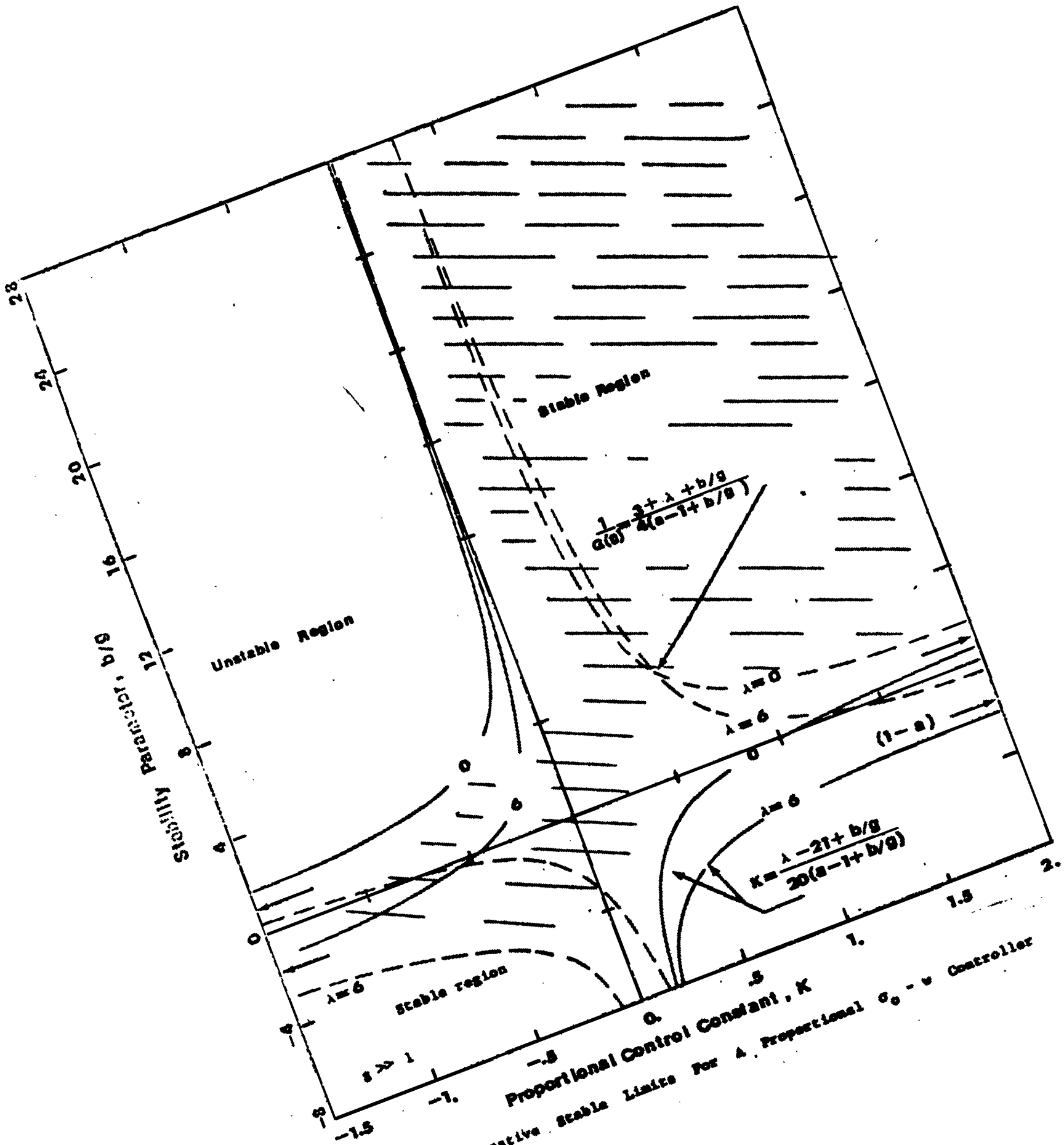

Figure 26 Illustrative Stable Limits For A Proportional σ_o - w Controller

$$\frac{21-\frac{b}{g}-\lambda}{\lambda} > K > -\frac{3+\lambda+\frac{b}{g}}{\lambda} \qquad (9.18)$$

As before we need for good control $K > -1/G(o)$ or

$$k > \frac{3+\frac{b}{g}+\lambda}{\lambda}$$

We note that this is possible as long as $21 - b/g - \lambda > 3 + b/g + \lambda$. Therefore, such a control is possible only for $(b/g + \lambda) < 9$. On the other hand, to insure that K is not excessively large, $(3 + b/g + \lambda)/\lambda$ should be no more than two or three. This control scheme therefore requires a minimum value of λ, which depends on b/g. One has, therefore, to be very careful in operating this control scheme, as the stability margins ($k_{max}/(-1/G(o))$ are quite small. A similar control scheme ($\bar{r} - w_o$) is often used for manual control, and similar considerations apply to this case.

For the σ - w controller, we see from Fig. 23 that σ is an increasing function of w. Accordingly we adopt the feedback convention A of Fig. 14 and write

$$\frac{\hat{\delta w}}{w} = -K\,\frac{\hat{\delta\sigma}}{\sigma} \qquad (9.19)$$

With the transfer function G(s)

$$\frac{\hat{\delta\sigma}}{\sigma} = G\,\frac{\hat{\delta w}}{w} \qquad (9.20)$$

given from (7.22), the stability characteristic

$$1 + GK = 0$$

becomes

$$(s+1)^4 + ge^{-\lambda} \sum_{i=1}^{3} (s+1)^i + (b + \lambda g)e^{-\lambda}$$

$$-K\left\{ \sum_{i=1}^{3} (s+1)^i + ge^{-\lambda} - (b+\lambda g)e^{-\lambda} \right\} = 0 \qquad (9.21)$$

and an application of the Routh-Hurwitz criterion gives for the stability condition with proportional control for large b, g and finite b/g

$$-\frac{\frac{b}{g} + \lambda + 3}{\frac{b}{g} + \lambda - 1} < K < \frac{21 - \frac{b}{g} - \lambda}{\frac{b}{g} + \lambda - 1} \qquad (9.22)$$

$(-1/G(o))$ for this case is equal to $(3+b/g+\lambda)/(1-b/g-\lambda)$. We note that this case is very similar to the control scheme $\bar{r}$-w, discussed in Chapter 8, and has the same disadvantages. It cannot be used to stabilize an unstable system, and is not applicable if b/g is close to unity.

The two last controllers do not as we see have any especially useful or interesting stable ranges, and we accordingly drop them from further consideration.

We conclude our stability analysis of the crystal surface controllers by seeing how the nonlinear system responds to them. Our first illustrative calculations are for the

application of the proportional σ_o-w_o and σ_o-w controllers to a crystallizer with point fines trap. The method of calculation is by means of the moment equations (7.9) as for the crystal size controller discussed earlier. The calculation proceeds by putting an initial disturbance on the system and solving the differential equations forward in time. The results are presented as plots of number density μ_o (normalized on μ_{oe}) versus time t (normalized on θ_e). Several cases have been calculated, all with linear growth kinetics and with Mier nucleation kinetics with exponent 1. In all cases, where the linear analysis indicated stability, the numerical calculations showed stable behavior. Where the linear analysis indicated instability, the numerical calculations showed sometimes cyclic behavior, sometimes (the sign of K permitting) the approach to an extraneous steady state. Fig. 27 shows a case, unstable in open loop, stabilized by various values of the σ_o- w feedback gain. Fig.28 shows a stable case, regulated by various of the σ_o - w feedback gain. In Fig. 29, we take up the σ_o - w_o controller, and for the same stable case as in Fig. 28, show how the operation is regulated by various values of the feedback gain.

The calculations for the finite fines trap crystallizer with proportional σ_o - w_o control conclude the present analysis.

The calculation are made by means of the full nonlinear partial differential equations of the system, as in the open loop dynamic calculations of our prior work. The plots again show μ_o (normalized on μ_{oe}) against t(normalized on θ_e). In Fig. 30, we present calculat ons about a stable steady-state point where σ_o is a decreasing function of w_o. The λ and b/g here are the same as in Figs. 28, 29 and we may see how this case is again regulated by positive values of the feedback gain.

Figure 27-1 Illustrative Dynamics of A Point Fines Trap Crystallizer With σ_o - w Control : Unstable Case

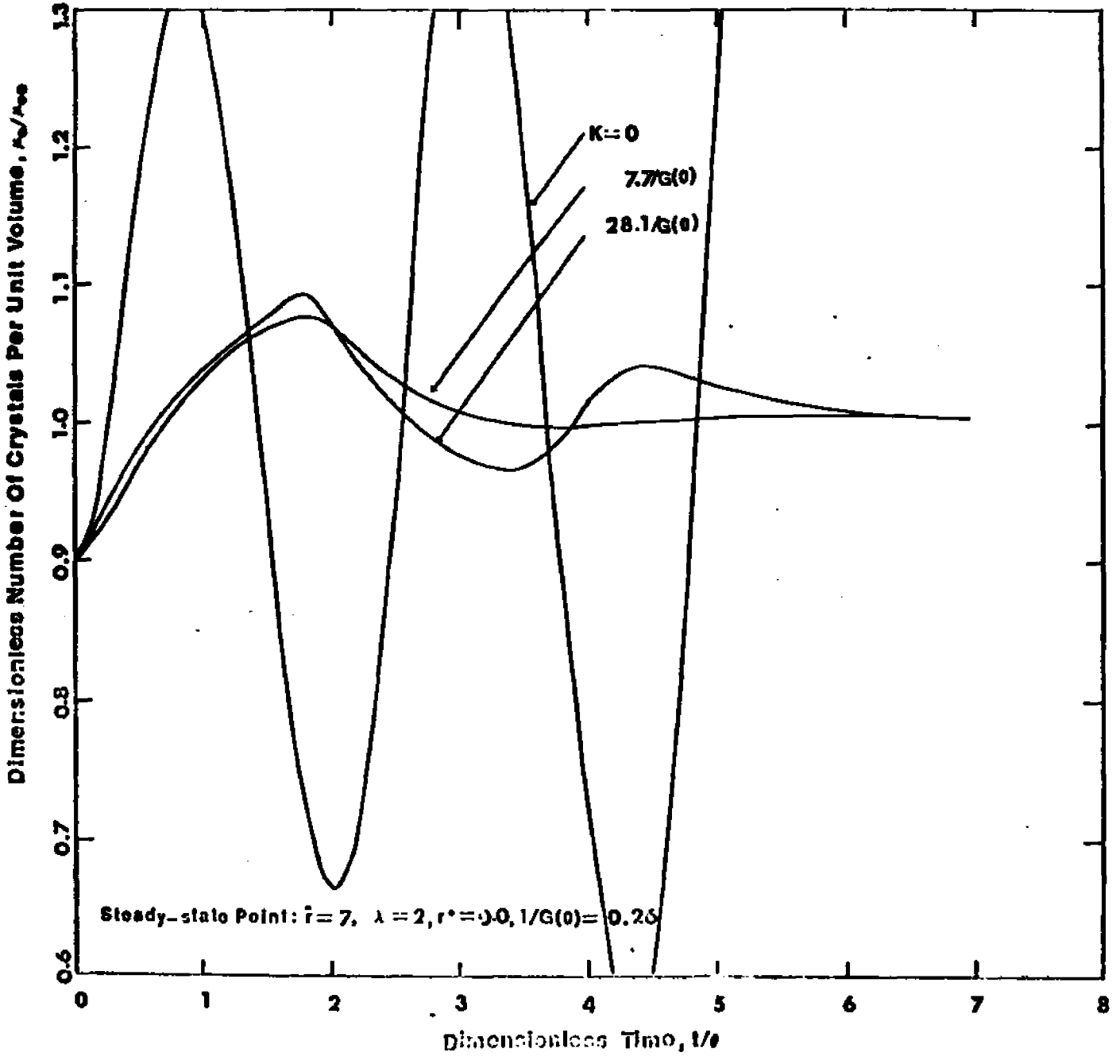

Figure 27-2 Illustrative Dynamics Of A Point Fines Trap Crystallizer With σ_o - w Control : Unstable Case

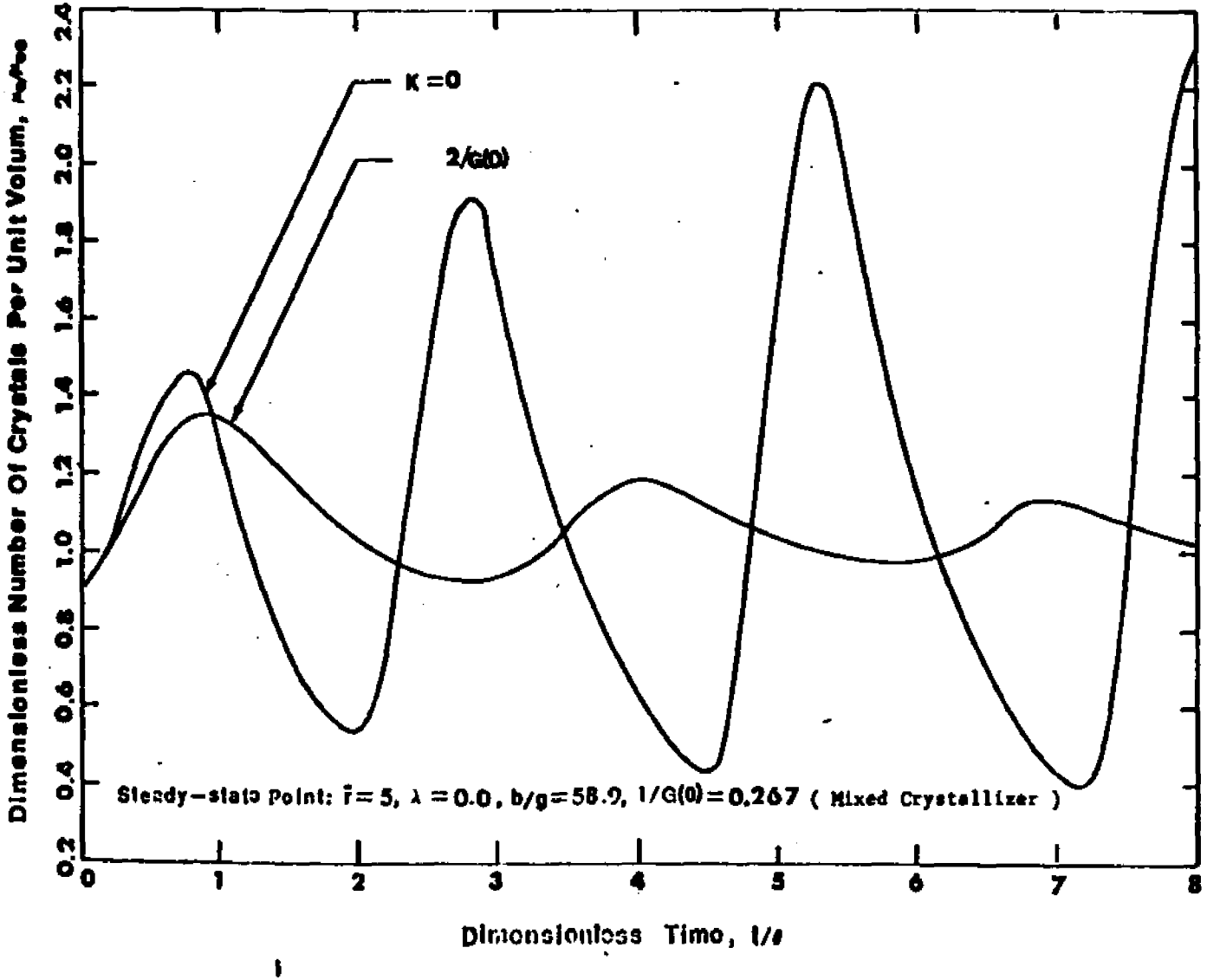

Figure 28-1 Illustrative Dynamics Of A Point Fines Trap Crystallizer With

σ_o - w Control: Stable Case

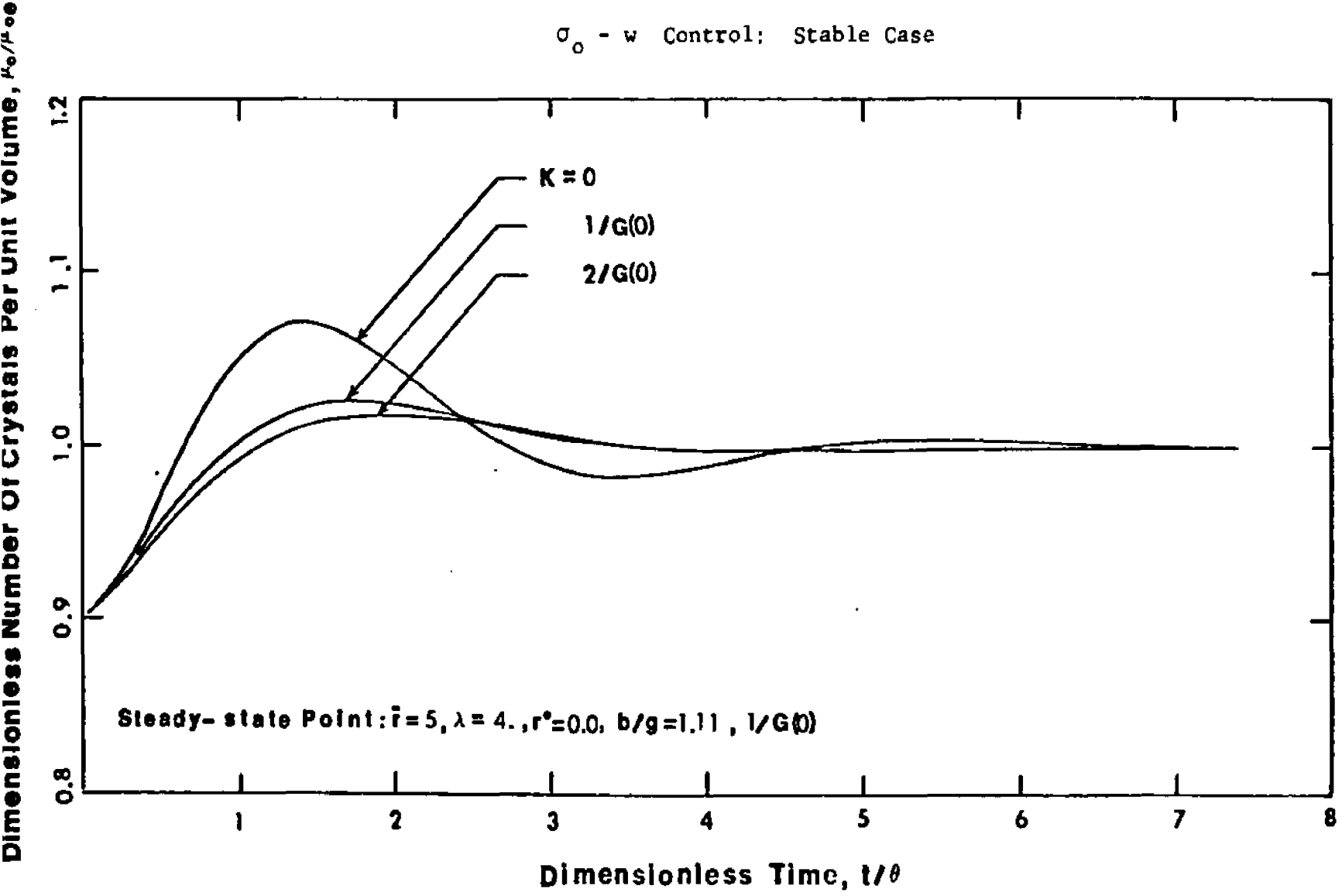

Figure 28-2 Illustrative Dynamics Of A Point Fines Trap Crystallizer With

σ_o - w Control : Stable Case

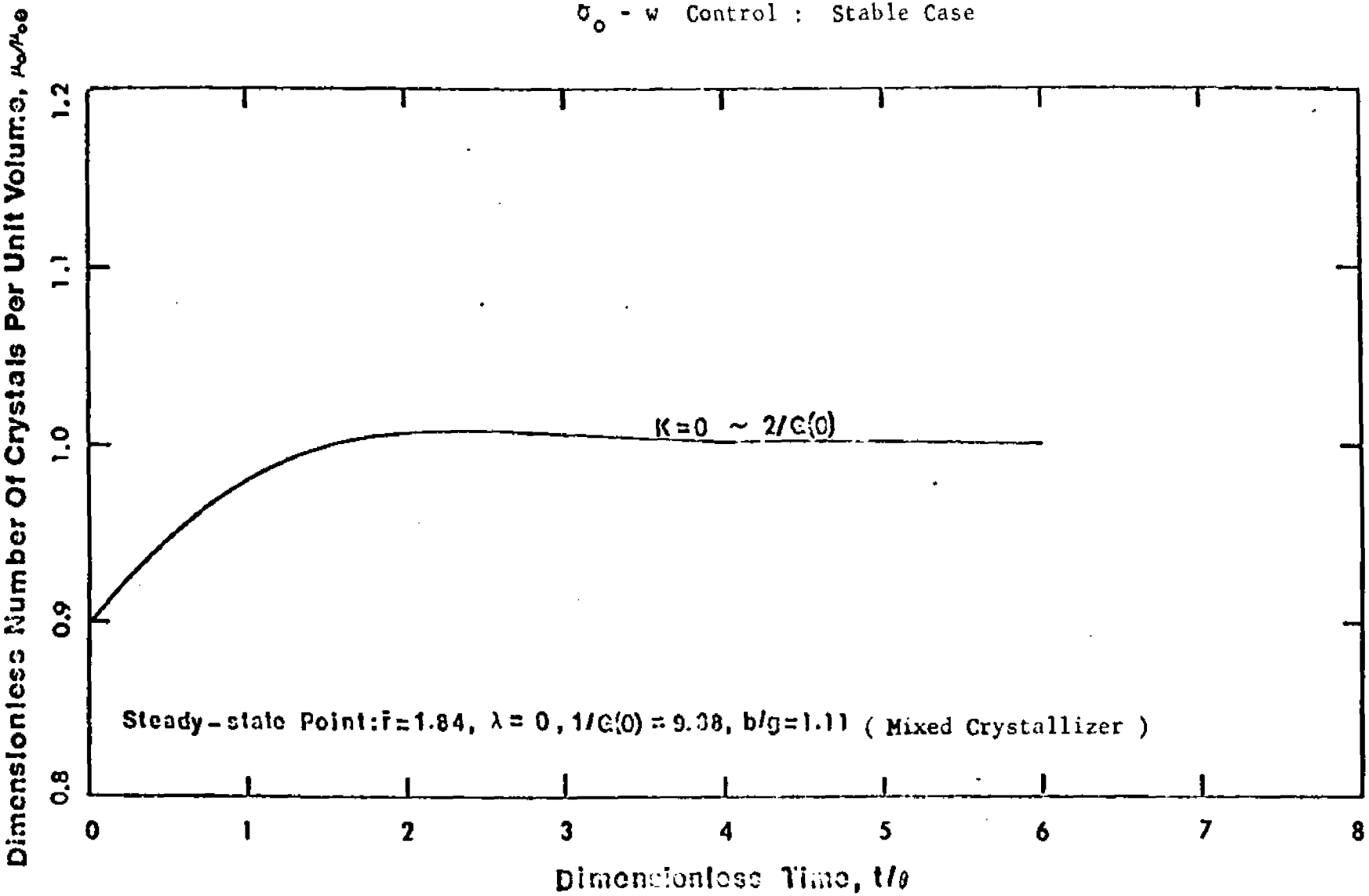

CHAPTER 10

Discussion of Closed-Loop Operation

The control schemes investigated here all control a flow rate. The two flow rates chosen were the flow rate to the crystallizer and the flow rate through the fines trap. Both methodes can lead to satisfactory control schemes. The most important factor in achieving a satisfactory control is the measured variable. Measuring overall properties of the product mix leads very often to difficulties. In the absence of a fines trap, such a scheme is practical in a very narrow range of b/g ($3 < b/g < 7$). With a fines trap one can control the flow through the fines trap, measuring some parameter of the overall particle size distribution. This is often done in practice by the operator. As shown in the text this is satisfactory as long as the system in the absence of control is stable. To achieve a reasonable control action, $(b/g + \lambda)$ must be less than nine for an ideally mixed crystallizer. If these is any classification occurring, $(b/g + \lambda)$ must be considerably less than in the stable limit without control. One notes, therefore, that it is quite easy for the operator to introduce instabilities by using a too large control action ($K = -(1/G(o))$ will already be unstable in many cases).

There is a strong advantage in using a control based on the parameters of the stream leading to the fines trap such as

σ_o. This is not surprising as σ_o for a point fines trap measures a quantity related to the instantaneous nucleation rate. The time delay between a perturbation in nucleation rate and the time a significant effect on overall size distribution is noticed is thereby eliminated. It is this time delay which makes control schemes based on the properties of the total crystal mix so difficult to operate especially at higher values of b/g. In a real and finite fines trap this time delay is not zero but related to r_o/G. As long as r_o is small compared to the average particle size, this time delay will have a relatively small effect. Measurement of any overall property of the size distribution in the fines trap will lead to superior control than use of a corresponding property of the size distribution in the crystallizer itself. The total surface σ_o in the fines trap was chosen as it is relatively easily accessible, by light transmission measurement, but if other properties such as total crystal mass in the fines trap are available they could serve just as well.

What is somewhat surprising in the results are the complications arising when the flow through the fines trap, or in other words, the amount of fines destroyed is used as a control variable. This is due to the fact that for variable flow through

the fines trap, σ_o is not uniquely related to the instantaneous nucleation rate. The initial effect of sudden increase of w_o is always to decrease σ_o, as more crystals are destroyed in the trap. After some time the decreased effective nucleation rate will cause an increase in supersaturation, thereby increasing the real nucleation rate. The effective nucleation rate (the amount surviving to a size larger than r_o) will always decrease as w_o is increased, but σ_o will not necessarily decrease. In facr for h gh values of b/g it increases. This has a simple explanation. For high values of b/g a small change in supersaturation cuases a high increase in nucleation rate. Fewer will survive than before but the stream entering the fines trap will have a larger number of samll crystals. At high values of w_o, b/g always decreases and therefore, at high values of w_o we will always reach a region in which the static $d\sigma_o/dw_o$ is negative. To insure stable and effective control one has to insure that the instantaneous and the static responses in the same direction. If b/g ($\lambda = 0$) is less than (13) this is true for every w_o and this control is satisfactory. The system is stable and as shown in Fig. 29 shows a fast and smooth response. Though the system is always stable we would prefer to avoid the region in which -1/G(o) is large as in this case

a large K has to be used. We want to be in an area where σ_o is sensitive to w_o.

For $\lambda = 4$, and b/g less than 3, $-1/G(o)$ is less than unity and as all K are stable this leads to a good and smooth control, as can be seem from Fig. 29 and 30. Now fines traps are very often used to increase particle size in systems in which b/g ($\lambda = 0$) is close to unity. For such cases this control scheme has significant advantages as upsets in nucleation are reduced before they effect the particle size.

If the control is used to stabilize unstable systems, then a σ_o-w controller seems to have significant advantages. If the instability is due to a too high value of λ, and the system is stable for $\lambda = 0$, then the σ_o- w_o control can be used to both control and stabilize the crystallizer.

All of our above considerations start with ideally mixed crystallizers. One could use the same method to study a classified crystallizer, but this is outside the scope of this study. However, the results allow some intuitive comments. For all controls involving the overall size distribution the stability limit $21 - (b/g + \lambda)$ determines the allowable value of K, and as no stabilization is possible, also the limit of stable control. Partial classification which always occurs in all crystallizers

will therefore reduce the range of stable operation (which is already very limited for the ideal case). In the case of the fines trap control we have a control circuit around the fines trap maintaining a stable nucleation rate, and one would therefore expect that with a sufficiently large K one should be able to stabilize the system even in the presence of classification. Such arguments are however speculative and await confirmation.

Figure 29 Illustrative Dynamics Of A Point Fines Trap Crystallizer With

$\sigma_o - w_o$ Control

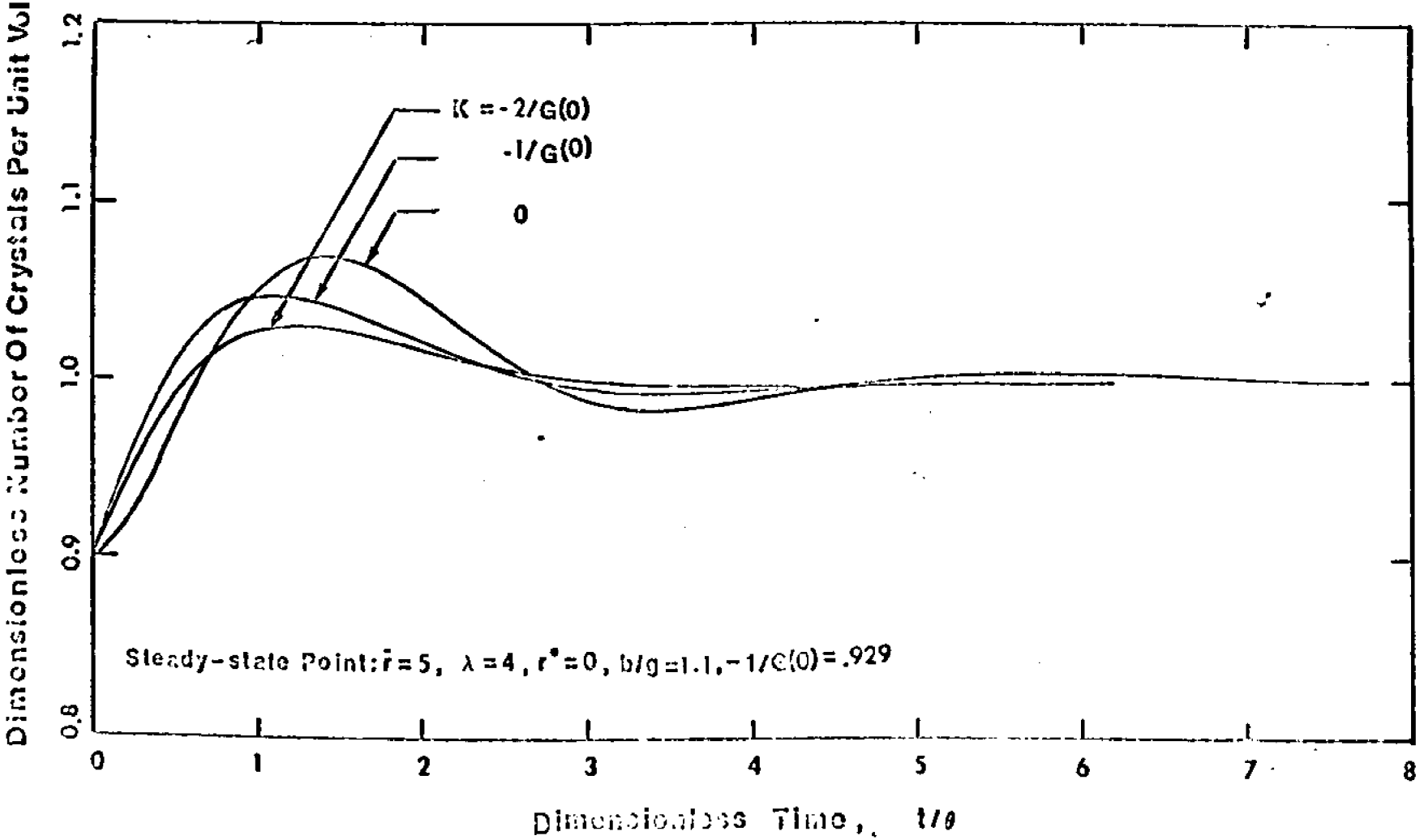

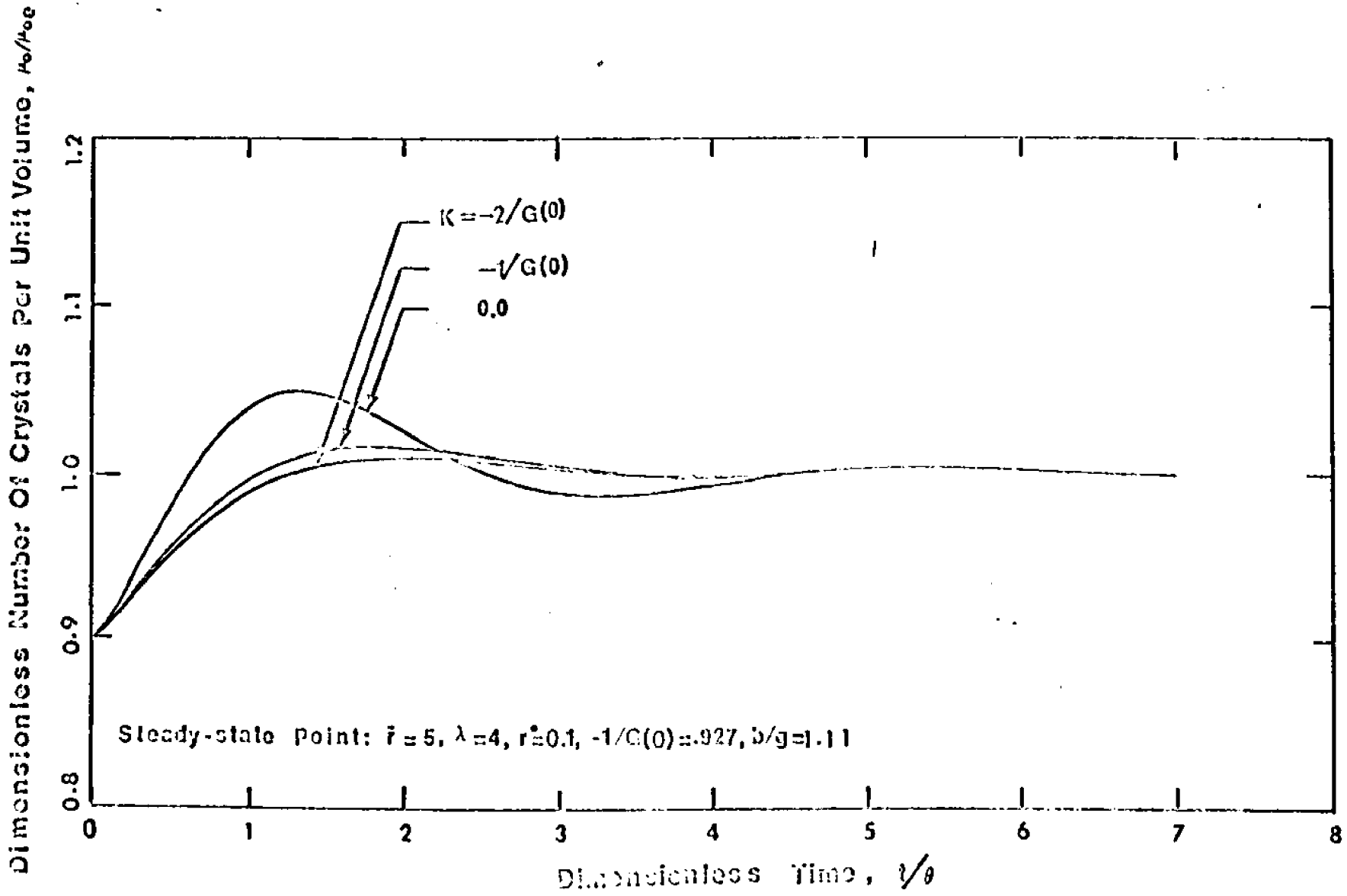

Figure 30-1 Illustrative Dynamics Of A Finite Fines Trap Crystallizer With $\sigma_o - w_o$ Control

Figure 30-2 Illustrative Dynamics Of A Finite Fines Trap Crystallizer With σ_o - w_o Control

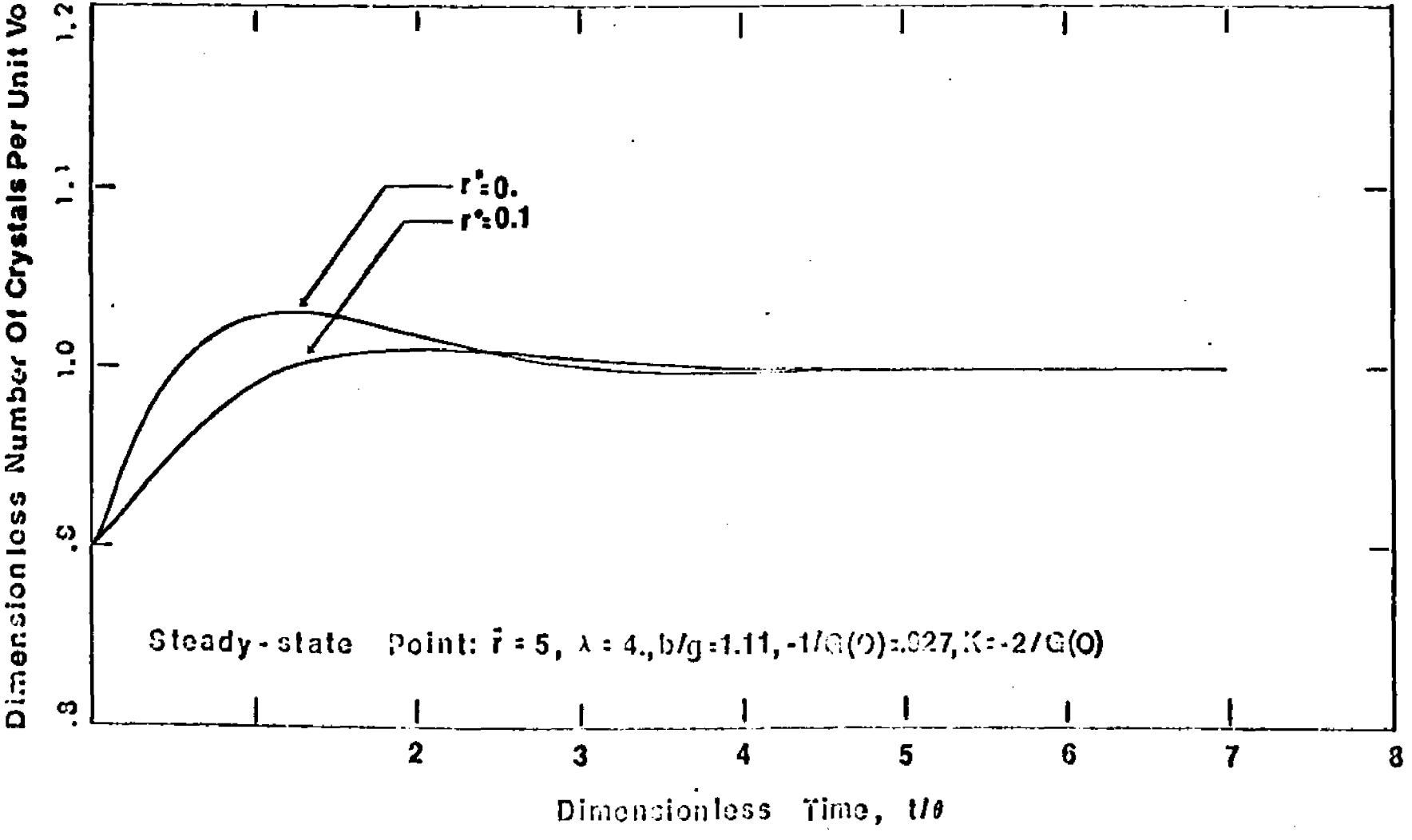

Appendix I

The Characteristic Equation via Spectral Analysis

We sketch here the derivation of the characteristic equation (4.12,4.13) for the linearized crystallizer equations (4.8, 4.9). Our procedure will be to write the dynamic equations (4.8,4.9) in the form

$$\frac{\partial}{\partial t}\begin{Bmatrix}\delta\omega\\ \delta f\end{Bmatrix} = \mathcal{L}\begin{Bmatrix}\delta\omega\\ \delta f\end{Bmatrix} \qquad \text{(AI.1)}$$

so as to identify the linear operator $\mathcal{L}$, and then carry out a formal spectral analysis on $\mathcal{L}$ by solving the eigenvalue problem

$$\mathcal{L}\begin{Bmatrix}\delta\omega\\ \delta f\end{Bmatrix} = s\begin{Bmatrix}\delta\omega\\ \delta f\end{Bmatrix} \qquad \text{(AI.2)}$$

The conditions on s that (AI.2) have solutions then give just the characteristic equation (spectral equation) of the system (AI.1). We shall of course assess the stability of the system by whether the solutions of the spectral equation lie in the left half s-plane.

In (AI.1) we recognize that, apart from their dependence on t, $\delta\omega$ is simply a scalar, but δf a function of r. Consulting (4.8,4.9) we may accordingly write

$$\mathcal{L}\left\{\begin{matrix}\delta\omega\\ \delta f(r)\ ;\ r>0\end{matrix}\right\} = \left\{\begin{matrix}-\delta\omega\\ -\frac{\partial(\delta f(r))}{\partial r} - [1+R\eta(r)]\delta f(r)\\ +g(1+R\eta(r))\left(e^{-r-R\int_0^r \eta}\right)\left(\delta\omega - \int_0^\infty \frac{r^3}{6}\,\delta f\right);\ r>0\end{matrix}\right\} \qquad \text{(AI.3)}$$

and we must be careful to complete the description of the operator by setting down the boundary condition

$$\delta f(o) + (b-g)\int_o^\infty \frac{r^3}{6}\,\delta f - (b-g-\alpha)\,\delta\varphi = o \qquad \text{(AI.4)}$$

For (AI.3, AI.4), the eigenvalue problem (A1.2) becomes

$$\begin{cases} -\delta\dot{\varphi} = s\cdot\delta\varphi \\ -\dfrac{\partial(\delta f(r))}{\partial r} - (1+R\eta(r))\delta f(r) \\ +g(1+R\eta(r))e^{-r-R\int_o^r\eta}\left(\delta\varphi - \displaystyle\int_o^\infty \frac{r^3}{6}\,\delta f\right) = s\,\delta f(r);\ r>0 \\ \delta f(0) + (b-g)\ \dfrac{r^3}{6}\cdot\delta f - (b-g-\partial)\cdot\delta\varphi = 0 \end{cases} \qquad \text{(AI.5)}$$

From the first line of (AI.5) we see that either $\delta\varphi=o$ or $s=-1$, and since we are only interested in what the eigenvalue analysis can tell us about possible instabilities, we summarily set $\delta\varphi=o$. This leaves

$$\begin{cases} \dfrac{\partial(\delta f(r))}{\partial r} + (s+1+R\eta(r))\,\delta f(r) \\ +g(1+R\eta(r))e^{-r-R\int_o^r\eta}\cdot\displaystyle\int_o^\infty \frac{r^3}{6}\cdot\delta f = 0;\ r>0 \\ \delta f(o) + (b-g)\displaystyle\int_o^\infty \frac{r^3}{6}\cdot\delta f = o \end{cases} \qquad \text{(AI.6)}$$

solving (AI.6) as a boundary value problem in $\delta f(r)$ gives

$$\delta f(r) = \lambda \cdot \exp.\left\{ -(s+1)r - R\int_o^r \eta \right\}.$$

$$\left(-(b-g) - g\int_o^r \left[1+R\eta(x)\right] e^{sx}\, dx\right) \quad ; \quad r \geq o \qquad \text{(AI.7)}$$

where λ is the moment integral

$$\lambda = \int_o^\infty \frac{r^3}{6} \cdot \delta f(r) dr$$

But λ must be computable also from the $\delta f(r)$ of (AI.7), and this requires

$$\int_o^\infty \frac{r^3}{6} \cdot e^{-(s+1)r - R\int_o^r \eta(y)dy} \cdot \left[-(b-g) - g\int_o^r \left(1+R\eta(x)\right) e^{sx} \cdot dx\right] dr = 1 \qquad \text{(AI.8)}$$

The equation (AI.8) is just the characteristic equation of the system (AI.1), that is, of (4.8,4.9), and can readily be rearranged into the form (4.12,4.13).

Appendix II

The Characteristic Equation for A Finite Fines Trap

We develop here the full expression for the characteristic equation (4.21) of the finite fines trap. Our starting point is the general characteristic equation (4.21), with H and K given by

$$H(s) = \int_0^\infty e^{-sr} \cdot \frac{r^3}{6} e^{-\int_0^r (1+R\eta)} dr \qquad \text{(AII.1)}$$

$$K(s) = \int_0^\infty e^{-sr} \cdot \frac{r^3}{6} e^{-\int_0^r (1+R\eta)} dr \int_0^r e^{sx}(1+R\eta(x))dx \qquad \text{(AII.2)}$$

from (4.13). By interchanging the order of integration, we can rearrange the equation (AII.2) for K into the somewhat more convenient form

$$K(s) = \int_0^\infty e^{-sr} dr \int_0^\infty \frac{(r+x)^3}{6} e^{-\int_0^{r+x} (1+R\eta)} (1+R\eta(x))dx \qquad \text{(AII.3)}$$

For the finite fines trap, we take $\eta(r) = h(r/r^*)$, where h is the unit square pulse of (4.14). The expression (AII.1, AII.2) can then readily be evaluated to give

$$H(s) = \frac{1}{(S+R+1)^4(S+1)^4} \left\{ (s+1)^4 + \left((S+R+1)^4 \sum_{i=0}^{3} \frac{(s+1)^i r^{*i}}{i!} - (s+1)^4 \sum_{i=0}^{3} \frac{(S+R+1)^i r^{*i}}{i!} \right) \cdot \exp\left[-(S+R+1) r^* \right] \right\} \qquad \text{(AII.4)}$$

$$K(s) = \frac{e^{-(R+1)\cdot r^*}}{S}\left[\sum_{i=0}^{3}\frac{r^{*i}}{i!} - \frac{1}{(R+1)^3}\cdot\sum_{i=0}^{3}\frac{(R+1)^i r^{*i}}{i!}\right]$$

$$+\frac{1}{S\cdot(R+1)^3} - \frac{R+1}{S(S+R+1)^4} + \frac{R\cdot e^{-(R+1)r^*}}{S(S+1)^4} \qquad \text{(AII.5)}$$

$$\cdot\sum_{i=0}^{3}\frac{(S+1)^i r^{*i}}{i!} + \frac{(R+1)e^{-(S+R+1)r^*}}{S(S+1)^4(S+R+1)^4}$$

$$\cdot\left\{(S+1)^4\cdot\sum_{i=0}^{3}\frac{(S+1+R)^i r^{*i}}{i!} - (S+R+1)^4\sum_{i=0}^{3}\frac{(S+1)^i r^{*i}}{i!}\right\}$$

To assemble the characteristic equation, we bring (AII.4, AII.5) to (4.12), and rearrange the resulting equation into the form of equation (4.21). The polynomial P turns out to be of 9th degree, Q, of 7th degree. We write them in the form

$$P(s) = \sum_{j=0}^{9} M_j\cdot S^j$$

$$Q(s) = \sum_{j=0}^{7} N_j\cdot S^j$$

We proceed to set down expressions for these coefficients in terms of b, g, R and r*. For convenience, we write

$$D = 1 + R$$

$$E = \frac{6}{(1+R)^3} + \left\{3\cdot r^{*2} + 6r^* + 6 - \frac{3r^{*2}}{1+R} - \frac{6r^*}{(1+R)^2} - \frac{6}{(1+R)^3}\right\}$$

$$\cdot\ \exp.\ (-(1+R)r^*)$$

Then the coefficients m_j are given by

$$m_9 = 6.$$

$$m_8 = 24\,D + 24 + E\,g$$

$$m_7 = 36\cdot D^2 + 96\cdot D + 36\cdot D + g\cdot\left\{E(4D+4) + R\cdot e^{-Dr^*}\cdot r^{*3}\right\}$$

$$m_6 = 24\cdot D^3 + 144D^2 + 144D + 24 + g\cdot\left\{E(6D^2+16D+6) + R\cdot e^{-Dr^*}\left[(4D+3)r^{*3} + 3r^{*2}\right]\right\}$$

$$m_5 = 6D^4 + 96D^3 + 216D^2 + 96D + 6 + 6b + g\left\{(4D^3+24D^2+24D+4) - 6 + R\cdot e^{-Dr^*}\left[(6D^2+12D+3)r^{*3} + (12D+6)r^{*2} + 6r^*\right]\right\}$$

$$m_4 = 24D^4 + 144D^3 + 144D^2 + 24D + 24b + g\left\{E(D^4+16D^3+36D^2+16D+1) - 6D - 24 + R\cdot e^{-Dr^*}\left[(4D^3+18D^2+12D+1)r^{*3} + (18D^2+24D+3)r^{*2} + (24D+6)r^* + 6\right]\right\}$$

$$m_3 = 36D^4 + 96D^3 + 36D^2 + 36b + g\left\{E(4D^4+24D^3+24D^2+4D) - 24D - 36 + R\cdot e^{-Dr^*}\left[(D^4+12D^3+18D^2+4D)\,r^{*3} + (12D^3+36D^2+12D)r^{*2} + (36D^2+24D)r^* + 24D\right]\right\}$$

$$m_2 = 24D^4 + 24D^3 + 24b + g\left\{E(6D^4+16D^3+6D^2) - 36D - 24 + R\cdot e^{-Dr^*}\left[(3D^4+12D^3+6D^2)r^{*3} + (3D^4+24D^3+18D^2)r^{*2} + (24D^3+36D^2)\,r^* + 36\,D^2\right]\right\}$$

$$m_1 = 6D^4 + 6b + g\{E(4D^4 + 4D^3) - 24D - 6 + R\cdot e^{-Dr^*}[(3D^4 + 4D^3)r^{*3} + (6D^4 + 12D^3)r^{*2} + (6D^4 + 24D^3)r^* + 24D^3]\}$$

$$m_o = g \cdot E^{\prime} \cdot D^4 - 6D + R\cdot e^{-Dr^*}.D^4.(r^{*4} + 2r^{*2} + 6r^{*4} + 6)$$

and the n_j by

$$n_7 = (b-g) \cdot r^{*3} \cdot R \cdot e^{-Dr^*}$$

$$n_6 = R\cdot e^{-Dr^*}\{b[(3D + 3)r^{*3} + 6r^{*2}] - g[(4D + 3)r^{*3} + 6r^{*2}]\}$$

$$n_5 = R \cdot e^{-Dr^*}\{b[(3D^2 + 9D + 3)r^{*3} + (15D + 15)r^{*2} + 18r^*] - g[(6D^2 + 12D + 3)r^{*3} + (21D + 15)r^{*2} + 18r^*]\}$$

$$n_4 = R \cdot e^{-Dr^*}\{b[(D^3 + 9D^2 + 9D + 1)r^{*3} + (12D^2 + 36D + 12)r^{*2} + (36D + 36)r^* + 24] - g[(4D^3 + 18D^2 + (2D+1)r^{*3} + (27D^2 + 51D + 12)r^{*2} + (54D + 36)r^* + 24]\}$$

$$n_3 = R \cdot e^{-Dr^*}\{b[(3D^2 + 9D^2 + 3D)r^{*3} + (3D^3 + 27D^2 + 27D + 3)r^{*2} + (24D^2 + 60D + 24)r^* + 36(D+1)] - g[(D^4 + 12D^3 + 18D^2 + 4D)r^{*3} + (15D^3 + 63D^2 + 39D + 3)r^{*2} + (60D^2 + 96D + 24)r^* + 60D + 36]\}$$

$$n_2 = R \cdot e^{-Dr^*} \Big\{ b\big[(3D^2+3D^2)r^{*3}+(6D^3+18D^2+6D)r^{*2}$$
$$+(6D^3+30D^2+30D+6)r^*+24(D^2+D+1)\big]-g\big[(3D^4$$
$$+12D^3+6D^2)r^{*3}+(3D^4+33D^3+45D^2+90)r^{*2}$$
$$+(30D^3+90D^2+54D+6)r^*+60D^2+60D+24\big]\Big\}$$

$$n_1 = R\cdot e^{-Dr^*}\Big\{ b\big(Dr^{*3}+3(D^3+D^2)r^{*2}+6(D^3+D^2+D)r^*$$
$$+6(D^3+D^2+D+1)\big]-g\big[(3D^4+4D^3)r^{*3}+(6D^4+21D^3+9D^2)r^{*2}$$
$$+(6D^4+36D^3+36D^2+12D)r^*+30D^3+30D^2+30D+6\big]\Big\}$$

$$n_o = -R\cdot e^{-Dr^*} g\big[D^4r^{*3}+3(D^3+D^2)r^{*2}+6(D^3+D^2+D)r^*$$
$$+6(D^3+D^2+D+1)\big]$$

Appendix III

Numerical Methods for the Nonlinear System Dynamics

We sketch here the numerical procedures employed to solve the nonlinear dynamic equations (3.1-3.3) for the crystallizer. Our method is to make, as far as possible, with the moments of the particle population and of the subpopulation of fines. Besides the moments, it turns out to be necessary to introduce the value of the number density f at the fines cut-off size r_o, and a numerical procedure is interested to develop this value as well.

Denote the moments of the particle populations as a value by μ_j

$$\mu_j(t) = \int_o^\infty r^j f(r,t)dr \qquad ; \quad j = 0, 1, 2 \ldots\ldots$$

and the corresponding moments of the fines population by μ_j^*

$$\mu_j^*(t) = \int_o^\infty r^j \eta(r) \cdot f(r,t) \qquad ; \quad j = 0, 1, 2\ldots\ldots$$

from (3.1), we note that

$$\epsilon = 1 - k\mu_3$$

and an integration of (3.3) or (3.3a) then gives

$$\frac{d\mu_o}{dt} = (1-k\mu_3)B(c) - \frac{1}{\theta}\mu_o - \frac{1}{\theta_o}\mu_o^* \qquad \text{(AIII.1)}$$

To get corresponding equation in the higher moments, we multiply equation (3.3) or (3.3a) by r^j and integrate, finding

$$\frac{d\mu_j}{dt} = j\mu_{j-1}G(c) - \frac{1}{\theta}\mu_j - \frac{1}{\theta_o}\mu_j^* \qquad ; \quad j = 1, 2, \ldots \qquad \text{(AIII.2)}$$

Because of the apperance of μ_3 on the right side of (AIII.1), the equations (AIII.2) must be carried at least through $j = 3$. One may of course want to carry higher moments in order to develop more informat on about the distribution.

The equation (AIII.1, AIII.2) involve the fines moments μ_j^*, we turn accordingly to the development of differential equations for them. For the square unit pulse selection curve η of (3.4) we may develop these euqations by multiplying (3.3a) by r^j and integrating up to r_o, we find

$$\frac{d\mu_o^*}{dt} = (1-k\mu_3)B(c) - \left(\frac{1}{\theta} + \frac{1}{\theta_o}\right)\mu_o^* - f(r_o)\,G(c) \qquad \text{(AIII.3)}$$

and, for the higher moments

$$\frac{d\mu_j^*}{dt} = j\cdot\mu_{j-1}^*\,G(c) - \left(\frac{1}{\theta} + \frac{1}{\theta_o}\right)\mu_j^* - r_o^j\,f(r_o)G(c)$$

$$j = 1, 2, \ldots. \qquad \text{(AIII.4)}$$

The equations (AIII.4) must be carried at least through the same value of j as (AIII.2)

The equations (AIII.3, AIII.4) involve the value of the number density f at the fines cut-off size r_o, and we turn now to a computing procedure for this value. This is a matter of solving the boundary value problem (3.3a), and there are of course various ways of driving this. The one we adopt here is simply to take

a grid of equally spaced points in r, and replace $\partial f/\partial r$ by a backword difference formula. The value of f at r = 0 is given by the boundary condition

$$f(o) = (1 - k\mu_3)B(c)/G(c) \qquad \text{(AIII.5)}$$

and for successive values of r on the grid, the partial differential equation gives

$$\frac{\partial f(nr_o/N)}{\partial t} = -G(c)\ \frac{f(nr_o/N) - f((n-1)r_o/N)}{r_o/N}$$

$$- \left(\frac{1}{\theta} + \frac{1}{\theta_o}\right) f(nr_o/N) \qquad n = 1, 2, \ldots N \quad \text{(AIII 6)}$$

Here we have taken the grid spacing r_o/N, and the differential euqations (AIII.6) defined in turn the values of f at r_o/N, etc. up to the critical value $Nr_o/N = r_o$ which appears in the equation (AIII.3, AIII.4). For numerical purpose, values of N of the order of several tens were found to give satisfactory results.

It remains only to incorporate the overall material balance (3.2) to have a self-sustained set of algebraic equation. This can conveniently be done in terms of a total solute-crystal resource function ψ

$$\psi = (1-k\mu_3)C + k\mu_3\rho$$

The differential equation (3.2) becomes

$$\frac{d\psi}{dt} = \frac{1}{\theta}\ (C_i - \psi) \qquad \text{(AIII.7)}$$

and we may recover the solute concentration C as

$$C = \frac{\varphi - k\mu_3\rho}{1 - k\mu_3} \qquad \text{(AIII.8)}$$

The equations (AIII.1-AIII.8) form a self-contained set of equations for the dynamic behavior of the crystallizer. The quantities C and f(o) are given by albebraic equations, (AIII.8) and (AIII.5) respectivly. The remaining equations are first order ordinary differential equations, and define jointly the behavior of the moments μ_j and μ_j^* for j = 0, 1, 2, etc., of the distributional values $f(nr_o/N)$ for n = 1, 2, ...,N and of the resource function φ. Carring both sets of moment equations up to j=J gives N + 2J + 3 differential equations, to gether with the two algebraic equations in C and f(0). Calculations were made for various steady states of interest, by taking initial departures from these steady states and following the resulting free transients. The variables were scaled on their steady-state values. The resulting systems of differential equations were solved by a Runge-Kutta scheme. Calculations were carried out on the IBM 360/50 computer of the City College Computing Center.

Appendix IV
Undesired Steady States through Positive Feedback

Suppose a process, with driving force x and response y, to have the steady-state operating characteristic

$$y = f(x) \qquad \text{(AIV.1)}$$

The process is designed to operate at the steady-state values

$$x = x_e, \quad y = y_e$$

so that

$$y_e = f(x_e) \qquad \text{(AIV.2)}$$

Operation is maintained at the point, x_e, y_e with the help of a feedback control system, which we take in the form

$$x - x_e = \frac{-K}{f'(x_e)} \quad (y - y_e) \qquad \text{(AIV.3)}$$

where $f'(x_e)$ is the derivative of the steady-state characteristi (AIV.1) at the set point x_e. The normalization of the controller gain K with this derivative provides a convenient dimensionless form for K, with positive sign when negative feedback is being applied.

The steady-state behavior of the closed loop system is described by the equations (AIV.1-AIV.3). These have always the solution $x = x_e$, $y = y_e$, and any other solution must satisfy

$$k = -f'(x_e) / \frac{f(x) - f(x_e)}{x - x_e} \qquad \text{(AIV.4)}$$

Now as long as f is steadily increasing or decreasing over its whole working range, the right hand side of (AIV.4) is negative, and extraneous solutions of (AIV.4) can only exist for negative K. That is, undesired steady states of the closed loop system can only arise when positive feedback is being applied.

This line of argument of course fails when f is not monotonic, since the difference quotient in (AIV.4) may then well have different sign from the derivative at the setpoint

References

1. Bennett, R.C., C.E.P. Vol.58, No.9, 76 (1962).
2. Newman, H.H. and Bennett, R.C., C.E.P. Vol.55, No.3, (1959).
3. Bennett, R.C., Swenson Evaporator Co., Personal Communication.
4. Bransom, S.H. and Palmer, A.G.C., British Chemical Engineering, Vol.9, No. 10, 672 (1964).
5. Caldwell, H.B., I. & E.C., Vol.53, No.2, 115 (1961).
6. Murray, D.C. & Larson, M.A., A.I.Ch.E. Journal, Vol. 11, No. 4, 728 (1965).
7. Kirwan, K.J. and Pigford, R.L., A.I.Ch.E. Meeting, May 1968, Preprint, New York.
8. Randolph, A.D. and Larson, M.A., A.I.Ch.E. Journal, Vol. 8, No. 5, 639 (1962); C.E.P. symposium series Vol. 61, 147, (1965), and 95, Vol. 65, P.1 (1969).
9. Melia, T.P. and Moffitt, W.P., I. & E.C. Fundamental, Vol. 3, No. 4, 313 (1964).
10. Randolph, A.D., A.I.Ch.E. Journal, Vol. 11, No. 3, 424 (1965).
11. Rumford, F. and Bain, J., Trans. Insts Chem Engrs., Vol. 38, 11 (1960).
12. Saeman, W.C., I. & E.C., Vol. 53, No.8, 612 (1961) and Vol. 53, No. 8 191 (1961).
13. Saeman, W.C., U.S. Patent # 2,883,273 (1959)
    # 2,737,451 (1956).
14. Schoen, H.M., I. & E.C., Vol. 53, No.8, 607 (1961).
15. Sherwin, M.B. & Shinnar, R. & Katz, S., A.I.Ch.E Journal, Vol. 13, No.6, 114 (1967).
16. Sherwin Martin, Shinnar, Reuel and Katz, Stanley, C.E.P. Symposium Series, No. 95, Vol. 65, P.75 (1969).
17. Ealton, Alan G., Science, Vol. 148, 601 (1965).
18. Hulburt, H.M. and Katz, S., C.E.S. 19, 555 (1964).
19. Hulburt, H.M. and Stefango, D.G., Chem. Eng. Progress Symp. Series, 95, Vol. 65, P. 50 (1969).

Autobiographical Statement

Shang-jen Lei was born November 24, 1938 in a small town of the northern part of Taiwan, China. He graduated from Tainan Ist Middle School with an academic diploma in June 1958. His college education was completed in Tunghai University, Taichung, Taiwan. There he received a Bachelor of Chemical Engineering degree in June 1962.

Between 1962 and 1963, he served in the Chinese Marine Corps as Second Lieutenant in Ordnance Maintenance. Upon completion of military service, he taught high school courses in his home town.

January 1964 Mr. Lei came to this country. He worked part time as an instructor at the freshman chemistry and unit operation laboratorys in Stevens Institute of Technology, Hoboken, New Jersey. September 1965, he received a Master of Chemical Engineering degree from Stevens. Upon the notification of honoring a research fellowship, he came to City College, and worked toward his Ph. D. degree. August 1969, after fullfilment of the major part of the Ph. D. requirements, he accepted an engineering research position at American Machine & Foundary Company in Stamford, Conneticut. May 1970 he completed his disertation.